TEASING APART THE ROLE OF THE MAMMALIAN MOLECULAR CIRCADIAN CLOCK AND THREE-DIMENSIONAL CHROMATIN INTERACTIONS IN RHYTHMIC TRANSCRIPTION

A Dissertation

by

JOSHUA ROBERT BEYTEBIERE

Submitted to the Office of Graduate and Professional Studies of
Texas A&M University
in partial fulfillment of the requirements for the degree of

DOCTOR OF PHILOSOPHY

Chair of Committee,	Jerome S. Menet
Committee Members,	Alan E. Pepper
	Christine Merlin
	Craig D. Kaplan
Head of Department,	Tom McKnight

December 2019

Major Subject: Biology

ABSTRACT

The mammalian molecular circadian clock is composed of a transcriptional-translational feedback loop. The positive arm of this loop is composed of the transcription factor CLOCK:BMAL1 which activates the transcription of their target genes *Per* and *Cry*. PER and CRY then feedback to inhibit their own transcription. The molecular circadian clock is also responsible for the activation of many clock-controlled genes. Recent data suggest that genes expressed in a circadian manner have little overlap among the tissues. The goal of this study is to determine the mechanisms by which the circadian clock can drive tissue-specific rhythmic gene expression.

To identify the genes targeted by the circadian clock, we performed BMAL1 chromatin immunoprecipitation with massively parallel DNA sequencing (ChIP-seq) in the mouse liver, kidney, and heart. We determined the majority of binding to be tissue-specific, and this was largely accounted for by differences in the permissiveness of the chromatin, and binding with tissue-specific transcription factors. The majority of genes targeted by BMAL1 were still transcribed arrhythmically, suggesting that BMAL1 binding alone is insufficient to drive rhythmic gene expression. To determine if enhancer-enhancer interactions play a role in rhythmic transcription, we performed POL II ChIA-PET at ZT6 (middle of the day) and ZT18 (middle of the night). Our data show that rhythmically expressed BMAL1 targets exhibit day night differences in interactions between BMAL1 bound DHS and neighboring DHS. Our data suggest that BMAL1-mediated rhythmic transcription relies on the transcriptional activity of the BMAL1 bound DHS, neighboring DHS, and on the ability of BMAL1 to regulate the activity of

neighboring DHS. To address the role of enhancer-enhancer interactions and the intrinsic activity of enhancers in coordinating rhythmic gene expression we developed a technique to measure the intrinsic activity of enhancers *in vivo* by cloning the enhancers into plasmids and delivering them to the liver via hydrodynamic tail vein injection. Our results indicate transfection of ten percent of liver cells and expression from the vector with our enhancer of interest suggesting that it likely will be a viable means to measure the intrinsic enhancer activity.

DEDICATION

This dissertation is wholeheartedly dedicated to my family. First my parents Curt and Jana who have always been there for me with love and support. Thank you for always believing in me. My sisters who have provided good times and encouragement along the way. Last but certainly not least I would also like to dedicate this dissertation to my dog Cesar who has also been there for me as a best friend and a companion in anything life has thrown our way until he passed away.

ACKNOWLEDGEMENTS

The course of my Ph.D. and life over the last five years has been filled with peaks and valleys. The first thing my Ph.D. taught me was about failure. My Ph.D. taught me that although for the first few years I seemed to only be climbing small hills to end up in even lower valleys that sometimes you must cross the valleys to get to the peaks. Without all the failed experiments and trial and error I would never have achieved the publications or Ph.D. that I have today. I would like to take these pages to say thank you to all the people that have helped me along the way in my growth both as a scientist and a person.

First, I would like to say thank you to Dr. Jerome Menet. You showed me what good science is and were the best mentor that I have seen. I have to say the experience was tough, but eventually you made me realize this is a good thing and discussion can promote better scientific thought. I know you always have the best intentions for us in mind when you do things and want what is best for us, and I think this is part of what makes you the best advisor. Your scientific knowledge and the rigor that is put into the science is rarely seen and has made me the scientist that I am today, so I thank you so much for that.

I would like to thank my committee members Dr. Alan Pepper, Dr. Christine Merlin, and Dr. Craig Kaplan who have added invaluable insight and helped steer my project in the best possible direction. Your insight has also taught me how to approach scientific challenges and how to become a better scientist. I would also like to thank all

members of the clock journal club at Texas A&M University for your insightful comments, suggestions, and fun times at conferences.

I am grateful for my laboratory members that I have had along the way. They were a major part of making the laboratory feel like a family. I would first like to thank Alexandra Trott who was a mentor and like a big sister to me and was the only graduate student in the laboratory when I arrived. Thank you for your support, feedback, help on projects, and for all the wondering memories we have made. I would also like to thank Ben Greenwell and Collin Osborne for their input and collaborations on projects as well. They have also been largely responsible for creating a friendly and inviting atmosphere. I would also like to thank Aishwarya Sahasrabudhe for helping me learn how to mentor people. Ash, I may have taught you techniques but you have also helped me learn how to be a better mentor.

I would like to thank my family who have been there for me whenever I have needed them. Your continuous support of my goals and aspirations has been invaluable. I would like also like to thank my dog Cesar for being my walking partner and the main reason I have kept my sanity.

CONTRIBUTORS AND FUNDING SOURCES

Contributors

Research done in this dissertation was supervised by my advisory committee consisting of Dr. Jerome Menet (chair), Dr. Christine Merlin, Dr. Alan Pepper from the Biology Department of Texas A&M University, and Dr. Craig Kaplan formerly at the Biochemistry and Biophysics Department of Texas A&M University, and currently from University of Pittsburgh Department of Biological Sciences.

The work done in chapter Chapter II was conceived and designed by myself and Dr. Jerome Menet. I performed the majority of the experiments and the bioinformatics analysis. Dr. Jerome Menet performed the ChIA-PET experiments with help from Alexandra Trott and myself. Ben Greenwell, Collin Andrew Osborne and Dr. Jerome Menet helped with bioinformatics analysis. Jessica Spence and Helene Vitet performed ChIPs at early stages of the project. Seung-Hee Yoo, Zheng Chen, and Joseph S. Takahashi contributed the BMAL1 antibody used for the ChIP-seq experiments. Noushin Ghaffari helped with ChIA-PET bioinformatics analysis. Dr. Craig Kaplan, Dr. Christine Merlin, Dr Alan Pepper, and Aldrin Lugena provided insightful suggestions at various stages of the project. Michael Rosbash, Kate Abruzzi, Ryanne Spann, Charles Johnson, and Richard Metz for help with sequencing of the ChIP-seq and ChIA-PET libraries.

The work done in Chapter III was conceived and designed by myself and Dr. Jerome Menet. I performed the majority of the experiments and the bioinformatics analysis. Ben Greenwell and Jerome Menet helped with bioinformatics analysis.

Aishwarya Sahasrabudhe helped with experiments performing RNA extractions and qPCR.

The work done in Chapter IV and V was conceived and designed by myself and Dr. Jerome Menet. The feeding experiments were performed by myself, Aishwarya Sahasrabudhe, Jordan Thompson, and Jared Easterling. The bioinformatics and data analysis were performed by myself with assistance from Ben Greenwell and Jerome Menet.

Funding Sources

The studies and experiments performed in this study were supported by the Texas A&M University / Department of Biology Start Up Funds to Jerome S Menet.

TABLE OF CONTENTS

LIST OF FIGURES

Page

CHAPTER I

INTRODUCTION AND LITERATURE REVIEW

1.1 The mammalian circadian clock

The circadian clock is ubiquitously found throughout life from cyanobacteria to plants to insects and mammals (Bell-Pedersen et al., 2005; Dunlap, 1999). The circadian clock allows for the anticipation of rhythmic daily changes in the environment (Paranjpe and Sharma, 2005). The anticipation of changes that occur with a twenty-four-hour period in the environment have proven to be extremely important for responses to environmental factors such as nutrient availability and differences in predation (Rodriguez et al., 2016). In mammals, the master circadian clock is located in the suprachiasmatic nucleus (SCN) and is entrained by light dark cycles that are sensed by the intrinsically photosensitive retinal ganglion cells (IPRGC's) in the eye (Chen et al., 2011). The light dark cycles are conventionally referred to with Zeitgeber Time (ZT), and ZT0 denotes lights on while ZT12 denotes lights off. The circadian clock is entrained by zeitgebers ("time giver"), which are environmental cues that can synchronize the circadian clock. There are many different zeitgebers such as light, temperature, and feeding rhythms to name a few. Innervation from the eye to the SCN allows for the setting of the master circadian clock in the SCN (Chen et al., 2011). The master circadian clock then sends out signals that set the peripheral circadian clocks located throughout the body (Albrecht, 2012; Mohawk et al., 2012). These peripheral clocks can in part then drive tissue-specific rhythmic gene expression (Panda et al., 2002; Storch et al., 2002; Zhang et al., 2014). This circadian gene expression has

proven to be crucial for regulating many processes in a circadian manner such as metabolism and blood pressure (Gnocchi et al., 2015a; Wang et al., 2008; Xie et al., 2015). Disruption of the circadian clock has shown to affect these pathways and lead to diseases such as obesity and cancer (Hatori and Panda, 2015). REV-ERB proteins are components of the secondary feedback loop of the circadian clock that repress biological functions that cancer cells need such as cellular division and cell metabolism (Sulli et al., 2018).

1.2 The mammalian molecular circadian clock is composed of a transcriptional-translational feedback loop

The same molecular clockwork mechanism is found in every cell, *i.e*., in the master circadian clock in the SCN as well as in peripheral clocks such as the liver (Fig 1A). The peripheral clocks are able to respond to certain inputs individually depending on the signal of entrainment, and this in turn can contribute to tissue-specific rhythmic physiological outputs. The mammalian molecular circadian clock is composed of a transcriptional-translational feedback loop. CLOCK:BMAL1 form a heterodimer that acts as the positive arm of the feedback loop which activates the transcription of *Per 1*, *2*, and *3* and *Cry 1* and *2* by binding to E-boxes. The CLOCK:BMAL1 preferred binding motif is a perfect E-box CACGTG, however binding to degenerate E-boxes has been noted and certain degenerate motifs are preferred binding locations as compared to other degenerate motifs (Yoshitane et al., 2014). It has been found that the motif most associated with CLOCK:BMAL1 binding is a dual E-box with a six or seven base pair spacer (Yoshitane et al., 2014). PER and CRY then form a heterodimer and feedback to

inhibit CLOCK:BMAL1 activated transcription (Fig 1A). CLOCK:BMAL1 do not only drive the transcription of PER and CRY, but also drive the transcription of many clock controlled genes. The positive arm of the circadian clock CLOCK:BMAL1 act largely as a transcriptional activator, and the heterodimer binds to thousands of locations in the genome allowing for the regulation of transcription of many genes that are not circadian clock components. The genome wide binding sites of the circadian clock components CLOCK:BMAL1 have been mapped. Transcription factor binding sites are often determined by chromatin immunoprecipitation sequencing (ChIP-seq), a technique that relies on cross-linking of DNA-protein interactions, followed by sonication of DNA to shear the DNA, followed by an immunoprecipitation and size selection before library preparation and sequencing. The technique allows for many of the DNA binding sites of a protein of interest to be determined. BMAL1 binding locations have been determined via ChIP-seq and it has been found that the genome-wide peak binding phase of BMAL1 DNA binding is at ZT6 (Koike et al., 2012; Menet et al., 2014; Rey et al., 2011).

Figure 1. The molecular circadian clock is composed of a transcriptional-translational feedback loop.
The circadian clock is composed of a transcriptional-translational feedback loop with CLOCK:BMAL1 heterodimer forming the positive arm and driving transcription of *Per* and *Cry*. PER and CRY then form a heterodimer and feedback to inhibit CLOCK:BMAL1 activated transcription. CLOCK:BMAL1 does not only activate transcription of Per and Cry, they also activate the transcription of many clock controlled genes. The diagram show the molecular clock coming from the suprachiasmatic nucleus (SCN) the location of the master circadian clock. The liver shows an example of a tissue with a peripheral circadian clock as it is not the master circadian clock.

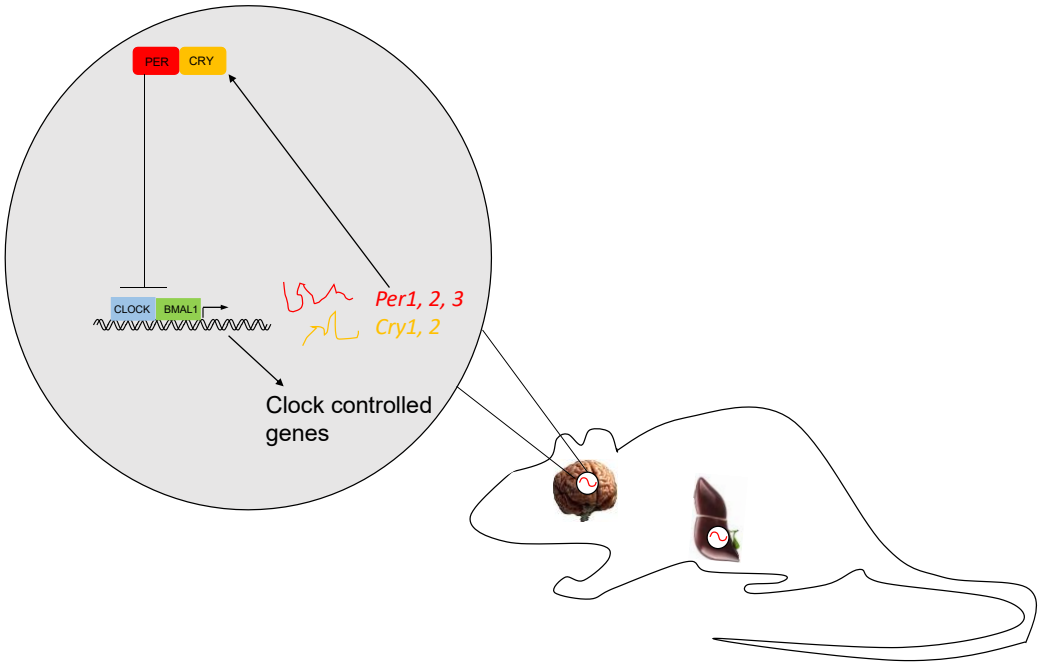

1.3 Chromatin structure and regulation of transcription in mammals

Gene expression is extremely important in biology and is a necessity for the production of proteins. Gene expression is broken down into several key steps, the first of which is transcription. Transcription is the process of making mRNA transcripts from DNA. DNA in cells is found in the form of chromatin. Certain regions of the chromatin called enhancers and promoters are permissible and regulate transcription and are also regions were transcription factors and other regulatory factors bind to regulate transcription. Chromatin is the substance that makes up chromosomes and consists of DNA and proteins, the major protein components are histones which allow for the

compaction of the DNA. Chromatin is a dynamic structure where the nucleosomes can shift up and down the DNA, referred to as nucleosome positioning, as well as be displaced from the DNA which often occurs due to the action of ATP-dependent remodeling complexes. Chromatin is composed of DNA wrapped around nucleosomes. Chromatin is composed of DNA wrapped around histones proteins. Eukaryotic nucleosomes are composed of four core canonical histones (H3, H4, H2A, H2B) that form an octamer with two of each protein wrapped nearly twice by the DNA (Venkatesh and Workman, 2015). Chromatin can then come in two varieties heterochromatin which is a highly condensed form and euchromatin which is less condensed. The chromatin is a means of packing the DNA more tightly and regulating the accessibility of the DNA for transcription.

1.4 Nucleosome position and a permissive chromatin landscape

Nucleosomes at the transcription start site can inhibit the binding of RNA polymerase II and transcription from taking place (Soboleva et al., 2014). Nucleosome positioning is controlled by many different factors including: nucleosome sequence preferences, DNA methylation, histone variants, post-translational modifications, and competition between transcription factors and nucleosomes (Segal and Widom, 2009). Histone variants such as H2A.Z and H3.3 can replace H2A and H3 respectively and are correlated with active transcription. Histones can also undergo many different post-translational modifications such as acetylation, methylation, ubiquitylation, and sumoylation that can affect the structure of the chromatin and the rate of transcription. The histone modifications are able to affect the chromatin structure and the rate of

transcription by interacting with chemical structures in the nucleosome, neighboring nucleosomes, or by affecting the histone-DNA interactions (Venkatesh and Workman, 2015). Active cis-regulatory enhancer elements are defined by both H3K27ac and high levels of H3K4me1 relative to H3K4me3 (Gates et al., 2017), while repressed genes have a higher density of nucleosomes and can be marked by H3K9 methylation, H3K27me3, and H4K20me3 (Gates et al., 2017). The structure of the chromatin is not the only thing that has been shown to regulate transcription.

1.5 Enhancers and promoters influence transcriptional output

Enhancers and promoters are regions of the DNA that have been shown to have a major impact on the output of transcription. Enhancers are devoid of nucleosomes most of the time and in these regions, nucleosomes will compete with transcription factors for access to DNA. Enhancers are regions of DNA to which regulatory proteins bind, and they can be vast distances from the genes that they influence. Promoters are the DNA region where RNA polymerase binds to initiate transcription and are often binding sites for additional transcription factors. These enhancer and promoter regions can interact with one another through long-range chromatin interactions to help regulate transcriptional outputs.

1.6 Transcription Initiation and Elongation in Mammals

Transcription in mammals involves many steps and begins with the initiation of transcription which is carried out by RNA polymerase II at gene promoters. RNA polymerase II is responsible for the transcription of all protein-coding genes and several

other types of RNA as well. RNA polymerase relies on the general transcription factors for correct positioning at the promoter of the target gene, and for the release of RNA polymerase II into the elongation phase to begin transcribing the target gene. These general transcription factors are denoted as such since they are needed at nearly all the promoters that are used by RNA polymerase II. The general transcription factors form the pre-initiation complex or PIC along with RNA polymerase II. First, TFIID, through its TATA binding protein (TBP), will bind to the TATA box. TFIID binding to the TATA box will allow for adjacent binding of TFIIB. Then the rest of the general transcription factors along with RNA polymerase II will assemble at the promoter of the target gene. TFIIH will then use its helicase activity to separate the strands of DNA exposing the template strand for transcription. TFIIH will also phosphorylate RNA polymerase II which will allow for release of RNA polymerase II and the beginning of the elongation phase. Serine5 is phosphorylated during initiation and recruits capping enzyme, while serine2 is recruited during elongation (Yu et al., 2015), which suggests that phosphorylation of the carboxyl-terminal domain (CTD) of RNA polymerase II (POL II) governs stage-specific interactions with different cellular machines (Ahn et al., 2004; Bowman and Kelly, 2014; Corden, 1990; Nemec et al., 2019). Transcription elongation is followed by transcription termination, and RNA processing events. The nascent RNA will be processed such that a 5’ 7-methylguanosine cap will be added, introns are spliced, and the poly (A) tail is added. The production of mRNA can be regulated from the transcription initiation to the post-transcriptional processing, but transcription initiation is generally the main step controlling gene expression (Ogata et al., 2003).

1.7 The role of transcription factors in driving gene expression

Transcription initiation can be regulated in many ways, one such way is the binding of transcriptional activators and repressors which is extremely important for the circadian clock as it is composed of a transcriptional-translational feedback loop. Previous research has shown that transcription factors in mammals often bind together and aid the binding of additional transcription factors (Stefflova et al., 2013). It has also been shown by the encode consortium that transcription factors bind in open chromatin (chromatin that is permissible to cutting by DNase I) 97.7% of the time (Thurman et al., 2012a; Yue et al., 2014a). DNase I Hypersensitive sites (DHS) are sites that are preferentially digested by a mild DNase I treatment, and which therefore identify accessible chromatin regions within the genome by DNase-seq on intact nuclei (Fig 2). These open chromatin regions correspond to enhancers and promoters which are largely responsible for regulating transcription and are major sites of transcription factor binding. DNase-seq is the technique used to map these open chromatin regions and begins with a mild DNase I digestion, then a size selection for small DNA fragments, library preparation and sequencing. In addition, mild DNase I treatment can also be used to determine if transcription factors are bound in the enhancer via DNase footprinting because they will shield the DNA from being cut and allow for the mapping on transcription factor footprints (Fig 2). By mapping the 5' most base pair of the DNase-seq reads, the initial cut location can be identified. For transcription to take place, transcription factors will bind to permissible chromatin regions such as enhancer and promoters, which will in turn allow for the recruitment of the pre-initiation complex, and mediator (Allen and Taatjes, 2015; Sainsbury et al., 2015). The mediator complex is

responsible for relaying regulatory signals from transcription factors and the PIC to RNA polymerase II. Recent findings revealed that the mediator and POL II create a functional bridge between enhancers and promoters rather than an architectural bridge, and that cohesion is required to tether regulatory DNA while mediator and POL II are not (El Khattabi et al., 2019). A functional bridge is created instead of an architectural bridge as the mediator impacts promoter-enhancer contacts indirectly, by the recruitment of architectural proteins. The mediators' structure is pliable and allows for the integration and transmission of regulatory signals.

Transcription factors and histones have been shown to have major roles in the regulation of DHS activity. Transcription factors and histones compete for access to DNA, and some transcription factors have shown to bind DNA and reposition or displace histones (Magnani et al., 2011; Zaret and Carroll, 2011). BMAL1 has been shown to aid in the rhythmic removal of nucleosomes independent of its transcriptional output (Menet et al., 2014; Trott and Menet, 2018a). Prior research has shown that BMAL1 does not directly contribute to the activity of its enhancers, but instead opens the chromatin to facilitate the binding of additional transcription factors (Trott and Menet, 2018a). These findings indicate that BMAL1 alone is insufficient to create a transcriptionally active enhancer, and that BMAL1 relies on the binding of additional ubiquitously expressed transcription factors (Trott and Menet, 2018a). Common characteristics of transcriptionally active enhancers are nucleosome depletion, p300, and chromatin remodelers binding, eRNA, POL II ChIP-seq signal and H3K27ac. Instances of enhancers with nucleosome depletion, p300, and chromatin remodeler binding have been found to be transcriptionally inactive, as they lacked H3K27ac and

are therefore termed poised enhancers (Calo and Wysocka, 2013; Rada-Iglesias et al., 2011). Many of these enhancers have been found to be tissue-specific, and the majority of BMAL1 binding has been shown to occur in enhancer regions (Beytebiere et al., 2019; Dunham et al., 2012; Sobel et al., 2017a; Thurman et al., 2012a; Trott and Menet, 2018a). Current research in the field indicates that the tissue-specific chromatin landscape is one major factor controlling the tissue-specific binding of CLOCK:BMAL1, and this in turn is one of the factors contributing to tissue-specific rhythmic gene expression (Beytebiere et al., 2019; Perelis et al., 2015).

Figure 2. DNase-seq and DNase footprinting allows for the identification of open chromatin regions and transcription factor binding.

DNase-seq is performed with a mild DNase I digestion of chromatin. Open chromatin will be the first regions digested and DNA purification with a size selection of short fragments is then performed. Library preparation must then occur for sequencing to take place. After this sequencing and genome mapping allows for the determination of enhancer regions. Mapping of the 5' most base pair allows for the determination of transcription factor binding locations as this DNA is protected by the transcription factor from DNase I digestion.

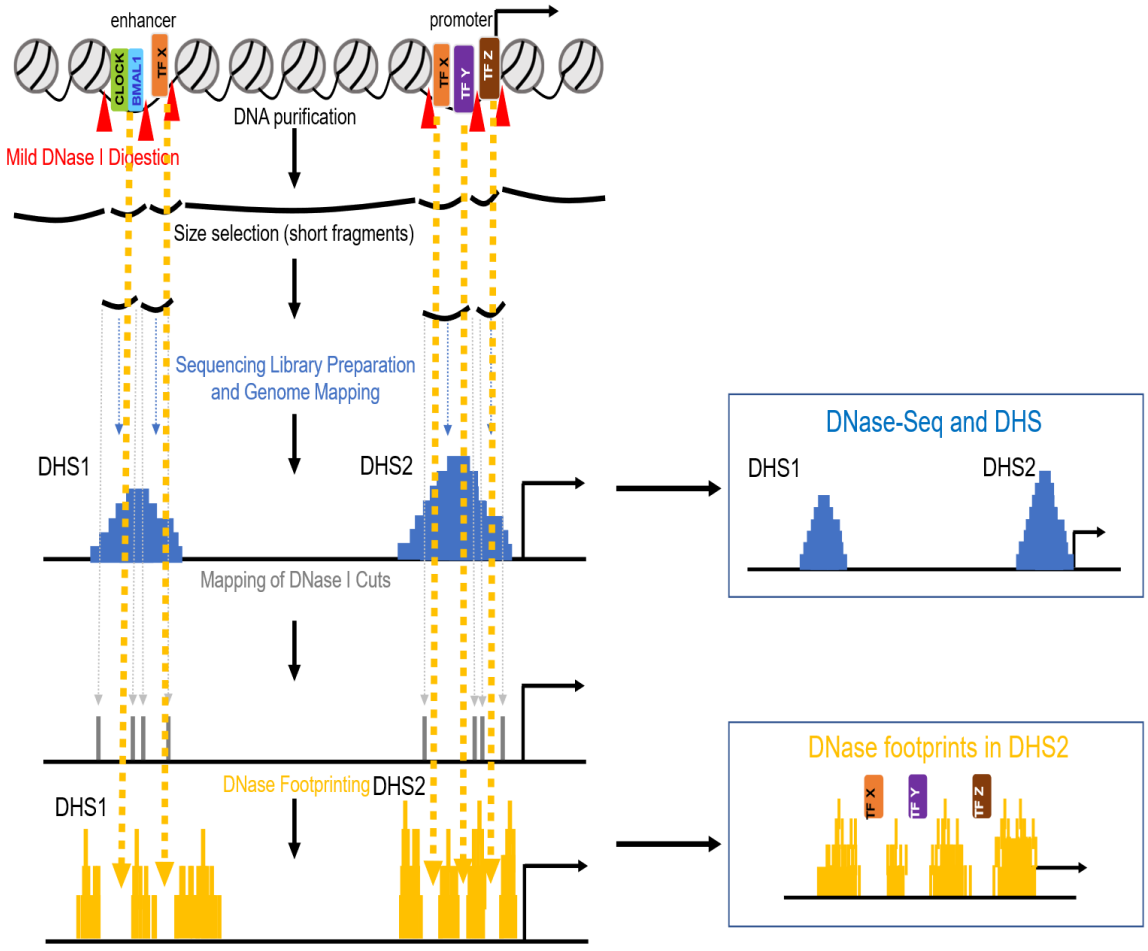

1.8 The three-dimensional chromatin structures role in circadian transcription

The three-dimensional chromatin structure or gene looping has been shown to be important in transcriptional outputs and recent findings have shown that it is also very important for circadian transcription regulation (Aguilar-Arnal and Sassone-Corsi,

2013; Beytebiere et al., 2019; Kim et al., 2018a; Mermet et al., 2018; Yeung et al., 2018). Previous research shows that these three-dimensional chromatin interactions are not random events but are coordinating gene expression for related biological functions. One protein that has been shown to play a large role in mediating long-range interactions is CCCTC-binding factor (CTCF). CTCF has been shown to bind DNA, recruit cohesin, and organize chromatin into topologically associated domains (TAD) (Cho et al., 2005; Giorgetti et al., 2016; Rubio et al., 2008; Wendt et al., 2008). Recent findings in the circadian field suggest that enhancer-enhancer interactions play a large role in the rhythmic transcription (Aguilar-Arnal and Sassone-Corsi, 2013; Beytebiere et al., 2019; Kim et al., 2018a; Mermet et al., 2018; Yeung et al., 2018). These findings all show that circadian enhancers bound by components of the circadian clock interact with non-circadian enhancers to drive the transcription of their target genes, while these interactions can take place over long distances, many of the interactions can also occur within the same gene. These chromatin interactions have been shown to be important for both BMAL1 regulated transcription and for REV-ERBα (a transcriptional repressor involved in the secondary loops of the circadian clock) mediated transcription, suggesting that this may occur for the primary and secondary circadian clock loops (Aguilar-Arnal et al., 2013; Beytebiere et al., 2019; Kim et al., 2018a; Mermet et al., 2018; Yeung et al., 2018). Disorganization of the three-dimensional genome has been shown to be a common hallmark found in cancers (Barutcu et al., 2015; Flavahan et al., 2016; Hnisz et al., 2016; Seaman et al., 2017; Taberlay et al., 2016). The three-dimensional genome structure has also shown to be important for many other diseases.

These diseases include congenital limb formations, autoimmune diseases, Cooks Syndrome, and sex reversal (Darío et al., 2015; Franke et al., 2016; Martin et al., 2015).

1.9 Regulation of circadian transcription

Over fifteen percent of the mouse liver transcriptome is rhythmic and over half of the total transcriptome is rhythmic in at least one tissue (Menet et al., 2014; Mure et al., 2018b; Trott and Menet, 2018a; Zhang et al., 2014). There is a great deal of tissue-specificity in both rhythmically transcribed genes and rhythmic biological functions. One interesting observation is that the majority of CLOCK:BMAL1 targets are not rhythmically expressed in phase with CLOCK:BMAL1 binding (Menet et al., 2014; Trott and Menet, 2018a). The transcriptional output of CLOCK: BMAL1 targets has been shown to be highly heterogenous. It has been shown that this is largely accounted for by the binding of additional ubiquitously expressed transcription factors at CLOCK:BMAL1 enhancers (Trott and Menet, 2018a). It was also shown previously that the binding of tissue-specific transcription factors did not play a major role in whether a gene would be expressed rhythmically in-phase with BMAL1 binding, rhythmically out-of-phase with BMAL1 binding, arrhythmic, or not expressed (Trott and Menet, 2018a). Previous findings reveal CLK:CYC, the positive arm of the circadian clock in drosophila, bind in a tissue-specific manner due to the binding of tissue-specific transcription factors (Meireles-Filho et al., 2014). Together these data suggest that there may be a role for ubiquitously expressed transcription factors such as NF-KB and CTCF, that is different from tissue-specific transcription factors. Recent findings also suggest that circadian transcription is not only influenced by the cell autonomous molecular circadian clock but

that rhythms in feeding and other external cues can aid in the driving of rhythmic gene expression (Greenwell et al., 2019). CLOCK:BMAL1 has been shown to promote a transcriptionally permissive landscape rather than directly activating transcription which provides a novel framework to explain the reprogramming of the circadian clock by environmental and pathological conditions (Trott and Menet, 2018a). Some mechanisms that have shown to reprogram the circadian clock are high-fat diet, antibiotic treatment in the liver, and LPS treatment in the lungs (Eckel-Mahan and Sassone-Corsi, 2013; Eckel-Mahan et al., 2013; Haspel et al., 2014; Murakami et al., 2016). The model that CLOCK:BMAL1 binding facilitates the binding of additional TFs provides a mechanistic framework for how the circadian clock could be reprogrammed by environmental conditions such as LPS, antibiotic treatment, and high-fat diet. The circadian clock is largely responsible for the coordination of rhythmic transcription which has been shown to coordinate many metabolic pathways with important physiological impacts. However, when circadian clock desynchrony is observed as with shift-workers, many adverse physiological and metabolic impacts have been observed.

1.10 Impacts of desynchrony of the circadian clock

The circadian clock when disrupted has been shown to have many impacts of physiology and often results in diseases such as obesity, metabolic diseases, cancer, coronary heart disease, mood disruption, and dementia (Hatori and Panda, 2015). These impacts have been observed in human shift workers as well as in circadian clock knockouts in mice. In the circadian field, knockouts of core clock genes are often used for a mechanistic dissection of the clock to study the impact of the clock on different

outputs, and many of the same sort of pathologies are seen in animals that have had their clock knocked out. In *Bmal1*$^{-/-}$ mice, detrimental health effects have been observed such as sarcopenia, cataracts, decrease in subcutaneous fat, organ shrinkage, infertility, defective glucose homeostasis, and ossification of ligaments and tendons, reduced life-span, and a number of premature aging pathologies (Kondratov, 2006). These physiological impacts have also been observed in mice with knockout mutations in other core clock components (Liu et al., 2007; Sun et al., 2017; Turek et al., 2005). This suggests that the circadian clock has a crucial role in many different metabolic and biochemical pathways. There is an ever increasing need to mitigate the negative health effects of an out-of-sync circadian clock as shiftwork is becoming more common in society. Previous studies have shown that knockout mice do not have the same rhythms in behavior as wild-type mice in terms of locomotor activity and feeding (Bunger et al., 2000; Marcheva et al., 2010). Currently more research is needed to address ways to mitigate the negative effects of circadian desynchrony, and clock knockouts in mice are one model system that could allow for this. One thing of importance is that in *Bmal1* conditional knockouts where the gene was knocked out using Cre-Lox recombination there were not issues with life span, fertility, body weight, blood glucose levels, and age-dependent arthropathy, suggesting that some of these impacts may also be developmental (Yang et al., 2016).

Figure 3. Effects of *Bmal1*$^{-/-}$ on circadian rhythms, physiology, and metabolism.

The circadian clock is composed of a transcriptional-translational feedback loop. *Bmal1*$^{-/-}$ mice experience a loss of many rhythms though some behaviors do have dampened rhythms due to the masking effect and photophobia of mice. Many physiological and metabolic disorders are observed in *Bmal1*$^{-/-}$ mice.

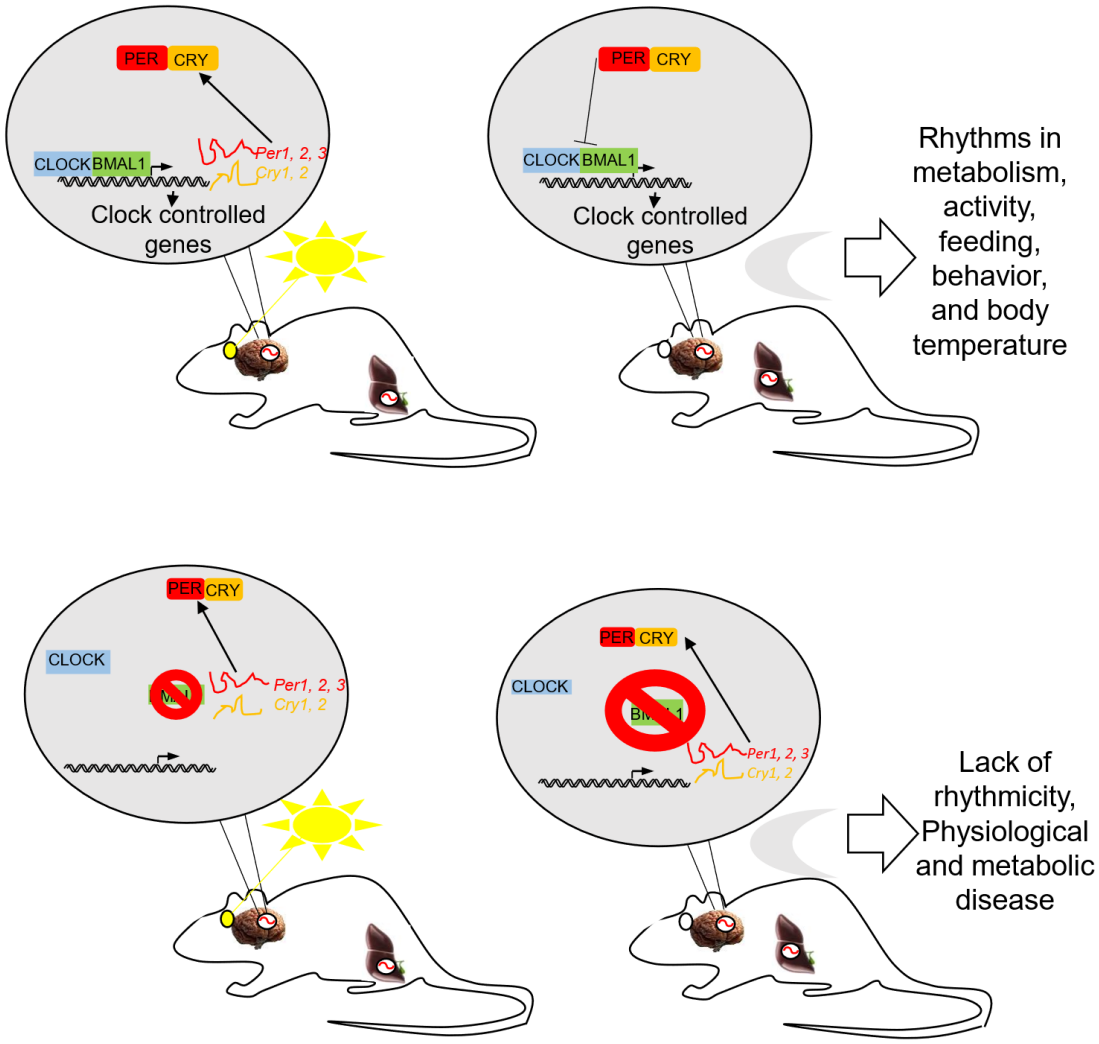

1.11 Implications of circadian temporal food preferences in mice

Feeding behavior can be broken down into three critical aspects: what food is eaten, when food is eaten, and how much food is eaten. Feeding behavior can also be divided into quantity and quality of food consumed. The quality of food consumed would

comprise what food is eaten and when food is eaten. These feeding behaviors can be determined by the homeostatic systems and hedonic system in the brain of the organism (Sasaki, 2017). The homeostatic system would consist of the body maintenance and needs of the organism while the hedonic system would cover the pleasure and desires of the organism. A wealth of research has been conducted into the quality of feeding behavior and this has largely addressed these two topics, macronutrient-based diet selection and feeding patterns.

Macronutrient based diet selection has shown to be influenced by humoral factors, homeostatic feeding mechanisms, the hedonic system, and genetics (Sasaki, 2017). Humoral factor FGF21 has been shown to regulate carbohydrate preferences (Larson et al., 2019; Stephanie et al., 2016; Talukdar et al., 2016). Ghrelin has been shown to regulate macronutrient preferences, however, its role is likely context-dependent and is somewhat controversial (Kojima et al., 1999; Perello et al., 2010; Skibicka et al., 2011; Skibicka et al., 2012). The central melanocortin system is the most important system involved in the homeostatic control of energy balance, and it regulates the quantity of feeding. However recently it has also been shown to have an important role in macronutrient preference. In POMC-null mice, which lack the agonist for the melanocortin receptor, an elevated fat preference was observed, and a reduced carbohydrate preference was also observed in other mouse models affecting the melanocortin receptor (Koegler et al., 1999; Tung et al., 2007). In the hypothalamus, galanin stimulates the release of the opioid enkephalin throughout the brain which promotes fat preference (Nogueiras et al., 2012; Toll et al., 2016). Neuropeptide Y and melanocyte concentrating hormone have shown to positively regulate carbohydrate

preference and oxytocin has shown to negatively regulate carbohydrate preference (Domingos et al., 2013; Klockars et al., 2015; Slawecki et al., 2000; Stanley et al., 1985). The hedonic system is important for regulating food preference, and glucose-containing sugars and fat, have a potent reward of dopamine. While the role of the dopamine system in reward is evident, its role in the regulation of macronutrient preference remains unclear at this time. Opioid receptor mu 1 gene has been implicated in increasing preference for fat and protein consumption (Haghighi et al., 2014).

Feeding patterns play an extremely important role in controlling weight and health (Asher and Sassone-Corsi, 2015). Ingesting the same amount of food at different times of day has different consequences on health, because systemic metabolic efficiency will fluctuate over the course of the day (Bray et al., 2010). Correcting the feeding schedule of mice fed a high fat diet relieved them of high-fat diet-induced obesity (Fuse et al., 2012; Hatori et al., 2012; Sherman et al., 2012). Different zeitgebers (external signals that set the internal clock) have different effects on the SCN and the peripheral circadian clocks. Mice consume the majority of their food during their active phase the night which is denoted ZT12-ZT24 and less during the day which is denoted ZT0-ZT12 (Yang et al., 2009).

Currently a gap in the field exists that is if there are temporal preferences for different macronutrients. One prior study in wild-caught wood mice suggests that they have a preference for sugars early in the night but did not find a preference for protein later in the night (Jensen, 1993). One reason for this could be that they used food with mixed macronutrients instead of pure macronutrient sources. Previous studies have indicated that rodents will go for the highest caloric gain per unit of time spent foraging

(Hansson, 1985), however this may not apply when the mice are given the macronutrients individually instead of in mixed sources. We hypothesized that carbohydrates and fats peak consumption would be earlier in the night, and that protein peak consumption would be later in the night. One reason for this is that glycogen is the main energy source used by many areas of the body and is used to provide energy to all cells, and it can be acquired from food or from fatty acids that are beta-oxidized, and gluconeogenesis (Slavin and Carlson, 2014). Glycogen represent the first choice of energy storage and use, and when glycogen needs are met the animals will switch to storing lipids in adipocytes, and protein in muscles (Lu et al., 2014).

Figure 4. Diagram of expected food consumption of different biomolecules based on the hypothesized temporal food consumption of mice.

Proposed model of food consumption. Carbohydrates are consumed first as glycogen is the first choice of energy storage and use (Lu et al., 2014). Then protein is consumed later in the active phase when the glycogen needs are met. Kcal of fat are expected to be consumed at the highest rate as they are the most caloric choice of the three biomolecules (Hansson, 1985).

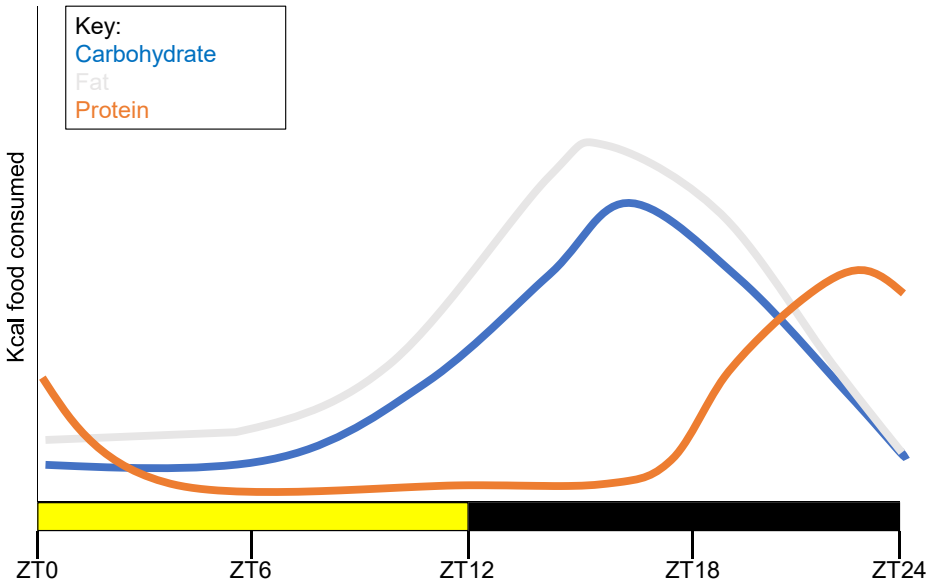

1.12 Project aims

Almost all mammalian cells have a circadian clock that allows for the anticipation of daily rhythmic oscillations. These circadian clocks rely on a transcriptional-translational feedback loop where the positive arm is composed of the heterodimeric transcription factor CLOCK:BMAL1 (Fig. 1). The circadian clock coordinates rhythmic transcription of about fifteen percent of the liver transcriptome and coordinates rhythmic transcription of over half the transcriptome in at least one tissue. The rhythmic transcription is then able in turn to drive rhythms of many key metabolic and biochemical pathways. As discussed above, there is very little overlap in the genes that are rhythmically expressed in each tissue. Recent findings have shown a great deal of tissue-specificity in rhythmic gene expression in mice, suggesting that the circadian clock may be able to drive tissue-specific gene expression in a rhythmic manner. This suggests that the targets of the circadian clock may be tissue-specific or that, alternatively, some regulatory mechanisms occur in a tissue-specific manner to generate tissue-specific rhythmic gene expression despite common target genes in each tissue.

The first aim of my Ph.D. (Chapter 2) was to determine if the circadian clock has tissue-specific gene targets, and if so, what are the mechanisms by which the circadian clock can target genes in a tissue-specific manner. To address this question, we performed Chromatin Immunoprecipitation sequencing (ChIP-seq) experiments in the mouse heart, kidney, and liver, and determine if BMAL1 is binding is tissue-specific. We found that the majority of BMAL1 binding was indeed tissue-specific, and the main drivers of tissue-specific binding were tissue-specific DHSs and co-binding with ts-TFs.

The second aim (Chapter 2) was to determine how the circadian clock can drive tissue-specific rhythmic gene expression. To address this aim we compared the binding sites of the CLOCK:BMAL1 with publicly available mRNA time courses with collections every four hours over the course of forty-eight hours in the heart, kidney, and liver. We found the majority of the rhythmic mRNA expression was tissue-specific. We found that the major reasons for the tissue-specific rhythms were differences in the activity of BMAL1-bound enhancers in tissues, BMAL1 binding to different enhancers in tissues, and enhancer-enhancer interactions. In accordance with recent findings showing that the circadian clock coordinates rhythmic transcription by promoting rhythmic enhancer-enhancer interactions, we found that BMAL1 bound enhancers have more enhancer-enhancer interactions at ZT6 (when CLOCK:BMAL1 are bound to DNA) than ZT18. These data suggest that there is a day-night difference in BMAL1 enhancer interactions, and that rhythmic gene expression is regulated by multiple non-mutually exclusive factors.

The third aim (Chapter 3) was to setup a technique to assay the role of the intrinsic activity of enhancers and compare this with the role enhancer-enhancer interactions in rhythmic gene expression. To determine the drivers of rhythmic gene expression, we want to measure the intrinsic activity of the enhancers in an episomal context *in vivo*, *i.e.*, when the enhancer is removed from any chromatin context and not subject to enhancer-enhancer interaction. To measure the intrinsic activity of enhancers, we cloned the enhancers into plasmids that were injected through the mouse tail using a technique known as hydrodynamic tail vein injection. The data show that we can measure the intrinsic activity of an enhancer *in vivo* and we can compare

this to the ChIA-PET allowing for the determination of both aspects in driving rhythmic gene expression.

The fourth aim (Chapter 4) was to determine whether *Bmal1*$^{-/-}$ mice eat in a rhythmic manner and whether *Bmal1*$^{-/-}$ mice experience health benefits from strong external rhythms. We found that *Bmal1*$^{-/-}$ mice eat in an arrhythmic manner when fed *ad libitum*, and that they are able to be entrained to a night-restricted eating pattern without a drop in the amount of Kcal consumed. These results will be useful to determine the role of rhythmic food intake vs. the molecular circadian clock in the regulation of rhythmic gene expression as we will be able to determine if night-restricted feeding restores rhythmic gene expression and behavior patterns.

The fifth aim (Chapter 5) was to design a system to assess the temporal food preferences in mice for different biomolecules. Our data suggest that mice prefer eating carbohydrates and lipids earlier in the active phase and then protein later in the active phase. While additional biological replicates will be needed to complete our study, our data confirm previous findings showing that mice prefer sugars early in the active period (Jensen, 1993), and extend the rhythms in nutrient preference to lipids and proteins.

1.13 References

Aguilar-Arnal, L., and Sassone-Corsi, P. (2013). The circadian epigenome: how metabolism talks to chromatin remodeling. Curr Opin Cell Biol.

Ahn, S.H., Kim, M., and Buratowski, S. (2004). Phosphorylation of Serine 2 within the RNA Polymerase II C-Terminal Domain Couples Transcription and 3′ End Processing. *13*, 67-76.

Albrecht, U. (2012). Timing to Perfection: The Biology of Central and Peripheral Circadian Clocks. Neuron *74*, 246-260.

Allen, B.L., and Taatjes, D.J. (2015). The Mediator complex: a central integrator of transcription. Nature Reviews Molecular Cell Biology *16*, 155-166.

Asher, G., and Sassone-Corsi, P. (2015). Time for Food: The Intimate Interplay between Nutrition, Metabolism, and the Circadian Clock. Cell *161*, 84-92.

Barutcu, A.R., Lajoie, B.R., McCord, R.P., Tye, C.E., Hong, D., Messier, T.L., Browne, G., Van Wijnen, A.J., Lian, J.B., Stein, J.L.*, et al.* (2015). Chromatin interaction analysis reveals changes in small chromosome and telomere clustering between epithelial and breast cancer cells. Genome Biology *16*.

Bell-Pedersen, D., Cassone, V.M., Earnest, D.J., Golden, S.S., Hardin, P.E., Thomas, T.L., and Zoran, M.J. (2005). Circadian rhythms from multiple oscillators: lessons from diverse organisms. Nat Rev Genet *6*, 544-556.

Beytebiere, J.R., Trott, A.J., Greenwell, B.J., Osborne, C.A., Vitet, H., Spence, J., Yoo, S.-H., Chen, Z., Takahashi, J.S., Ghaffari, N.*, et al.* (2019). Tissue-specific BMAL1 cistromes reveal that rhythmic transcription is associated with rhythmic enhancer–enhancer interactions. Genes & Development *33*, 294-309.

Bowman, E.A., and Kelly, W.G. (2014). RNA Polymerase II transcription elongation and Pol II CTD Ser2 phosphorylation. *5*, 224-236.

Bray, M.S., Tsai, J.Y., Villegas-Montoya, C., Boland, B.B., Blasier, Z., Egbejimi, O., Kueht, M., and Young, M.E. (2010). Time-of-day-dependent dietary fat consumption influences multiple cardiometabolic syndrome parameters in mice. *34*, 1589-1598.

Bunger, M.K., Wilsbacher, L.D., Moran, S.M., Clendenin, C., Radcliffe, L.A., Hogenesch, J.B., Simon, M.C., Takahashi, J.S., and Bradfield, C.A. (2000). Mop3 is an essential component of the master circadian pacemaker in mammals. Cell *103*, 1009-1017.

Calo, E., and Wysocka, J. (2013). Modification of enhancer chromatin: what, how, and why? Mol Cell *49*, 825-837.

Chen, S.K., Badea, T.C., and Hattar, S. (2011). Photoentrainment and pupillary light reflex are mediated by distinct populations of ipRGCs. *476*, 92-95.

Cho, D.H., Thienes, C.P., Mahoney, S.E., Analau, E., Filippova, G.N., and Tapscott, S.J. (2005). Antisense Transcription and Heterochromatin at the DM1 CTG Repeats Are Constrained by CTCF. *20*, 483-489.
Corden, J.L. (1990). Tails of RNA polymerase II. *15*, 383-387.
Darío, Kraft, K., Heinrich, V., Krawitz, P., Brancati, F., Klopocki, E., Horn, D., Kayserili, H., John, Laxova, R.*, et al.* (2015). Disruptions of Topological Chromatin Domains Cause Pathogenic Rewiring of Gene-Enhancer Interactions. Cell *161*, 1012-1025.

Domingos, A.I., Sordillo, A., Dietrich, M.O., Liu, Z.-W., Tellez, L.A., Vaynshteyn, J., Ferreira, J.G., Ekstrand, M.I., Horvath, T.L., De Araujo, I.E.*, et al.* (2013). Hypothalamic melanin concentrating hormone neurons communicate the nutrient value of sugar.

Dunham, I., Kundaje, A., Aldred, S.F., Collins, P.J., Davis, C.A., Doyle, F., Epstein, C.B., Frietze, S., Harrow, J., Kaul, R.*, et al.* (2012). An integrated encyclopedia of DNA elements in the human genome. Nature *489*, 57-74.

Dunlap, J.C. (1999). Molecular bases for circadian clocks. Cell *96*, 271-290.

Eckel-Mahan, K., and Sassone-Corsi, P. (2013). Metabolism and the circadian clock converge. Physiol Rev *93*, 107-135.

Eckel-Mahan, K.L., Patel, V.R., de Mateo, S., Orozco-Solis, R., Ceglia, N.J., Sahar, S., Dilag-Penilla, S.A., Dyar, K.A., Baldi, P., and Sassone-Corsi, P. (2013). Reprogramming of the circadian clock by nutritional challenge. Cell *155*, 1464-1478.

El Khattabi, L., Zhao, H., Kalchschmidt, J., Young, N., Jung, S., Van Blerkom, P., Kieffer-Kwon, P., Kieffer-Kwon, K.-R., Park, S., Wang, X.*, et al.* (2019). A Pliable Mediator Acts as a Functional Rather Than an Architectural Bridge between Promoters and Enhancers. Cell.

Flavahan, W.A., Drier, Y., Liau, B.B., Gillespie, S.M., Venteicher, A.S., Stemmer-Rachamimov, A.O., Suvà, M.L., and Bernstein, B.E. (2016). Insulator dysfunction and oncogene activation in IDH mutant gliomas. Nature *529*, 110-114.

Franke, M., Ibrahim, D.M., Andrey, G., Schwarzer, W., Heinrich, V., Schöpflin, R., Kraft, K., Kempfer, R., Jerković, I., Chan, W.-L.*, et al.* (2016). Formation of new chromatin domains determines pathogenicity of genomic duplications. *538*, 265-269.

Fuse, Y., Hirao, A., Kuroda, H., Otsuka, M., Tahara, Y., and Shibata, S. (2012). Differential roles of breakfast only (one meal per day) and a bigger breakfast with a small dinner (two meals per day) in mice fed a high-fat diet with regard to induced obesity and lipid metabolism. J Circadian Rhythms *10*, 4.
Gates, L.A., Foulds, C.E., and O'Malley, B.W. (2017). Histone Marks in the 'Driver's Seat': Functional Roles in Steering the Transcription Cycle. Trends in Biochemical Sciences *42*, 977-989.

Giorgetti, L., Lajoie, B.R., Carter, A.C., Attia, M., Zhan, Y., Xu, J., Chen, C.J., Kaplan, N., Chang, H.Y., Heard, E.*, et al.* (2016). Structural organization of the inactive X chromosome in the mouse. *535*, 575-579.

Gnocchi, D., Pedrelli, M., Hurt-Camejo, E., and Parini, P. (2015). Lipids around the Clock: Focus on Circadian Rhythms and Lipid Metabolism. *4*, 104-132.

Greenwell, B.J., Trott, A.J., Beytebiere, J.R., Pao, S., Bosley, A., Beach, E., Finegan, P., Hernandez, C., and Menet, J.S. (2019). Rhythmic Food Intake Drives Rhythmic Gene Expression More Potently than the Hepatic Circadian Clock in Mice. Cell Reports *27*, 649-657.e645.

Haghighi, A., Melka, M.G., Bernard, M., Abrahamowicz, M., Leonard, G.T., Richer, L., Perron, M., Veillette, S., Xu, C.J., Greenwood, C.M.T.*, et al.* (2014). Opioid receptor mu 1 gene, fat intake and obesity in adolescence. *19*, 63-68.

Hansson, L. (1985). The food of bank voles, wood mice and yellow-necked mice, Vol 55.

Haspel, J.A., Chettimada, S., Shaik, R.S., Chu, J.-H., Raby, B.A., Cernadas, M., Carey, V., Process, V., Hunninghake, G.M., Ifedigbo, E.*, et al.* (2014). Circadian rhythm reprogramming during lung inflammation. *5*, 4753.

Hatori, M., and Panda, S. (2015). Response of peripheral rhythms to the timing of food intake. Methods Enzymol *552*, 145-161.

Hatori, M., Vollmers, C., Zarrinpar, A., Ditacchio, L., Eric, Gill, S., Leblanc, M., Chaix, A., Joens, M., James*, et al.* (2012). Time-Restricted Feeding without Reducing Caloric Intake Prevents Metabolic Diseases in Mice Fed a High-Fat Diet. Cell Metabolism *15*, 848-860.

Hnisz, D., Weintraub, A.S., Day, D.S., Valton, A.L., Bak, R.O., Li, C.H., Goldmann, J., Lajoie, B.R., Fan, Z.P., Sigova, A.A.*, et al.* (2016). Activation of proto-oncogenes by disruption of chromosome neighborhoods. *351*, 1454-1458.

Jensen, S.P. (1993). Temporal changes in food preferences of wood mice (Apodemus sylvaticus L.). *94*, 76-82.

Kim, Y.H., Marhon, S.A., Zhang, Y., Steger, D.J., Won, K.-J., and Lazar, M.A. (2018). Rev-erbα dynamically modulates chromatin looping to control circadian gene transcription. Science *359*, 1274-1277.
Klockars, A., Levine, A.S., and Olszewski, P.K. (2015). Central Oxytocin and Food Intake: Focus on Macronutrient-Driven Reward. *6*.

Koegler, F.H., Schaffhauser, A.O., Mynatt, R.L., York, D.A., and Bray, G.A. (1999). Macronutrient Diet Intake of the Lethal Yellow Agouti (Ay/a) Mouse. *67*, 809-812.

Koike, N., Yoo, S.H., Huang, H.C., Kumar, V., Lee, C., Kim, T.K., and Takahashi, J.S. (2012). Transcriptional architecture and chromatin landscape of the core circadian clock in mammals. Science *338*, 349-354.

Kojima, M., Hosoda, H., Date, Y., Nakazato, M., Matsuo, H., and Kangawa, K. (1999). Ghrelin is a growth-hormone-releasing acylated peptide from stomach. Nature *402*, 656-660.

Kondratov, R.V. (2006). Early aging and age-related pathologies in mice deficient in BMAL1, the core componentof the circadian clock. Genes & Development *20*, 1868-1873.

Larson, K.R., Chaffin, A.T.B., Goodson, M.L., Fang, Y., and Ryan, K.K. (2019). Fibroblast growth factor-21 controls dietary protein intake in male mice. Endocrinology.

Liu, A.C., Welsh, D.K., Ko, C.H., Tran, H.G., Zhang, E.E., Priest, A.A., Buhr, E.D., Singer, O., Meeker, K., Verma, I.M.*, et al.* (2007). Intercellular coupling confers robustness against mutations in the SCN circadian clock network. Cell *129*, 605-616.

Lu, B., Bridges, D., Yang, Y., Fisher, K., Cheng, A., Chang, L., Meng, Z.X., Lin, J.D., Downes, M., Yu, R.T.*, et al.* (2014). Metabolic Crosstalk: Molecular Links Between Glycogen and Lipid Metabolism in Obesity. *63*, 2935-2948.

Magnani, L., Eeckhoute, J., and Lupien, M. (2011). Pioneer factors: directing transcriptional regulators within the chromatin environment. Trends Genet *27*, 465-474.

Marcheva, B., Ramsey, K.M., Buhr, E.D., Kobayashi, Y., Su, H., Ko, C.H., Ivanova, G., Omura, C., Mo, S., Vitaterna, M.H.*, et al.* (2010). Disruption of the clock components CLOCK and BMAL1 leads to hypoinsulinaemia and diabetes. Nature *466*, 627-631.

Martin, P., McGovern, A., Orozco, G., Duffus, K., Yarwood, A., Schoenfelder, S., Cooper, N.J., Barton, A., Wallace, C., Fraser, P.*, et al.* (2015). Capture Hi-C reveals novel candidate genes and complex long-range interactions with related autoimmune risk loci. *6*, 10069.

Meireles-Filho, A.C., Bardet, A.F., Yanez-Cuna, J.O., Stampfel, G., and Stark, A. (2014). cis-regulatory requirements for tissue-specific programs of the circadian clock. Curr Biol *24*, 1-10.
Menet, J.S., Pescatore, S., and Rosbash, M. (2014). CLOCK:BMAL1 is a pioneer-like transcription factor. Genes Dev *28*, 8-13.

Mermet, J., Yeung, J., Hurni, C., Mauvoisin, D., Gustafson, K., Jouffe, C., Nicolas, D., Emmenegger, Y., Gobet, C., Franken, P.*, et al.* (2018). Clock-dependent chromatin topology modulates circadian transcription and behavior. Genes Dev *32*, 347-358.

Mohawk, J.A., Green, C.B., and Takahashi, J.S. (2012). Central and peripheral circadian clocks in mammals. Annu Rev Neurosci *35*, 445-462.

Murakami, M., Tognini, P., Liu, Y., Eckel-Mahan, K.L., Baldi, P., and Sassone-Corsi, P. (2016). Gut microbiota directs PPARgamma-driven reprogramming of the liver circadian clock by nutritional challenge. EMBO Rep *17*, 1292-1303.

Mure, L.S., Le, H.D., Benegiamo, G., Chang, M.W., Rios, L., Jillani, N., Ngotho, M., Kariuki, T., Dkhissi-Benyahya, O., Cooper, H.M.*, et al.* (2018). Diurnal transcriptome atlas of a primate across major neural and peripheral tissues. Science *359*, eaao0318.

Nemec, C.M., Singh, A.K., Ali, A., Tseng, S.C., Syal, K., Ringelberg, K.J., Ho, Y.H., Hintermair, C., Ahmad, M.F., Kar, R.K.*, et al.* (2019). Noncanonical CTD kinases regulate RNA polymerase II in a gene-class-specific manner. Nat Chem Biol *15*, 123-131.

Nogueiras, R., Romero-Picó, A., Vazquez, M.J., Novelle, M.G., López, M., and Diéguez, C. (2012). The Opioid System and Food Intake: Homeostatic and Hedonic Mechanisms. *5*, 196-207.

Ogata, K., Sato, K., and Tahirov, T.H. (2003). Eukaryotic transcriptional regulatory complexes: cooperativity from near and afar. Current Opinion in Structural Biology *13*, 262.

Panda, S., Antoch, M.P., Miller, B.H., Su, A.I., Schook, A.B., Straume, M., Schultz, P.G., Kay, S.A., Takahashi, J.S., and Hogenesch, J.B. (2002). Coordinated transcription of key pathways in the mouse by the circadian clock. Cell *109*, 307-320.

Paranjpe, D.A., and Sharma, V.K. (2005). Evolution of temporal order in living organisms. J Circadian Rhythms *3*, 7.

Perelis, M., Marcheva, B., Moynihan Ramsey, K., Schipma, M.J., Hutchison, A.L., Taguchi, A., Peek, C.B., Hong, H., Huang, W., Omura, C.*, et al.* (2015). Pancreatic cell enhancers regulate rhythmic transcription of genes controlling insulin secretion. Science *350*, aac4250-aac4250.

Perello, M., Sakata, I., Birnbaum, S., Chuang, J.-C., Osborne-Lawrence, S., Rovinsky, S.A., Woloszyn, J., Yanagisawa, M., Lutter, M., and Zigman, J.M. (2010). Ghrelin Increases the Rewarding Value of High-Fat Diet in an Orexin-Dependent Manner. Biological Psychiatry *67*, 880-886.

Rada-Iglesias, A., Bajpai, R., Swigut, T., Brugmann, S.A., Flynn, R.A., and Wysocka, J. (2011). A unique chromatin signature uncovers early developmental enhancers in humans. Nature *470*, 279-283.

Rey, G., Cesbron, F., Rougemont, J., Reinke, H., Brunner, M., and Naef, F. (2011). Genome-wide and phase-specific DNA-binding rhythms of BMAL1 control circadian output functions in mouse liver. PLoS Biol *9*, e1000595.

Rodriguez, A., Chiaradia, A., Wasiak, P., Renwick, L., and Dann, P. (2016). Waddling on the Dark Side: Ambient Light Affects Attendance Behavior of Little Penguins.

Rubio, E.D., Reiss, D.J., Welcsh, P.L., Disteche, C.M., Filippova, G.N., Baliga, N.S., Aebersold, R., Ranish, J.A., and Krumm, A. (2008). CTCF physically links cohesin to chromatin. *105*, 8309-8314.

Sainsbury, S., Bernecky, C., and Cramer, P. (2015). Structural basis of transcription initiation by RNA polymerase II. Nature Reviews Molecular Cell Biology *16*, 129-143.

Sasaki, T. (2017). Neural and Molecular Mechanisms Involved in Controlling the Quality of Feeding Behavior: Diet Selection and Feeding Patterns. Nutrients *9*.

Seaman, L., Chen, H., Brown, M., Wangsa, D., Patterson, G., Camps, J., Omenn, G.S., Ried, T., and Rajapakse, I. (2017). Nucleome Analysis Reveals Structure-function Relationships for Colon Cancer. molcanres.0374.0372.

Segal, E., and Widom, J. (2009). What controls nucleosome positions? Trends in Genetics *25*, 335-343.

Sherman, H., Genzer, Y., Cohen, R., Chapnik, N., Madar, Z., and Froy, O. (2012). Timed high-fat diet resets circadian metabolism and prevents obesity. FASEB J *26*, 3493-3502.

Skibicka, K.P., Hansson, C., Alvarez-Crespo, M., Friberg, P.A., and Dickson, S.L. (2011). Ghrelin directly targets the ventral tegmental area to increase food motivation. *180*, 129-137.

Skibicka, K.P., Hansson, C., Egecioglu, E., and Dickson, S.L. (2012). Role of ghrelin in food reward: impact of ghrelin on sucrose self-administration and mesolimbic dopamine and acetylcholine receptor gene expression. *17*, 95-107.

Slavin, J., and Carlson, J. (2014). Carbohydrates. Advances in Nutrition *5*, 760-761.

Slawecki, C.J., Betancourt, M., Walpole, T., and Ehlers, C.L. (2000). Increases in Sucrose Consumption, But Not Ethanol Consumption, Following ICV NPY Administration. *66*, 591-594.

Sobel, J.A., Krier, I., Andersin, T., Raghav, S., Canella, D., Gilardi, F., Kalantzi, A.S., Rey, G., Weger, B., Gachon, F.*, et al.* (2017). Transcriptional regulatory logic of the diurnal cycle in the mouse liver. PLOS Biology *15*, e2001069.

Soboleva, T.A., Nekrasov, M., Ryan, D.P., and Tremethick, D.J. (2014). Histone variants at the transcription start-site. *30*, 199-209.

Stanley, B.G., Daniel, D.R., Chin, A.S., and Leibowitz, S.F. (1985). Paraventricular nucleus injections of peptide YY and neuropeptide Y preferentially enhance carbohydrate ingestion. *6*, 1205-1211.

Stefflova, K., Thybert, D., Wilson, M.D., Streeter, I., Aleksic, J., Karagianni, P., Brazma, A., Adams, D.J., Talianidis, I., Marioni, J.C*., et al.* (2013). Cooperativity and rapid evolution of cobound transcription factors in closely related mammals. Cell *154*, 530-540.

Stephanie, Lucas, Peltekian, L., Meghan, Terry, Kristin, Adriana, Andreas, Ratner, C., Holst, B*., et al.* (2016). FGF21 Mediates Endocrine Control of Simple Sugar Intake and Sweet Taste Preference by the Liver. *23*, 335-343

Storch, K.F., Lipan, O., Leykin, I., Viswanathan, N., Davis, F.C., Wong, W.H., and Weitz, C.J. (2002). Extensive and divergent circadian gene expression in liver and heart. Nature *417*, 78-83

Sulli, G., Rommel, A., Wang, X., Kolar, M.J., Puca, F., Saghatelian, A., Plikus, M.V., Verma, I.M., and Panda, S. (2018). Pharmacological activation of REV-ERBs is lethal in cancer and oncogene-induced senescence. Nature *553*, 351-355.

Sun, Q., Zhao, Y., Yang, Y., Yang, X., Li, M., Xu, X., Wen, D., Wang, J., and Zhang, J. (2017). Loss of the clock protein PER2 shortens the erythrocyte life span in mice. Journal of Biological Chemistry *292*, 12679-12690.

Taberlay, P.C., Achinger-Kawecka, J., Lun, A.T.L., Buske, F.A., Sabir, K., Gould, C.M., Zotenko, E., Bert, S.A., Giles, K.A., Bauer, D.C*., et al.* (2016). Three-dimensional disorganization of the cancer genome occurs coincident with long-range genetic and epigenetic alterations. Genome Research *26*, 719-731.

Talukdar, S., Bryn, Song, P., Hernandez, G., Zhang, Y., Zhou, Y., William, Paratala, B., Turner, T., Smith, A*., et al.* (2016). FGF21 Regulates Sweet and Alcohol Preference. Cell Metabolism *23*, 344-349.

Thurman, R.E., Rynes, E., Humbert, R., Vierstra, J., Maurano, M.T., Haugen, E., Sheffield, N.C., Stergachis, A.B., Wang, H., Vernot, B*., et al.* (2012). The accessible chromatin landscape of the human genome. *489*, 75-82.

Toll, L., Bruchas, M.R., Calo, G., Cox, B.M., and Zaveri, N.T. (2016). Nociceptin/Orphanin FQ Receptor Structure, Signaling, Ligands, Functions, and Interactions with Opioid Systems. *68*, 419-457.

Trott, A.J., and Menet, J.S. (2018). Regulation of circadian clock transcriptional output by CLOCK:BMAL1. PLOS Genetics *14*, e1007156.

Tung, Y.C.L., Rimmington, D., O'Rahilly, S., and Coll, A.P. (2007). Pro-Opiomelanocortin Modulates the Thermogenic and Physical Activity Responses to High-Fat Feeding and Markedly Influences Dietary Fat Preference. *148*, 5331-5338.

Turek, F.W., Joshu, C., Kohsaka, A., Lin, E., Ivanova, G., McDearmon, E., Laposky, A., Losee-Olson, S., Easton, A., Jensen, D.R.*, et al.* (2005). Obesity and metabolic syndrome in circadian Clock mutant mice. Science *308*, 1043-1045.

Venkatesh, S., and Workman, J.L. (2015). Histone exchange, chromatin structure and the regulation of transcription. Nature Reviews Molecular Cell Biology *16*, 178-189.

Wang, N., Yang, G., Jia, Z., Zhang, H., Aoyagi, T., Soodvilai, S., Symons, J.D., Schnermann, J.B., Gonzalez, F.J., Litwin, S.E.*, et al.* (2008). Vascular PPARgamma controls circadian variation in blood pressure and heart rate through Bmal1. Cell Metab *8*, 482-491.

Wendt, K.S., Yoshida, K., Itoh, T., Bando, M., Koch, B., Schirghuber, E., Tsutsumi, S., Nagae, G., Ishihara, K., Mishiro, T.*, et al.* (2008). Cohesin mediates transcriptional insulation by CCCTC-binding factor. Nature *451*, 796-801.

Xie, Z., Su, W., Liu, S., Zhao, G., Esser, K., Schroder, E.A., Lefta, M., Stauss, H.M., Guo, Z., and Gong, M.C. (2015). Smooth-muscle BMAL1 participates in blood pressure circadian rhythm regulation. J Clin Invest *125*, 324-336.

Yang, G., Chen, L., Grant, G.R., Paschos, G., Song, W.L., Musiek, E.S., Lee, V., McLoughlin, S.C., Grosser, T., Cotsarelis, G.*, et al.* (2016). Timing of expression of the core clock gene Bmal1 influences its effects on aging and survival. *8*, 324ra316-324ra316.

Yang, S., Liu, A., Weidenhammer, A., Cooksey, R.C., McClain, D., Kim, M.K., Aguilera, G., Abel, E.D., and Chung, J.H. (2009). The role of mPer2 clock gene in glucocorticoid and feeding rhythms. Endocrinology *150*, 2153-2160.

Yeung, J., Mermet, J., Jouffe, C., Marquis, J., Charpagne, A., Gachon, F., and Naef, F. (2018). Transcription factor activity rhythms and tissue-specific chromatin interactions explain circadian gene expression across organs. Genome Res *28*, 182-191.

Yoshitane, H., Ozaki, H., Terajima, H., Du, N.H., Suzuki, Y., Fujimori, T., Kosaka, N., Shimba, S., Sugano, S., Takagi, T.*, et al.* (2014). CLOCK-controlled polyphonic regulation of circadian rhythms through canonical and noncanonical E-boxes. Mol Cell Biol *34*, 1776-1787.

Yu, M., Yang, W., Ni, T., Tang, Z., Nakadai, T., Zhu, J., and Roeder, R.G. (2015). RNA polymerase II-associated factor 1 regulates the release and phosphorylation of paused RNA polymerase II. *350*, 1383-1386.

Yue, F., Cheng, Y., Breschi, A., Vierstra, J., Wu, W., Ryba, T., Sandstrom, R., Ma, Z., Davis, C., Pope, B.D.*, et al.* (2014). A comparative encyclopedia of DNA elements in the mouse genome. Nature *515*, 355-364.

Zaret, K.S., and Carroll, J.S. (2011). Pioneer transcription factors: establishing competence for gene expression. Genes Dev *25*, 2227-2241.

Zhang, R., Lahens, N.F., Ballance, H.I., Hughes, M.E., and Hogenesch, J.B. (2014). A circadian gene expression atlas in mammals: implications for biology and medicine. Proc Natl Acad Sci U S A *111*, 16219-16224.

CHAPTER II

TISSUE-SPECIFIC BMAL1 CISTROMES REVEAL THAT RHYTHMIC TRANSCRIPTION IS ASSOCIATED RHYTHMIC ENHNACER-ENHANCER INTERACTIONS

2.1 Overview

The mammalian circadian clock relies on the transcription factor CLOCK:BMAL1 to coordinate the rhythmic expression of thousands of genes. Consistent with the various biological functions under clock control, rhythmic gene expression is tissue-specific despite an identical clockwork mechanism in every cell. Here we show that BMAL1 DNA binding is largely tissue-specific, likely because of differences in chromatin accessibility between tissues and co-binding of tissue-specific transcription factors. Our results also indicate that BMAL1 ability to drive tissue-specific rhythmic transcription is not only associated with the activity of BMAL1 bound enhancers, but also with the activity of neighboring enhancers. Characterization of physical interactions between BMAL1 enhancers and other cis-regulatory regions by RNA polymerase II ChIA-PET reveals that rhythmic BMAL1 target gene expression correlates with rhythmic chromatin interactions. These data thus support that much of BMAL1 target gene transcription depends on BMAL1 capacity to rhythmically regulate a network of enhancers.

2.2 Introduction

Circadian clocks are found ubiquitously across all kingdoms of life and provide a time-keeping mechanism for organisms to anticipate rhythmic environmental changes. In mammals, virtually every cell harbors the same circadian clockwork that regulates rhythmic gene expression along with temporal cues and systemic signals, such that biological functions occur at the most appropriate time of day. The mammalian circadian clock relies on transcriptional feedback loops initiated by the heterodimeric transcription factor CLOCK:BMAL1 (Partch et al., 2014; Takahashi, 2016). CLOCK:BMAL1 rhythmically binds DNA to drive the rhythmic transcription of the genes *Period* (*Per1*, *Per2*, *Per3*) and *Cryptochrome* (*Cry1* and *Cry2*), which upon translation form a repressive complex that feedbacks to inhibit CLOCK:BMAL1-mediated transcription. CLOCK:BMAL1 binds to E-boxes and activates transcription more potently during the middle of the day, and maximal repression occurs during the middle of the night (Koike et al., 2012; Rey et al., 2011). CLOCK:BMAL1 is also responsible for the transcriptional regulation of many clock controlled genes, which allows for rhythms in biochemistry, physiology, and behavior (Panda, 2016).

Characterization of the rhythmic transcriptional outputs driven by the circadian clock indicates that genes expressed in a rhythmic manner vary greatly between tissues in the mouse (Panda et al., 2002; Storch et al., 2002; Zhang et al., 2014). Similar findings in plants, insects, and primates also revealed that circadian gene expression is largely tissue-specific (Endo et al., 2014; Meireles-Filho et al., 2014; Mure et al., 2018a). However, it is still unknown how the same circadian clock mechanism can generate tissue-specific rhythmic gene expression. Previous work in *Drosophila* revealed that

CLOCK:CYC, the CLOCK:BMAL1 homolog, exhibits tissue-specific DNA binding between the body and head, and that much of this tissue-specificity is due to the co-operation between CLOCK:CYC and tissue-specific transcription factors (TFs) (Meireles-Filho et al., 2014). Tissue-specific binding of another mammalian clock component, *Rev-erbα*, has also been described, but the underlying mechanisms have not yet been characterized (Zhang et al., 2015).

To address the mechanisms by which the mammalian circadian clock generates tissue-specific circadian transcriptional programs, we performed BMAL1 chromatin immunoprecipitation at the genome wide level (ChIP-Seq) in the mouse liver, kidney, and heart. Our data revealed that the majority of BMAL1 DNA binding is tissue-specific, and suggest that accessibility of the chromatin (as defined by DNase I hypersensitive sites or DHSs; Thurman et al., 2012b) and co-binding of tissue-specific TFs (ts-TFs) account for much of this tissue-specificity. In addition, we found large discrepancies between BMAL1 DNA binding and rhythmic gene expression with, for example, many genes targeted by BMAL1 in all three tissues only exhibiting rhythmicity in a single tissue. Characterization of the underlying mechanism suggests that the ability of BMAL1 to drive tissue-specific rhythmic gene expression depends not only on how BMAL1 promotes the activity of the DHSs it binds to, but also of other neighboring DHSs. Together, our data suggest that BMAL1 transcriptional output is controlled through enhancer-enhancer interactions, and that BMAL1-driven rhythmic transcription depends on the capacity of BMAL1 to rhythmically regulate a network of DHSs.

Figure 5. BMAL1 binds rhythmically and the cistromes are largely tissue-specific.

(A)BMAL1 ChIP-qPCR signal at *Dbp* 1st intron over the course of the day in the mouse liver (blue), kidney (green), and heart (red). Tissues were collected in wild-type mice at ZT2, ZT6, ZT10, ZT14, ZT18, and ZT22, and in *Bmal1* knockout mice at ZT6 for negative control. ChIP-qPCR signal normalized to the input signal corresponds to the average ± s.e.m. of 3 biological replicates, and the ratio ChIP/input was set to 1 for the *Bmal1* knockout mice samples. **(B)** Genome browser view of BMAL1 ChIP-Seq signal in the liver (blue), kidney (green), and heart (red) at *Slc35a6* and *Gys2* gene loci. BMAL1 ChIP-Seq signal is tissue-specific, with kidney-specific BMAL1 binding at *Slc35a6*, and liver-specific BMAL1 signal at *Gys2*.

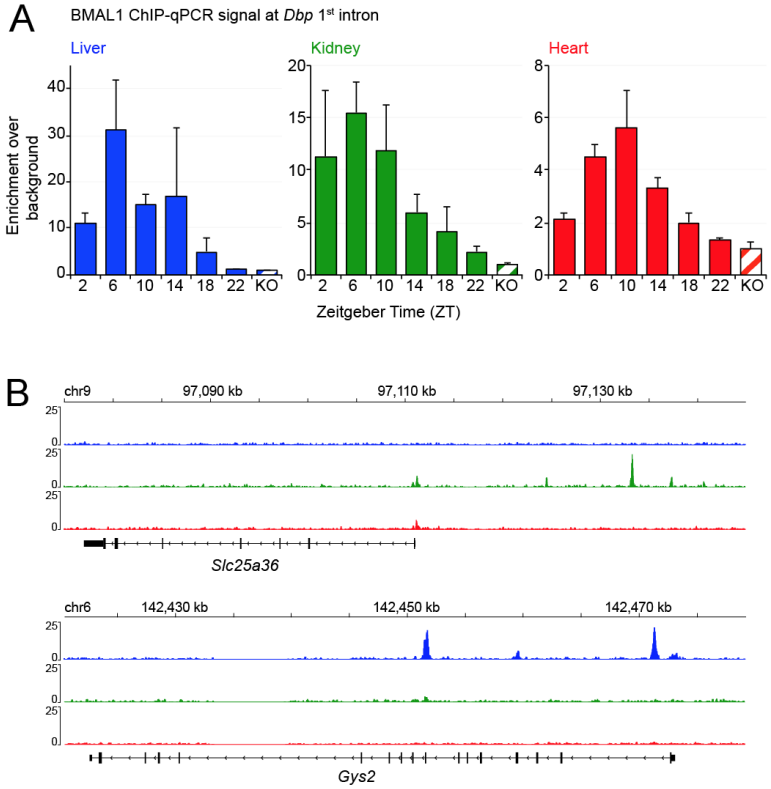

2.3 Results

2.3.1 BMAL1 DNA binding signal is largely tissue-specific

To determine if BMAL1 cistrome differs between tissues, we performed BMAL1 ChIP-Seq in the mouse liver, kidney and heart with three biological replicates per tissue. Because CLOCK:BMAL1 DNA binding sites in the liver are virtually identical over the light on signal). Identification of BMAL1 DNA binding sites using HOMER software (Heinz et al., 2010) revealed that most BMAL1 peaks were tissue-specific, with less

than 6% of BMAL1 peaks common to the liver, kidney and heart (Fig. 6A, B). Closer inspection revealed that tissue-specific BMAL1peaks were more often associated with BMAL1 signal below peak detection threshold in the other tissues rather than a complete absence of signal (Fig. 6B; 51B; see below). In addition, quantification of BMAL1 ChIP-Seq signal revealed that stronger BMAL1 binding is associated with peaks common to more than one tissue (Fig. 6C; see below).

To ensure that differences in BMAL1 ChIP-Seq signal between tissues represent true biological variation, we compared BMAL1 ChIP-Seq signal between each of the nine datasets and found a high degree of correlation between samples originating from the same tissue, but not between tissues (Fig. 6D). Inter-replicates variation between replicates was higher for the kidney than for the liver and heart; however, this might reflect the higher cell-type heterogeneity and the variability in the chromatin accessibility landscape that are observed in the kidney when compared to the heart and liver (Cusanovich et al., 2018). We also found that BMAL1 ChIP-Seq signal at core clock genes is nearly identical between all three tissues, further indicating that differences in BMAL1 binding signal between tissues stem from biological variations (Fig. 6E). Consistent with this finding, gene ontology analysis of BMAL1 target genes for each tissue revealed that while circadian rhythm and other general terms are enriched in all three tissues, tissue-specific biological processes are enriched in a tissue-specific manner (Fig. 6F). Many of these tissue-specific processes have been shown to be regulated by the circadian clock, such as glycogen synthesis, lipid metabolism and

Figure 6. BMAL1 cistromes are largely tissue-specific.
(A) Overlap of BMAL1 ChIP-Seq peaks in the mouse liver, kidney, and heart. **(B)** BMAL1 ChIP-Seq signal at BMAL1 peak center ± 2kb in the mouse liver, kidney, and heart, and parsed based on tissues in which BMAL1 peaks were detected. Group1: peaks common to all three tissues; group 2: peaks common to the liver and kidney; group 3: peaks common to the liver and heart; group 4: peaks common to the kidney and heart; group 5: liver-specific peaks, group 6: kidney-specific peaks; group 7: heart-specific peaks. **(C)** BMAL1 ChIP-Seq signal calculated at peak center ± 250 bp in the mouse liver, kidney, and heart. Groups with different letters are statistically different (Kruskal-Wallis test ; $p < 0.05$). **(D)** Spearman correlation coefficients of BMAL1 ChIP-Seq signal between each biological replicate (n = 3 per tissue) calculated at all 9,006 BMAL1 ChIP-Seq peaks. **(E)** Genome browser view of BMAL1 ChIP-Seq signal at *Nr1d1* and *Per1* gene loci. **(F)** Gene ontology analysis performed using BMAL1 peaks detected in the liver, kidney, or heart, and reporting functions enriched across the three tissues or in only one tissue (p-value < 0.05).

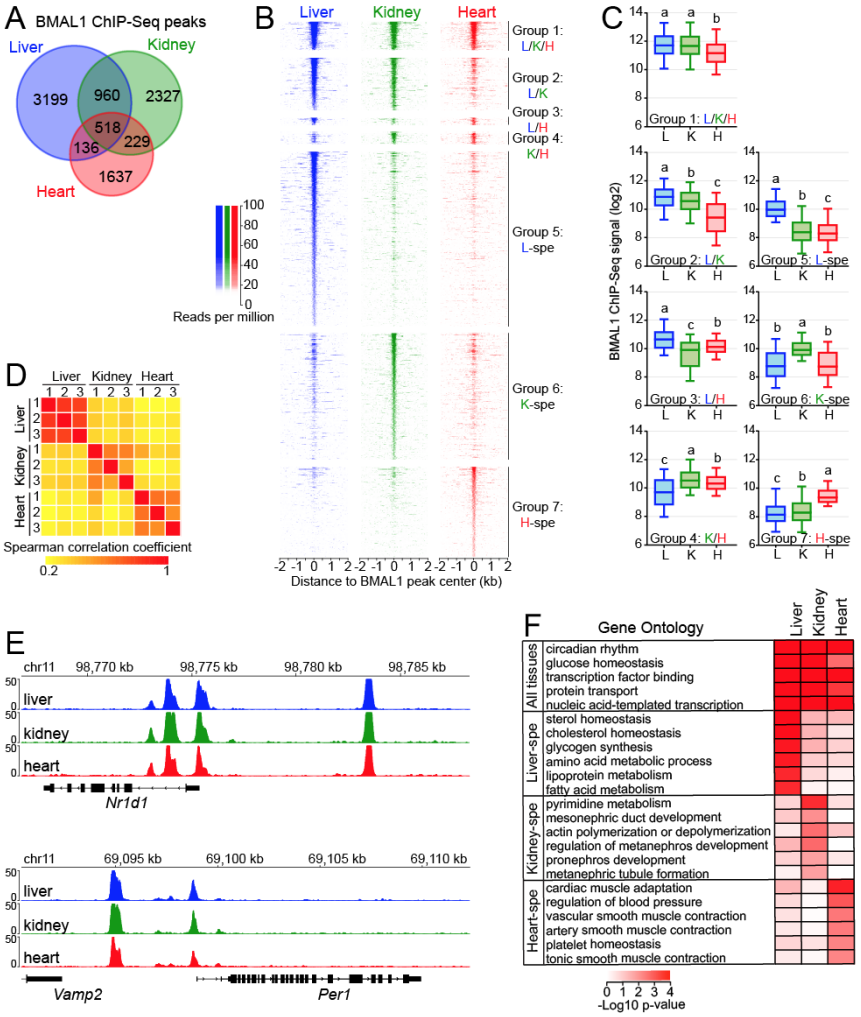

cholesterol homeostasis in the liver (Doi et al., 2010; Gnocchi et al., 2015b; Ma et al., 2015), and blood pressure and vascular smooth muscle contraction in the heart (Wang

et al., 2008; Xie et al., 2015). Together, these results indicate that BMAL1 predominantly binds DNA in a tissue-specific manner, and targets genes involved in the regulation of tissue-specific biological functions.

2.3.2 Chromatin accessibility contributes to tissue-specific BMAL1 DNA binding

To understand the large differences in BMAL1 ChIP-Seq signal between tissues, we set out to define the mechanisms that enable BMAL1 to bind DNA in a tissue-specific manner. Characterization of the chromatin landscape by the ENCODE consortium and others revealed that 94.4% of transcription factor (TF) ChIP-Seq peaks are located in an accessible chromatin region, *i.e*., a region that is hypersensitive to DNase I (Thurman et al., 2012b; Yue et al., 2014b). Because mouse liver CLOCK:BMAL1 DNA binding sites are predominantly located in DHSs (Sobel et al., 2017b; Trott and Menet, 2018b), we hypothesized that tissue-specific BMAL1 binding may be, at least in part, caused by differences in DNA accessibility between the liver, kidney and heart. To test our hypothesis, we used DNase-Seq datasets from the mouse ENCODE project (Vierstra et al., 2014; Yue et al., 2014b) and found that many tissue-specific BMAL1 peaks are located in a chromatin region that is only accessible in the corresponding tissue (Fig. 7A). Quantification of DNase-Seq signal at liver-, kidney-, and heart-specific BMAL1 peaks (named group 5, 6, and 7 hereafter, respectively) confirmed that tissue-specific BMAL1 peaks are associated with higher DNase-Seq signal (Fig. 7B). However, some DNase-Seq signal could be detected above background level in all three tissues, suggesting

Figure 7. The chromatin environment shapes tissue-specific BMAL1 binding.
(A) Genome browser view of BMAL1 ChIP-seq and DNase-seq signals in the mouse liver, kidney, and heart at twelve BMAL1 tissue-specific peaks. **(B)** DNase-seq signal calculated at BMAL1 peak center ± 250 bp in the mouse liver, kidney, and heart for tissue-specific BMAL1 peaks. Groups with different letters are statistically different (Kruskal-Wallis test; $p < 0.05$). **(C)** BMAL1 ChIP-seq, DNase-seq, and H3K27ac ChIP-seq signal at liver specific BMAL1 peaks, parsed based on the presence of a DNase I hypersensitive sites (DHS) peak in the liver, kidney, and heart. BMAL1 ChIP-seq and DNase-seq signals are displayed with a window of ± 2kb, whereas H3K27ac ChIP-seq signal is displayed with a window of ± 5kb. **(D-F)** Quantification of DNase-seq (D), BMAL1 ChIP-Seq (E), and H3K27ac ChIP-Seq (F) signals for liver specific BMAL1 peaks located at (top, group 5A) liver specific DHS or (bottom, group 5B) DHS peaks common to the liver, kidney and heart. Groups with different letters are statistically different (Kruskal-Wallis test; $p < 0.05$). Letters u-z denotes the outcome of the statistical analysis performed using groups 5A and 5B together.

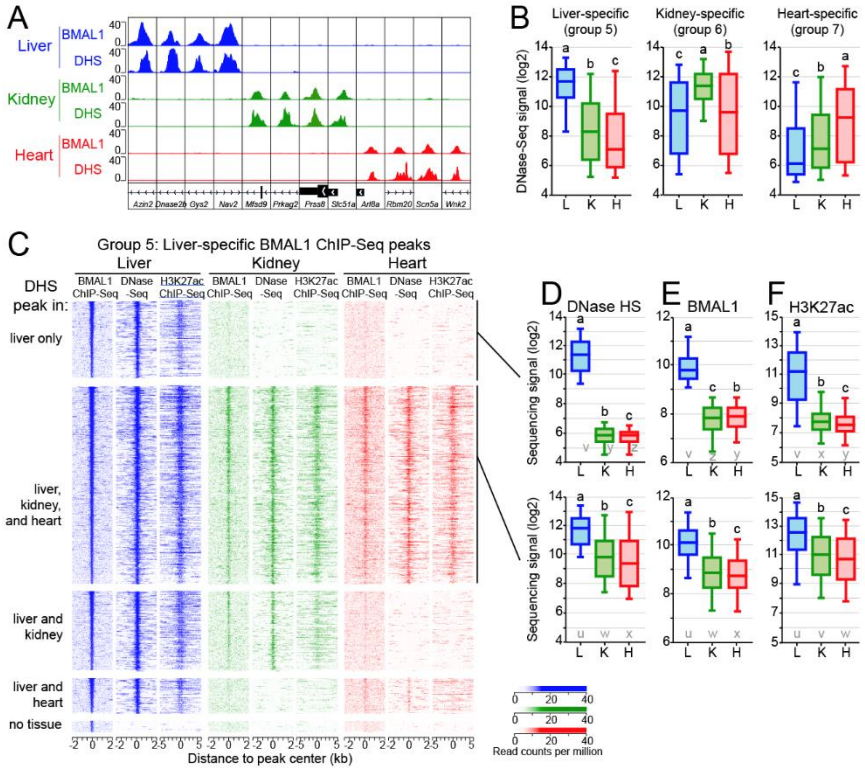

that tissue-specific BMAL1 peaks may not be always associated with a complete absence of DNase-Seq signal in other tissues.

To investigate if tissue-specific BMAL1 binding occurs at DHSs common to several tissues, we mapped the genomic location of DHSs in the liver, kidney and heart

(Fig. 8A), and determined the fraction of tissue-specific BMAL1 peaks found at tissue-specific DHSs or at DHSs common to more than one tissue, focusing primarily on liver-specific BMAL1 peaks. As expected, almost all mouse liver BMAL1 peaks (97.7%) are located in chromatin regions that are accessible in the mouse liver (Fig. 7C). However, only ~20% of liver-specific BMAL1 peaks are located at a liver-specific DHSs, *i.e*., most liver-specific BMAL1 peaks are located within chromatin regions that are also accessible in other tissues (Fig. 7C). Importantly, we found that while no BMAL1 signal is detectable in the kidney and heart at liver-specific DHSs, some BMAL1 signal is visible at common DHSs even if it is not defined as significant BMAL1 peaks by HOMER (Fig. 7C-E). Similar results were observed for kidney- and heart-specific BMAL1 peaks (Fig. 8B, C). Because DNase I hypersensitivity does not assess the activity of accessible chromatin regions, we also analyzed public ChIP-Seq datasets for histone modifications found at transcriptionally active/primed DHSs, *i.e*, acetylated lysine 27 of histone 3 (H3K27ac) and monomethylated lysine 4 of histone 3 (H3K4me1). Remarkably, both H3K27ac and H3K4me1 ChIP-Seq signals mirrored the DNase-Seq signal and were detected in particular at kidney and heart DHSs exhibiting liver-specific BMAL1 peaks (Fig. 7C, 7F, 8D).

Figure 8. The chromatin environment shapes tissue-specific BMAL1 binding.
(A) Venn diagram depicting the overlap of DNase hypersensitive sites (DHSs) between the mouse liver, kidney, and heart. DNase-Seq datasets were downloaded from the ENCODE project, and analyzed to define DHSs in each of the three tissues. Of the total 427,748 DHSs among the mouse liver, kidney, and heart, 100,009 are common to all three tissues. **(B)** H3K4me1 ChIP-seq signal (log2 scale) in the mouse liver, kidney, and heart at liver-specific BMAL1 peaks located in liver-specific DHSs (top), or at liver-specific BMAL1 peaks located at DHSs common to the liver, kidney and heart. H3k4me1 ChIP-Seq datasets were downloaded from the ENCODE project, and signal was calculated at BMAL1 peak center ± 1kb. **(C)** Left: Stacked bar chart representation of the percentage of kidney-specific BMAL1 peaks located within kidney-specific DHSs or DHSs found in other tissues. Right: Boxplot representation of BMAL1 ChIP-seq, DNase-seq, H3K27ac ChIP-seq and H3K4me1 ChIP-seq signals at kidney-specific BMAL1 peaks located at a kidney-specific DHSs or at a DHSs common to the liver, kidney and heart. Signal for BMAL1 ChIP-seq and DNase-seq was calculated at BMAL1 peak center ± 250 bp, and at BMAL1 peak center ± 500 bp for ChIP-seq of histone modifications. **(D)** Similar to panel C, but for heart-specific BMAL1 peaks.

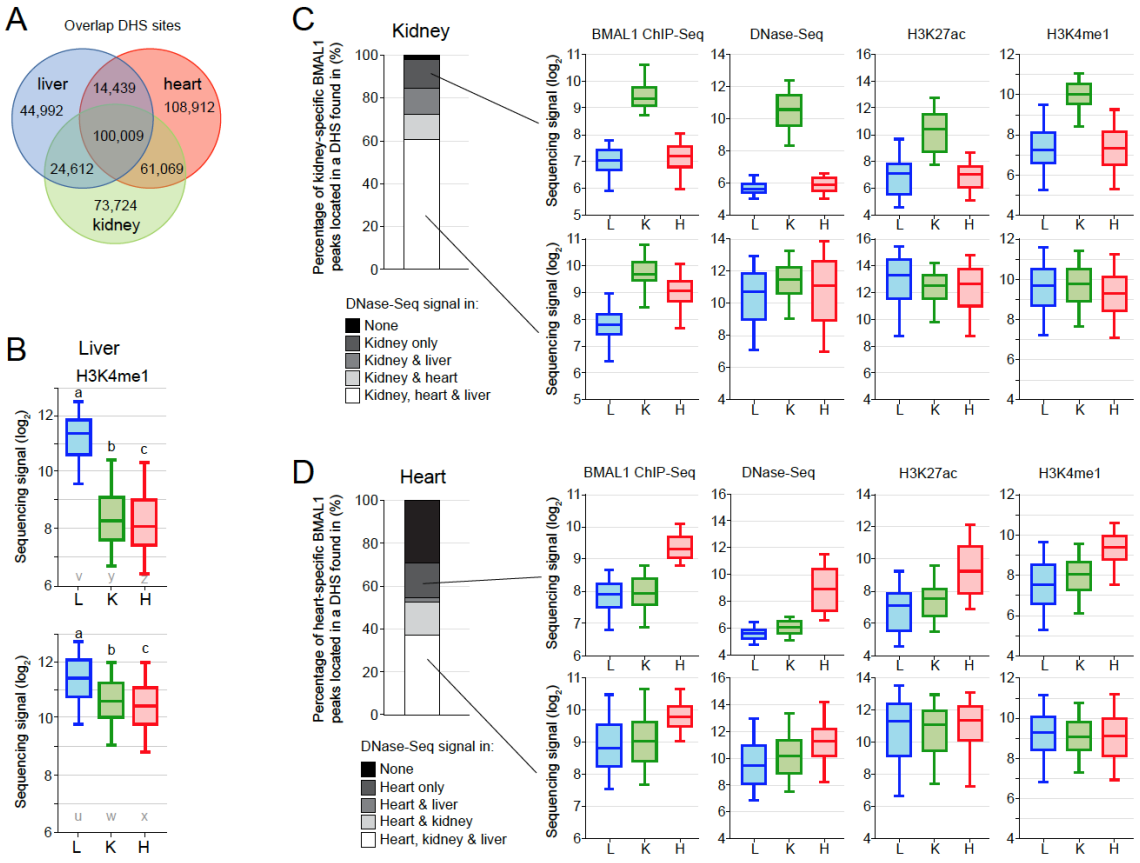

In summary, our data indicate that only a minority of BMAL1 binding sites are located at tissue-specific DHSs. For most tissue-specific BMAL1 peaks, chromatin is

accessible in other tissues and harbors histone modifications that mark transcriptionally active DHSs, albeit to lower levels. Importantly, some BMAL1 DNA binding can be detected at those sites, although at levels too low to be categorized as ChIP-Seq peaks by peak-calling algorithms.

2.3.3 Tissue-specific BMAL1 peaks are enriched for tissue-specific transcription factor DNA binding motifs

Several mechanisms may contribute to tissue-specific BMAL1 binding. First, BMAL1 DNA binding may only rely on the presence of its binding motif in an accessible DHS. Under this scenario, BMAL1 binding signal would correlate with DNase-Seq signal, and differences between tissues would mostly depend on the proportion of cells harboring an accessible DHS and/or the extent to which the DHS is accessible. Alternatively, tissue-specific BMAL1 binding may be, as suggested for some other TFs (Gertz et al., 2013; Hu and Gallo, 2010; Meireles-Filho et al., 2014), facilitated by tissue-specific TFs (ts-TFs) that bind at sites nearby BMAL1. Here, BMAL1 DNA binding signal would not correlate well with DNase-Seq signal, and motifs for ts-TFs would be enriched at tissue-specific BMAL1 peaks.

To assess if either or both of these mechanisms promote tissue-specific BMAL1 binding, we first compared BMAL1 ChIP-Seq signal with DNase-Seq signal at liver-, kidney-, and heart-specific BMAL1 peaks, and found that both signals were correlated in the heart, but not in the liver and kidney (Fig. 9A). Differences in BMAL1 ChIP-Seq signal of more than 16-fold are detected at liver DHSs displaying similar DNase-Seq signals, and similar BMAL1 ChIP-Seq signals were observed at DHSs harboring

Figure 9. Motifs and footprints for tissue-specific transcription factors are enriched at tissue-specific BMAL1 enhancers.
(A) Correlation between DNase-seq and BMAL1 ChIP-seq signals (calculated at BMAL1 peak center ± 250 bp) at liver-, kidney-, and heart-specific BMAL1 peaks. **(B)** Correlation between DNase-seq and BMAL1 ChIP-seq signal for liver specific BMAL1 peaks harboring one E-box only. **(C)** Enrichment of TF motifs at liver-, kidney-, and heart-specific BMAL1 peaks, performed using HOMER at BMAL1 peak center ± 100 bp. Enrichments are shown if q-value < 0.05. **(D)** Fold-enrichment of TF motif over background at tissue-specific BMAL1 peaks (BMAL1 peak center ± 100 bp; q-value <0.05). **(E)** mRNA expression in the mouse liver, kidney, and heart of *Bmal1* and TFs whose motifs were enriched at BMAL1 ChIP-Seq peaks. (RNA-Seq datasets from Zhang et al., 2014). Groups with different letters are significantly different (one-way ANOVA; p-value <0.05). **(F)** Distribution of DNase I footprints identified using pyDNase and detected at BMAL1 peak center ± 100 bp, and parsed based on the tissue(s) they were found in. **(G)** Motif enrichment of TFs performed at DNase I footprints identified in liver-, kidney-, and heart-specific BMAL1 peaks (footprint center ± 15 bp). Enrichments are displayed if q-value < 0.05, and colored in grey if no significant footprint is detected in any of the three tissues. **(H)** Heatmap representing DNase I cuts at BMAL1 peaks containing an E-box and an HNF6 motif (top) or a CEBP (bottom). DNase I cut signal is centered on the E-box and sorted based on the distance between the E-box and the liver-specific TF motif. **(I)** Quantification of DNase I cut signal at BMAL1 peaks containing an E-box and an HNF6 motif (top) or a CEBP (bottom) in the liver of wild-type (left) or *Bmal1*$^{-/-}$ (right) mice. Quantification was performed using signal centered on E-boxes (left) or on the ts-TF motif (middle). As control, quantification was also performed at HNF6 or CEBPA peaks that do not harbor a BMAL1 ChIP-Seq peak (right; signal corresponds to the average of 1,000 decile-normalized iterations).

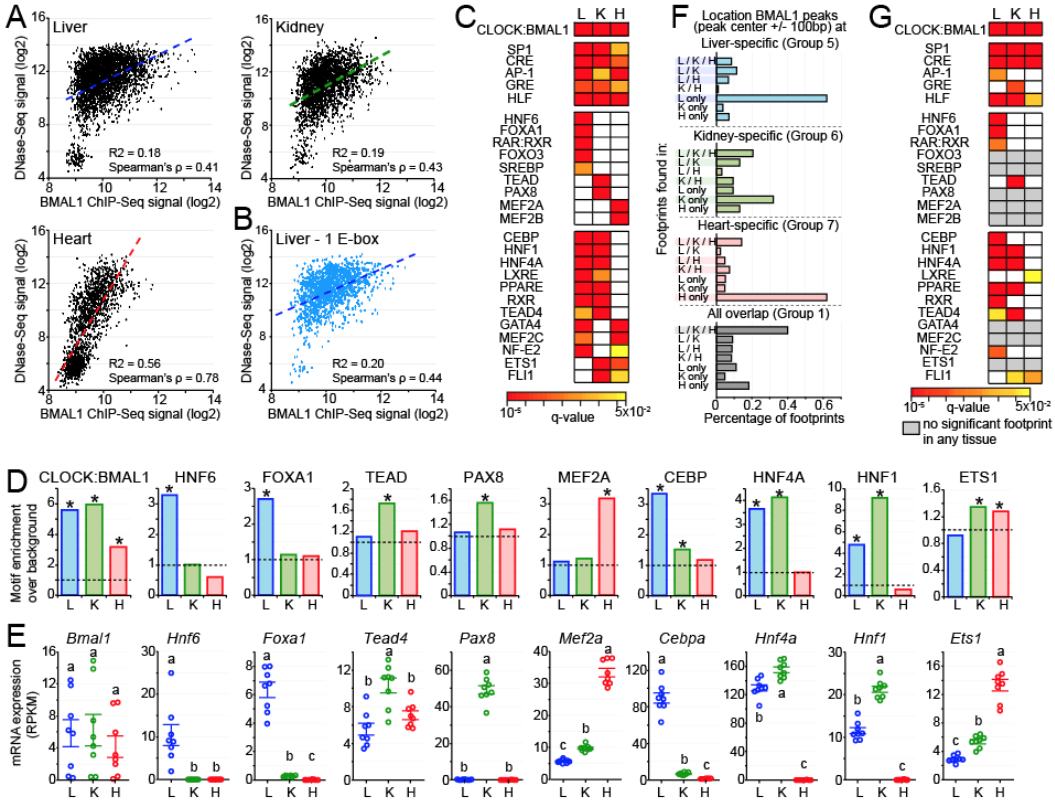

Figure 9 Continued.

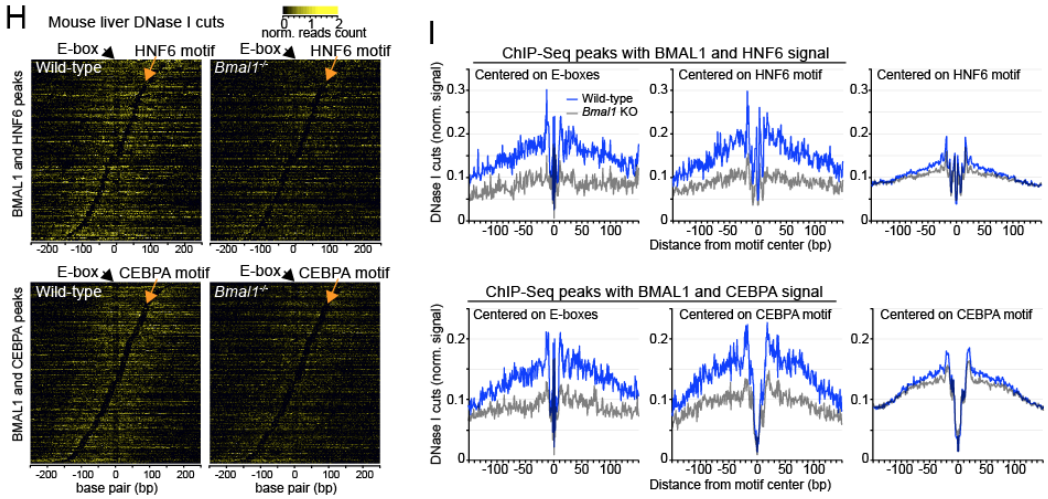

differences of DNase-Seq signal of more than 30-fold in both liver and kidney (Fig. 3A). Importantly, these differences are independent of the number of E-boxes within each DHS (Fig. 9B, 10A). These results thus indicate that, at least for the liver and kidney, the extent to which the chromatin is accessible cannot solely explain the differences in tissue-specific BMAL1 binding.

To determine if ts-TFs may be involved, we performed a motif enrichment analysis at tissue-specific BMAL1 peaks using HOMER. As expected, E-boxes are enriched at tissue-specific BMAL1 peaks for all three tissues, along with a few additional motifs for ubiquitously expressed TFs (u-TFs) (Fig. 9C, 9D). However, the majority of the motifs were significantly enriched in only one or two tissues, with many of them corresponding to binding sites of well-known ts-TFs like *Foxa1* and *Mef2a/b* (Fig 9C, 9D). To verify that these TFs are legitimate ts-TFs, we analyzed their levels of expression in the liver, kidney and heart using public mouse RNA-Seq datasets (Zhang et al., 2014) and the Genotype-Tissue Expression (GTEx) portal for human tissues

(Consortium, 2013). For almost all of the >20 TFs we examined, mRNA levels were specific to one or two tissues, confirming that these TFs are true ts-TFs (Fig 9E, 10B, 10C). Importantly, the tissue-specific pattern of expression matched particularly well with the tissue-specificity of the motif enrichment, suggesting that these TFs bind DNA in a tissue-specific.

Figure 10. Tissue-specific transcription factors may contribute to tissue-specific BMAL1 DNA binding.

(A) Correlation between DNase-seq signal and BMAL1 ChIP-seq signal for liver- (blue), kidney- (green) and heart- (red) specific BMAL1 peaks parsed based on the number of E-boxes. The E-boxes used in the analysis were CACGTG, CACGNG, and CACGTT. BMAL1 ChIP-seq signal and DNase-seq signal, which are represented in log2 scale, were calculated at BMAL1 peak center ± 250 bp. **(B)** mRNA expression in the mouse liver, kidney, and heart of *Bmal1* and transcription factors whose motifs were enriched at BMAL1 ChIP-Seq peaks. mRNA expression was calculated using public RNA-Seq datasets (Zhang et al., 2014) from samples collected over the course of the 24-hr day. **(C)** mRNA expression (RPKM) in human liver (blue), kidney (green), and heart (red, left ventricle and atrial appendage) for the tissue-specific transcription factors displayed in Fig. 9C, D, and E. Data were retrieved from the GTEx portal (https://www.gtexportal.org/home/) (Consortium, 2013). **(D)** Illustration of the DNase-Seq protocol, and the analysis of DNase I cuts that reveal footprints at DNase I hypersensitive sites (DHSs). Mild DNase I digestion of nuclei preserves closed chromatin and transcription factors/nucleosomes-bound regions from DNase I cutting. Thus, mapping regions uncut by DNase I at DHSs can reveal regions that are occupied by transcription factors and/or nucleosomes. **(E)** Genome browser view of DNase-seq signal, footprints p-value, DNase I cut sites, and BMAL1 ChIP-seq signal in the mouse liver (blue), kidney (green), and heart (red) at two BMAL1 DNA binding sites. DNase-Seq datasets were downloaded from the ENCODE project, and footprint p-value visualization files were generated using pyDNase (Piper et al., 2015; Piper et al., 2013). Mouse liver HNF6 ChIP-Seq signal, which was downloaded from a public dataset (Faure et al., 2012), is also displayed. Both BMAL1 peaks exhibit significant footprints at motifs corresponding to E-boxes, as well as to motifs for other transcription factors including the liver-specific transcription factor HNF6. **(F)** Distribution of DNase I footprints detected at the genomic coordinate of the DHSs bound by BMAL1, and parsed based on the tissue(s) they were found in. Analysis was performed at BMAL1 peaks that are liver-specific (blue), kidney-specific (green), heart-specific (red), or common to all three tissues (grey). **(G)** Motif enrichment of transcription factors performed at the DNase I footprints identified within the genomic coordinate of the DHS bound by BMAL1, for liver-, kidney-, and heart-specific BMAL1 peaks (footprint center ± 15 bp). Enrichments are displayed if q-value < 0.05, and colored in grey in no significant footprint is detected in any of the three tissues. **(G)** Heatmaps representing the DNase I cuts at BMAL1 peaks containing an E-box and a motif for another transcription factor. DNase I cut signal is centered on the E-box and sorted based on the distance between the E-box and the transcription factor motif. Scale corresponds to E-box center ± 250bp.

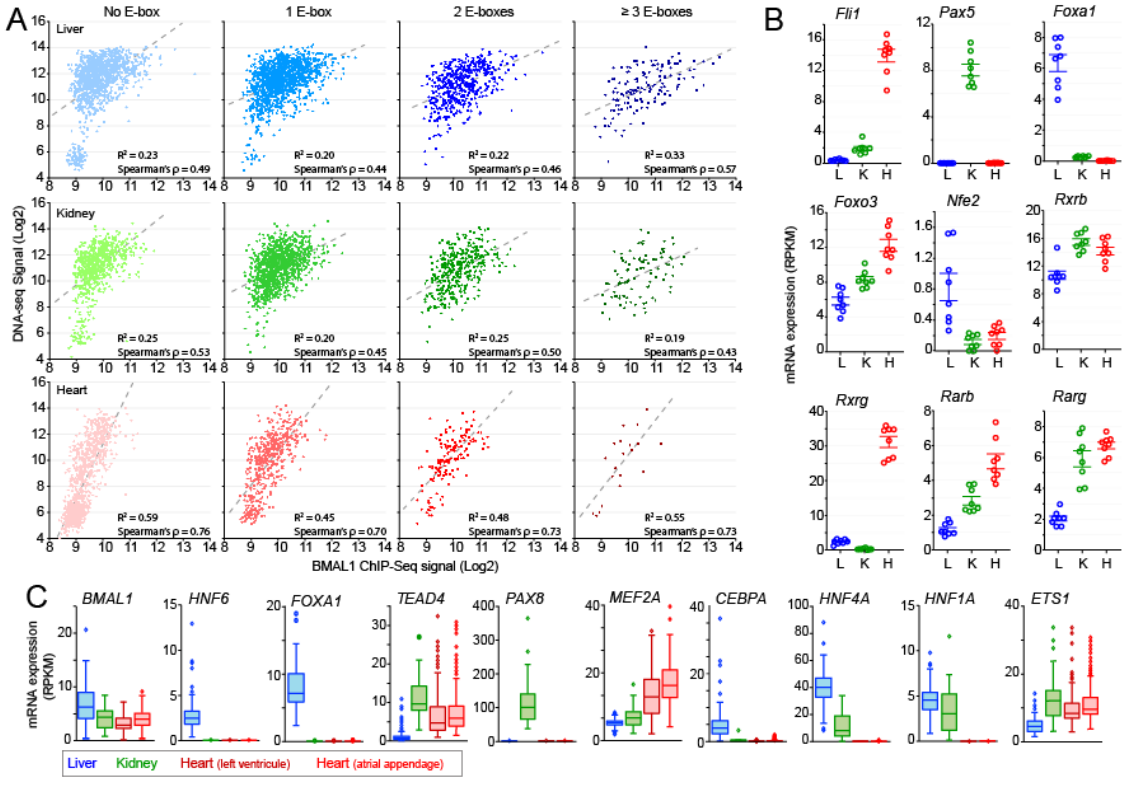

Figure 10 Continued.

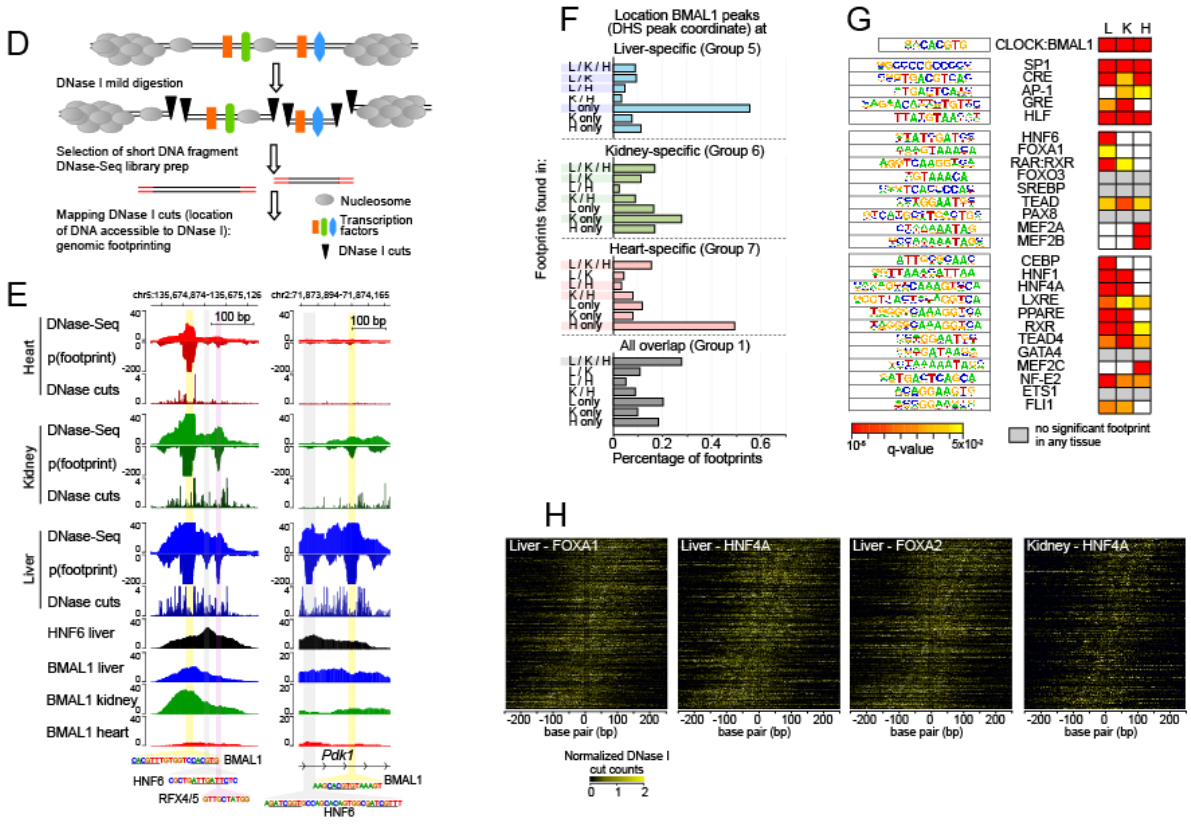

2.3.4 Genomic footprints for tissue-specific transcription factor are specifically enriched at tissue-specific BMAL1 peaks

The concordance between ts-TF motif enrichment and expression pattern (Fig. 9C-E, 10B, 10C) does not directly show that ts-TFs bind at BMAL1 DHSs in a tissue-specific manner. To further investigate this possibility, we took advantage of the genomic footprints left by chromatin-associated proteins following treatment with DNase I (Hesselberth et al., 2009). This analysis, which has been used successfully to define the genome-wide DNA binding profiles of dozens of TFs (Neph et al., 2012; Sherwood et al., 2014; Stergachis et al., 2014), exploits DNase-Seq datasets to uncover regions

within DHSs that are protected from DNase I activity by proteins bound to DNA (Fig. 10D, 10E). To this end, we analyzed the mouse liver, kidney, and heart DNase-Seq datasets using pyDNase (Piper et al., 2015) and identified the genome-wide location of TF footprints.

This analysis revealed that most footprints found at tissue-specific BMAL1 peaks are significantly enriched in the corresponding tissue. For example, 60% of the footprints found at liver-specific and heart-specific BMAL1 peaks are only detected in the liver and heart, respectively (Fig. 9F, 10F). Conversely, a large fraction of the footprints identified at common BMAL1 peaks are detected in all three tissues (Fig. 9F, 10F). To identify the proteins generating these footprints, we performed a motif analysis restricted to the footprint genomic locations found at liver-, kidney- and heart-specific BMAL1 peaks. While motifs for CLOCK:BMAL1 and some u-TFs are enriched in all three tissues, most significantly enriched motifs correspond to ts-TFs binding sites (Fig. 9G, 10G). For example, footprints are enriched at motifs for *Hnf6*, *Foxa1*, *Cebp*, *Hnf1*, and *Hnf4a* in the mouse liver, and for *Hnf1*, *Hnf4a*, and *Tead* in the kidney. We noticed that several ts-TFs whose motifs are enriched at BMAL1 DHSs (Fig. 9C) do not exhibit a significant footprint (*e.g.*, *Foxo3*, *Srebp*, Pax8, Gata4, and Ets1; Fig. 9G), suggesting that they do not bind to BMAL1 DHSs despite of the presence of a cognate motif. However, the absence of footprints may also reflect the inability of these TFs to generate distinctive footprints because of DNA residence time and DNase I cut bias, as previously shown for a few other TFs (He et al., 2014; Sung et al., 2014).

We then examined with heatmaps DNase I cuts at BMAL1 peaks and found that DHSs exhibit footprints at E-box and motifs for ts-TFs, suggesting that ts-TFs may be

bound to DNA concurrently with CLOCK:BMAL1 (Fig. 9H, 10H). Interestingly, quantification of DNase I cut signal in wild-type *vs. Bmal1*$^{-/-}$ mice revealed that *Bmal1* knockout decreases footprint signal for the ts-TFs HNF6 and CEPBA more potently at BMAL1 peaks than at control peaks (*i.e*., HNF6 and CEPBA peaks without BMAL1 ChIP-Seq signal), suggesting that BMAL1 may increase the binding of ts-TFs at tissue-specific DHSs (Fig. 9I).

2.3.5 Tissue-specific and common BMAL1 peaks are co-bound by different classes of transcription factors

To further assess if ts-TFs may contribute to tissue-specific BMAL1 binding, we determined the relative enrichment of footprints for several ts-TFs and u-TFs at BMAL1 peaks either specific to the liver (group 5) or common to all three tissues (group 1). We found that footprints for ts-TFs were preferentially detected at liver-specific BMAL1 peaks when compared to common BMAL1 peaks (Fig. 11A, 12A). Conversely, footprints for several u-TFs were enriched at BMAL1 peaks common to all three tissues, when compared to liver-, kidney-, or heart-specific BMAL1 peaks (Fig. 11A; Fig. 12A).

Figure 11. BMAL1 DNA binding sites common to the mouse liver, kidney, and heart exhibit unique features. **(A)** Percentage of footprints for BMAL1 (black), liver-specific TFs (blue), and u-TFs (orange) identified at liver-specific BMAL1 peaks (group 5) or at BMAL1 peaks common to all three tissues (group 1). **(B)** Percentage overlap between BMAL1 peaks and ChIP-Seq peaks for various TFs and Pol II in the mouse liver. Results are parsed based on tissues in which BMAL1 peaks were detected: G1: peaks common to all three tissues; G2: peaks common to the liver and kidney; G3: peaks common to the liver and heart; G4: peaks common to the kidney and heart; G5: liver-specific peaks, G6: kidney-specific peaks; G7: heart-specific peaks. **(C)** Heatmap representation of mouse liver ChIP-Seq signal for HNF6 (dataset from Faure et al., 2012), CEBPA (dataset from Faure et al., 2012) CRY1 (CT04, dataset from Koike et al., 2012), CREB (from Everett et al., 2013), and Pol II (ZT06, dataset from Sobel et al., 2017) at BMAL1 peaks ordered based on BMAL1 ChIP-Seq signal (as in Fig. 6B) for the group 1, 2, 3, and 5. **(D)** Correlation of BMAL1 ChIP-seq signal between the mouse liver, kidney, and heart for BMAL1 peaks common to all three tissues (group 1). **(E)** BMAL1 ChIP-Seq signal for BMAL1 peaks common to all tissues parsed based on the number of E-boxes (canonical E-box CACGTG and degenerate E-boxes CACGTT and CACGNG). **(F)** Fraction of BMAL1 peaks harboring a dual E-box motif (two E-boxes separated with 6 or 7 bp). **(G)** Location of BMAL1 peaks for each of the seven groups. Statistical analysis was performed using a chi square test, and *post-hoc* analysis was performed with Fisher's exact test. Groups with different letters are statistically different ($p < 0.01$). **(H)** Nucleosome signal at BMAL1 DNA binding sites parsed based on tissues in which BMAL1 peaks were detected (group 1 to 7, see above). Nucleosome signal was retrieved from mouse liver MNase-Seq datasets (Menet et al., 2014), which consists of 6 time points each separated by 4 hours with n = 4 mice for each time point, and is displayed as the average of the 24 datasets ± s.e.m.

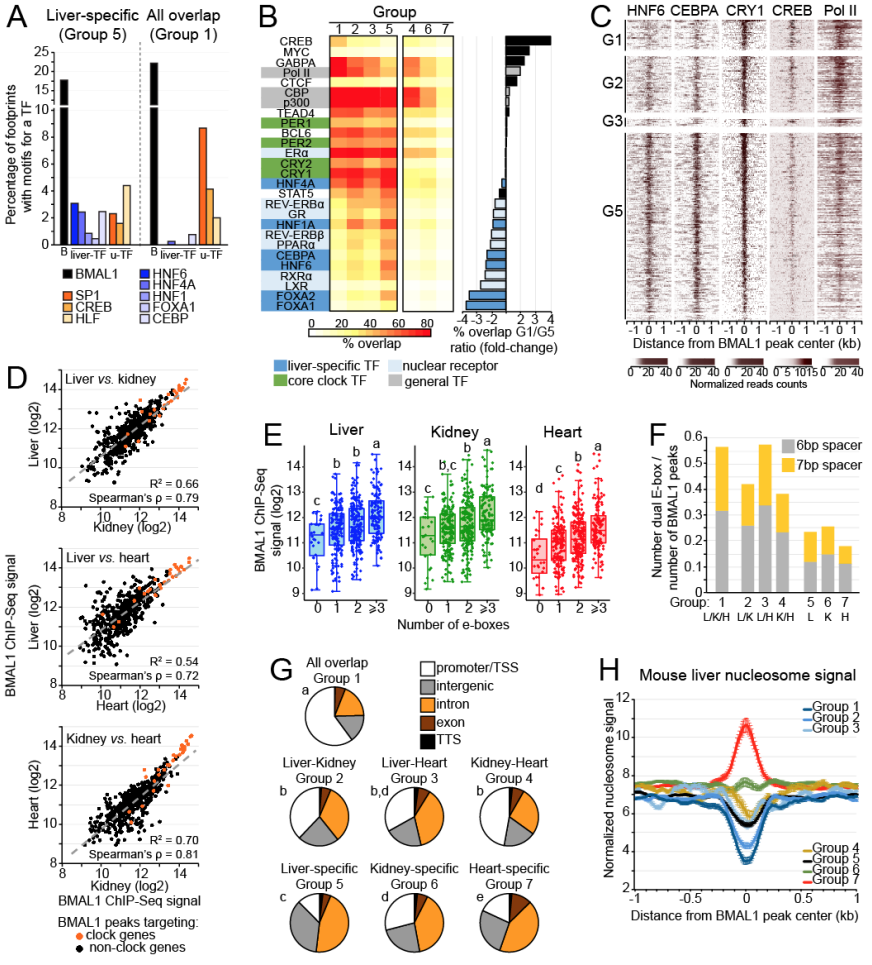

Differences in footprint enrichment between ts-TFs and u-TFs were also observed at liver-specific BMAL1 peaks based on whether DHS are liver-specific or ubiquitous, respectively (Fig. 12B). These results thus suggest that ts-TFs are more effectively recruited to tissue-specific BMAL1 peaks whereas u-TFs may be more effectively recruited to BMAL1 peaks common to different tissues.

To address this possibility more directly, we determined the relative distribution of TF ChIP-Seq peaks between tissue-specific and common BMAL1 peaks using public mouse liver ChIP-Seq datasets for more than 25 TFs. Results largely confirmed the footprint analysis, as ts-TF ChIP-Seq peaks were more potently found at liver-specific BMAL1 peaks than at peaks common to all three tissues (Fig. 11B, 11C, 12C). Moreover, ChIP-Seq peaks for RNA Polymerase II (Pol II) and the u-TFs CREB and GABPA were preferentially observed at common BMAL1 peaks. Intriguingly, we noticed that liver-specific BMAL1 peaks were also more frequently associated with ChIP-Seq for nuclear receptors (Fig. 11B, 11C). Taken together, these results thus indicate that BMAL1 peaks harbor a remarkable dissimilarity of TF bound near BMAL1, with ts-TFs and nuclear receptors being enriched at tissue-specific BMAL1 peaks while Pol II and some u-TFs being enriched at BMAL1 peaks common to different tissues.

2.3.6 BMAL1 peaks common to all three tissues exhibit stronger BMAL1 signal, harbor more E-boxes, are enriched at promoters, and display less nucleosome signal

More than 500 BMAL1 ChIP-Seq peaks targeting 294 genes are common to the liver, kidney and heart (Fig. 6A). These genes comprise all expected core clock genes and regulate biological processes that are ubiquitous to most mammalian tissues (Fig. 12D).

Figure 12. Differential binding of transcription factors between tissue-specific and common BMAL1 peaks. **(A, B)** Percentage of footprints for BMAL1 (black), liver-specific transcription factors (HNF6, HNF4A, HNF1, FOXA1, CEBP; blue), and ubiquitous transcription factors (SP1, CREB, HLF; orange) identified at (E) BMAL1 peaks common to all three tissues (group 1), BMAL1 peaks that are liver-specific (group 5), kidney-specific (group 6), and heart-specific (group 7), or at (F) liver-specific peaks that are located at a liver-specific DHS (group 5A) or located at a DHS that is common to the liver, kidney, and heart. **(C)** Heatmap representation of mouse liver ChIP-Seq signal for different transcription factors at BMAL1 peaks ordered based on BMAL1 ChIP-Seq signal (as in Fig. 6B) for the group 1 (peaks common to all three tissues), 2 (peaks common to the liver and kidney), 3 (peaks common to the liver and heart), and 5 (liver-specific peaks). ChIP-Seq datasets were retrieved from public depositories (see methods for details). **(D)** Gene ontology analysis of the genes targeted by BMAL1 peaks common to all three tissues (p-value < 0.05). **(E)** Correlation between DNase-seq and BMAL1 ChIP-seq signals for BMAL1 peaks that are common to all three tissues. Signal was calculated at BMAL1 peak center ± 250 bp in the mouse liver, kidney, and heart, and is displayed in log2 scale. **(F, G)** Enrichment for the motifs of clock genes (F) and u-TFs (G) at tissue-specific BMAL1 peaks (liver in blue, kidney in green, and heart in red) or BMAL1 peaks common to the three tissues (black). Asterisks illustrate a q-value < 0.05. **(H)** Nucleosome signal at BMAL1 DNA binding sites parsed based on tissues in which BMAL1 peaks were detected (group 1 to 7, see above). Nucleosome signal was retrieved from liver MNase-Seq datasets of wild-type and *Bmal1*$^{-/-}$ mice (Menet et al., 2014), which consists of 6 time points each separated by 4 hours with n = 4 mice for each time point, and is displayed as the average of the 24 datasets ± s.e.m.

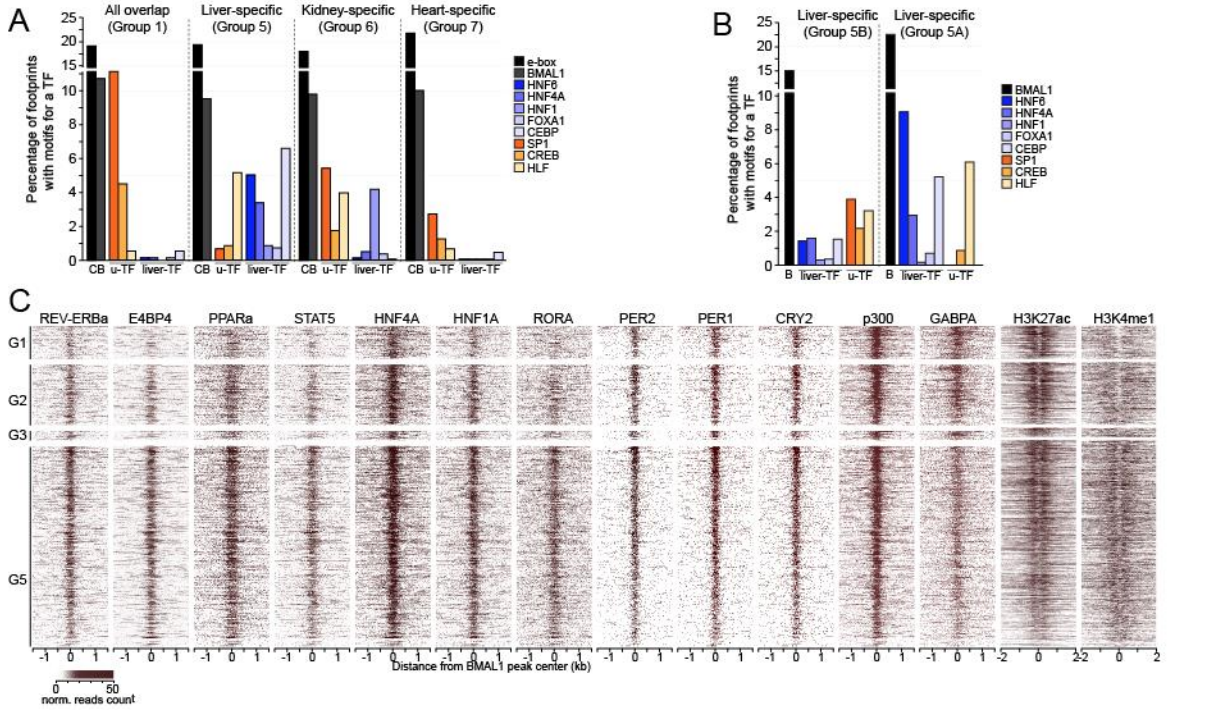

Figure 12 Continued.

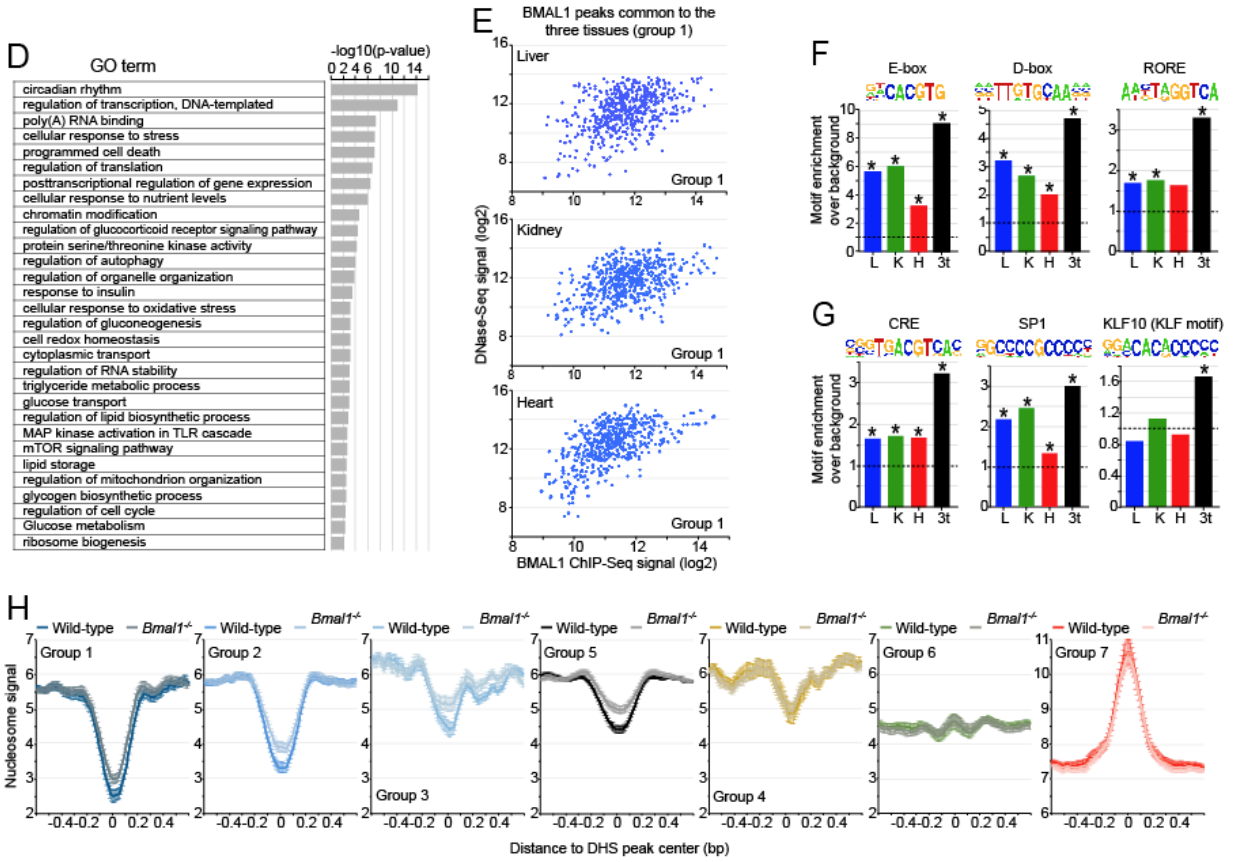

Consistent with the hypothesis that BMAL1 binding at peaks common to several tissues is less dependent on ts-TFs than tissue-specific BMAL1 peaks, we found that BMAL1 ChIP-Seq signal at common BMAL1 peaks is well correlated with DNase-Seq signal (Fig. 12E), and between tissues (Fig. 11D). Analysis of the DNA binding motifs at common BMAL1 peaks revealed that E-boxes were enriched along with motifs for the clock genes *Rev-erbα/β* and *Rorα/β/γ* (RORE) and *E4bp4*/*Dbp*/*Tef*/*Hlf* (D-box), as well as motifs for well-characterized u-TFs such as CREB, SP1 and HLF (Fig. 12F, 12G).

The reasons to why REV-ERBα/β DNA binding is lower at common BMAL1 peaks (Fig. 11B, 11C, 12C) in spite of RORE motif enrichment are unknown, but may include the recently described recruitment of REV-ERBα to DNA-bound ts-TFs like HNF6 (Zhang et al., 2015). To investigate if the higher enrichment for E-boxes at common BMAL1 peaks (Fig. 12F) may contribute to the increased BMAL1 ChIP-Seq signal at those sites (Fig. 6C), we quantified BMAL1 ChIP-Seq signal based on the number of E-boxes and found that BMAL1 signal was positively correlated with increasing number of E-boxes for all three tissues (Fig. 11E). Moreover, dual E-boxes, *i.e.* two E-box motifs separated by 6 or 7 nucleotides and which have been proposed to be a preferred CLOCK:BMAL1 binding site (Paquet et al., 2008), are also more enriched at common BMAL1 peaks (Fig. 11F). Characterization of the location of BMAL1 peaks revealed that peaks common to all three tissues were predominantly located at promoter/TSS, whereas tissue-specific BMAL1 peaks were more consistently located within introns and intergenic regions (Fig. 11G). Finally, nucleosome signal at common BMAL1 peaks was lower compared to other groups (Fig. 11H, 12H). This result, which is likely due to differences in BMAL1 peak location between groups, suggests that DNA is more accessible at peaks common to all three tissues.

Together, these results indicate that BMAL1 peaks common to all three tissues, which target genes that are involved in generic biological processes, are enriched for E-boxes, are predominantly localized at promoter regions/TSS, and exhibit less nucleosome signal. These features likely contribute to the higher BMAL1 ChIP-Seq signal observed at those sites.

2.3.7 BMAL1 DNA binding contributes only partially to rhythmic gene expression

To determine whether tissue-specific BMAL1 binding contributes to generating tissue-specific circadian transcription, we analyzed BMAL1 target gene expression in the mouse liver, kidney and heart using public datasets that assessed the rhythmic transcriptome in those tissues (Zhang et al., 2014). In agreement with the literature (Menet et al., 2012; Rey et al., 2011), genes targeted by BMAL1 exhibit a higher proportion of rhythmic mRNA expression than those not targeted by BMAL1. Specifically, rhythmic expression of BMAL1 targets in the liver, kidney and heart is increased by ~2-fold compared to all genes, and by ~1.3-1.5-fold compared to genes targeted by BMAL1 in other tissues (Fig. 13A). Surprisingly, genes targeted by BMAL1 in all three tissues (group 1) do not exhibit substantially more rhythmic expression despite increased BMAL1 ChIP-Seq signal, increased number of E-boxes, and preferential peak location at promoter/TSS (Fig. 13A). Moreover, the majority of BMAL1 target genes are not rhythmically expressed in any of the three tissues (Fig. 13A). These results thus suggest

Figure 13: Transcriptional activities of BMAL1 DHS and other DHS contribute to BMAL1-mediated rhythmic transcription.
(A) Percentage of rhythmically expressed gene for the seven groups of BMAL1 binding sites. Gene expression data originate from public microarray datasets (Zhang et al., 2014) and is considered rhythmic if q-value <0.05 using JTK-cycle. **(B)** Overlap of rhythmic expression for peaks common to all three tissues (group1), and for liver-, kidney-, and heart-specific BMAL1 peaks (groups 5, 6, and 7, respectively). The number of genes that are rhythmically expressed for the mouse liver (blue), kidney (green), and heart (red) is displayed, along with the number and percentage of non-rhythmically expressed genes (AR). **(C, D)** mRNA expression (left) and genome browser view (right) of BMAL1 ChIP-seq and DNase-seq signals in the mouse liver (blue), kidney (green), and heart (red). Rhythmic expression determined by JTK-cycle is defined as *** if q-value < 0.001, ** if q-value < 0.01, and * if q-value < 0.05. The genes *Coq10b* and *Abcf1* (C) represent two examples for which the activity of BMAL1 DHS likely contributes to the differences in mRNA expression, where the genes *Dusp7* and *Comt* (D) represent two examples for which the activity of other DHS likely contributes to BMAL1-mediated rhythmic transcription.

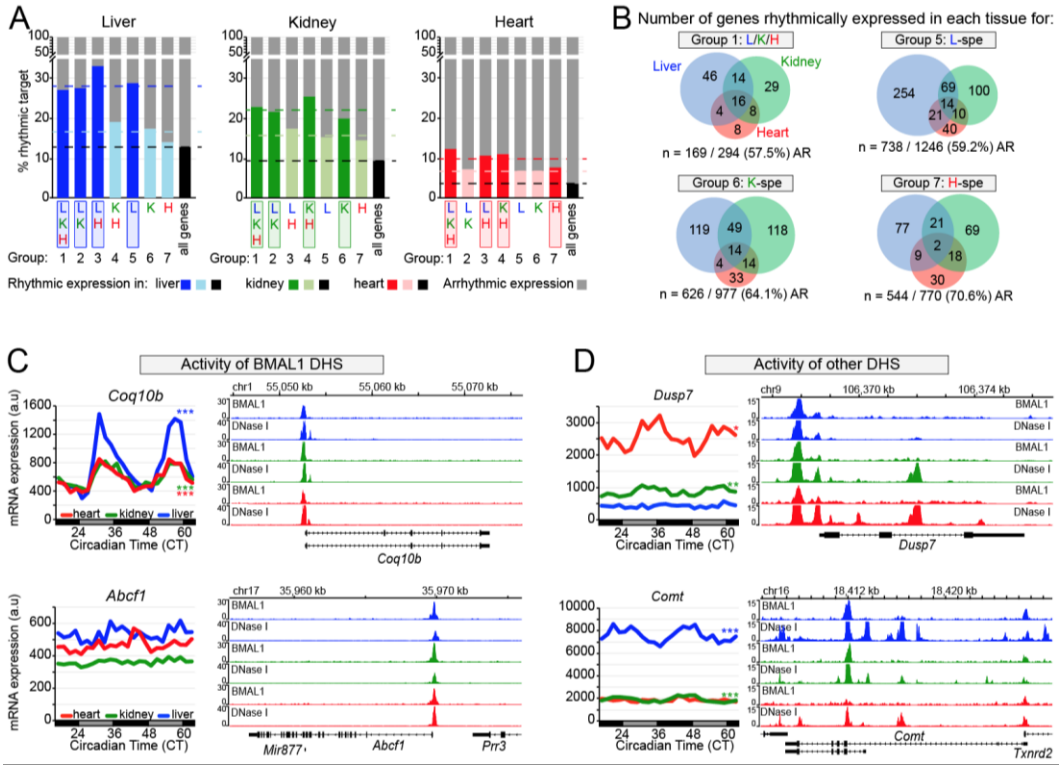

that although BMAL1 DNA binding contribute to increased rhythmic expression, it is not sufficient to drive rhythmic transcription.

Consistent with this notion, BMAL1 targets common to all three tissues display a widely heterogeneous rhythmic output, with most genes being rhythmic in only one tissue (83 genes out of 125 rhythmically expressed genes; Fig. 13B). In fact, only 16

genes targeted by common BMAL1 peaks are rhythmically expressed in all three tissues, and most of them are core clock genes. We also found that many genes targeted by BMAL1 in one tissue were rhythmic only in another tissue (Fig. 13B). To characterize the mechanisms underlying this poor overlap between BMAL1 binding and rhythmic gene expression, we examined the profiles of DNase-Seq and BMAL1 ChIP-Seq datasets in the liver, kidney, and heart. While we were unable to detect a unified mechanism that may explain the variability in BMAL1 transcriptional output, we identified two important features that likely contribute to rhythmic transcription. First, similar BMAL1 ChIP-Seq signal between tissues can result in significantly different levels and/or rhythmicity of target gene expression (Fig. 13C, 14A). This observation was made at genes targeted by a unique DHS, suggesting that factors other than just BMAL1 contribute to the activity of BMAL1-bound DHSs and to rhythmic BMAL1 target gene expression. Second, we found that rhythmicity of BMAL1 target genes was often associated with higher levels of expression and more DHSs, thus suggesting that rhythmic gene expression results from functional interactions between BMAL1 DHSs and other DHSs (Fig. 13D, 14B). We also found a few instances where more DHSs were associated with decreased expression, suggesting that interactions between multiple DHSs may also result in decreased transcription activation (Fig. 14C).

Figure 14: Tissue-specificity of rhythmic BMAL1 target gene expression relies on the transcriptional activities of DHS bound by BMAL1, but also other DHS.
(A-C) mRNA expression (left) and genome browser view (right) of BMAL1 ChIP-seq and DNase-seq signals in the mouse liver (blue), kidney (green), and heart (red). Rhythmic expression determined by JTK-cycle is defined as *** if q-value < 0.001, ** if q-value < 0.01, and * if q-value < 0.05. Panel A represents examples for which the activity of BMAL1 DHS likely contributes to the differences in mRNA expression, whereas panels B and C represent examples for which the activity of other DHS likely contributes to BMAL1-mediated rhythmic transcription. The activity of these other enhancers often enhances (rhythmic) target gene expression (B), but it can also lead to decrease (rhythmic) gene expression (C).

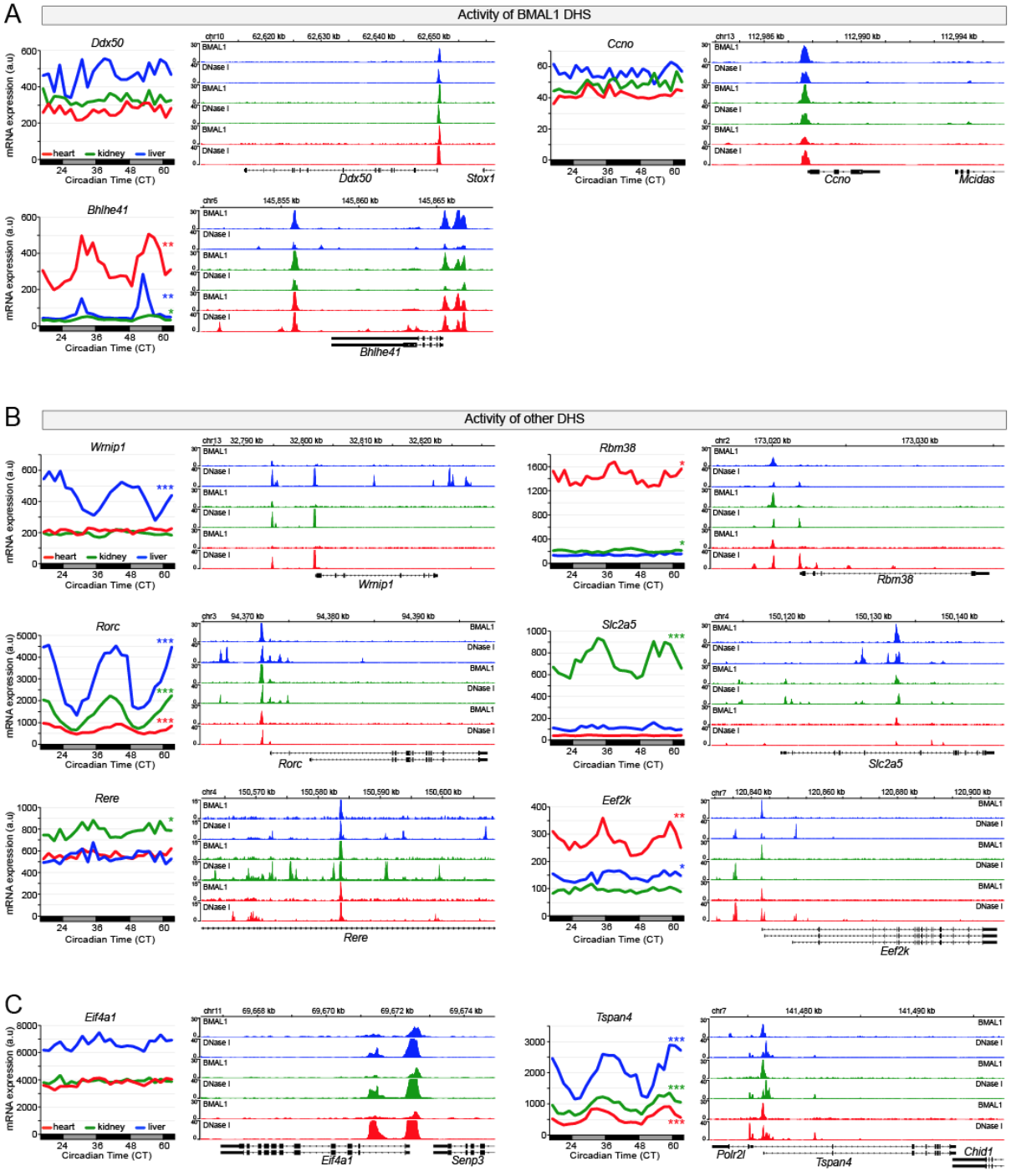

In summary, our results indicate that, as recently reported (Trott and Menet, 2018b), BMAL1 DNA binding is not sufficient to drive rhythmic transcription. They also suggest that rhythmic BMAL1 target gene expression likely results from (i) interactions between DHSs bound by BMAL1 and other DHSs, and (ii) the activity of each DHS, including those bound by BMAL1.

2.3.8 BMAL1-bound DHSs physically interact with other DHSs

To determine the extent to which BMAL1 target gene transcription relies on physical interactions between DHSs, we performed RNA Polymerase II (Pol II) Chromatin Interaction Analysis by Paired-End Tag Sequencing (ChIA-PET) in the mouse liver at ZT6 and ZT18 with 3 biological replicates per time point. By incorporating a Pol II ChIP step, this technique identifies interactions between enhancers and/or TSS of genes that are being transcribed (Fig. 15A) (Kieffer-Kwon et al., 2013; Li et al., 2012).

To assess the efficiency of our mouse liver Pol II ChIA-PET in detecting chromatin interactions at transcriptionally active genes, we determined the number of Paired-End Tags (PETs) mapped to a single gene based on gene transcription using public mouse liver Nascent-Seq datasets (Menet et al., 2012). We found that most PETs mapped to transcriptionally active genes, with 23.4% of all PETs located within the top 10% of genes transcribed in the mouse liver (Fig. 15B, 16A). Analysis of PETs with reads located in two different DHSs and visualization of chromatin interactions at mouse liver BMAL1 target genes further confirmed that actively transcribed genes harbor many PETs mapping to different DHSs, including some bound by BMAL1 (Fig.

13C, 15D). These data indicate that DHSs located within the same gene physically

interact

Figure 15: Analysis of chromatin interactions by RNA polymerase II ChIA-PET in the mouse liver.
(A) Illustration of the ChIA-PET technique. **(B)** Number of Paired-End Tags (PET) with both reads mapped to the same gene and parsed based on gene nascent RNA expression in the mouse liver. Red circles represent the average PET number for each decile ± 95% confidence intervals. **(C)** Average number of PET per gene in the mouse liver with both reads located in different DHS and mapped to the same gene, parsed based on gene nascent RNA expression. Error bars represent the 95% confidence intervals. **(D)** Genome browser view of mouse liver BMAL1 ChIP-seq (this study), DNase-seq (ENCODE), and Pol II ChIP-seq (from Sobel et al., 2017b). PET with both reads mapped to DHS are in red, while PETs with one read mapped to a DHS are in orange and those not mapped to a DHS are in grey. **(E-G)** Percentage of PETs detected at ZT6 (white bar and dashed black line) or ZT18 (grey bar and solid black line), displayed as the average ± s.e.m. of 3 independent experiments based on the type of PET, the rhythmicity of gene expression, and the phase of expression. * denotes $p < 0.05$ between ZT6 and ZT18, and # denotes an interaction found in the two-way ANOVA ($p < 0.05$) between the phase of expression and the time of the ChIA-PET experiment (ZT6 or ZT18). Triangles represent DHSs, and may be located within a gene or not.

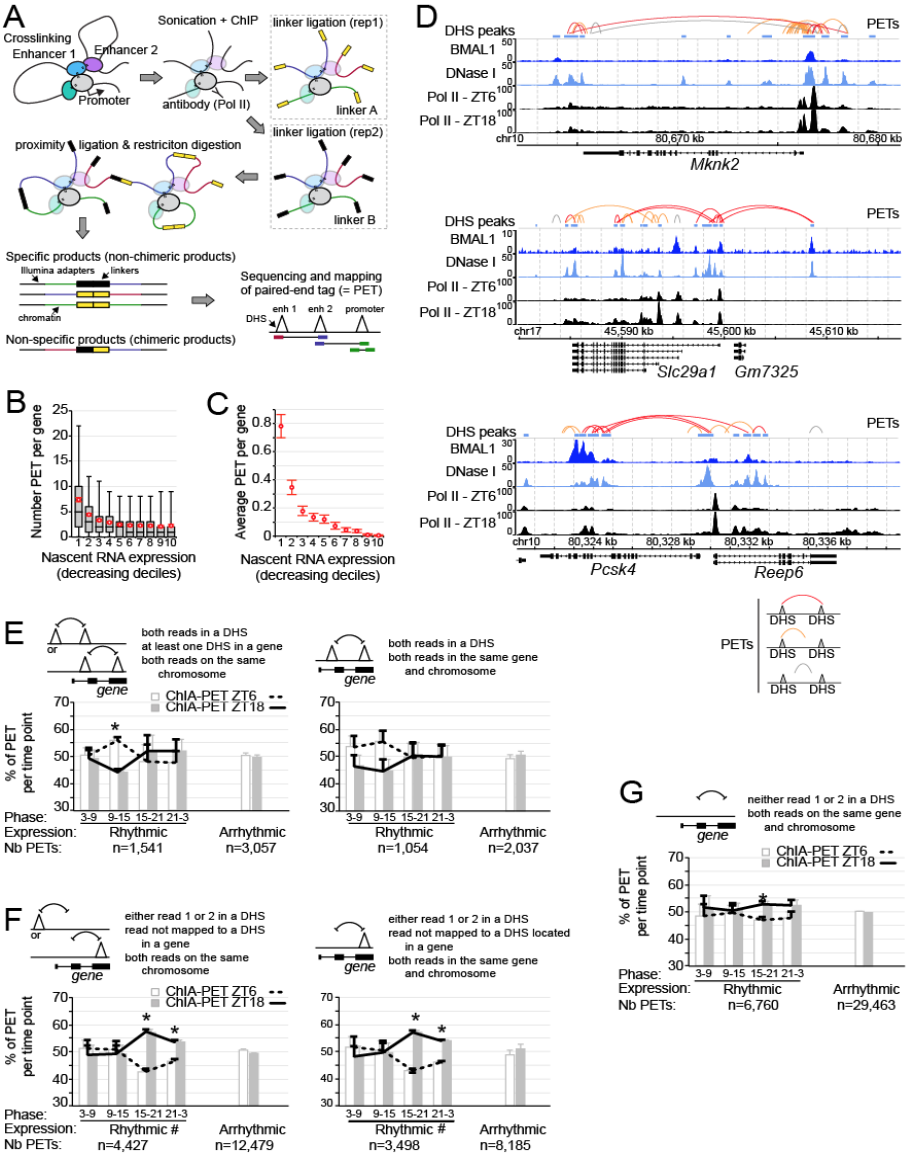

via gene looping, and suggest that transcriptional activation results from the synergistic interaction between DHSs. To assay if rhythmic gene expression is associated with changes in chromatin interactions, we determined the number of PETs between DHSs based on the phase of rhythmic gene expression. We found small day *vs.* night differences in chromatin interactions in the mouse liver, with about 10% more PETs between two DHSs at ZT6 for genes with a peak of expression at ZT9-15 (Fig. 15E). In addition, analysis of interactions between a DHS and a non-DHS site, *e.g*., a site with elongating Pol II that is expected to better reflect transcriptional activity revealed that DHS-non-DHS interactions exhibit day *vs.* night differences, with more interactions at ZT18 for genes expressed from ZT15 to ZT3 (Fig. 15F, 15G).

A few recent reports suggested that rhythmic interactions between BMAL1 DHSs and other DHSs underlie the rhythmic transcription of BMAL1 target genes (Aguilar-Arnal et al., 2013; Mermet et al., 2018; Yeung et al., 2017). To investigate this possibility, we quantified the number of PETs mapped to BMAL1 target genes. We found that, at rhythmically expressed BMAL1 target genes, the number of chromatin interactions between two DHSs containing at least one BMAL1 peak is higher at ZT6 when BMAL1 binding is maximal (Fig. 17A, 17B). This higher number of PETs at ZT6 *vs.* ZT18 was specifically observed for rhythmically expressed targets peaking at ZT3-ZT15, *i.e*., at times corresponding relatively well with BMAL1 DNA binding, and after incorporation of chromatin interactions involving distal BMAL1-bound DHSs, which account for ~15-20% of DHS-DHS interactions (Fig. 17A, 17B). In addition, analysis of

Figure 16: Pol II ChIA-PET datasets uncover interaction between DHS in the mouse liver.
(A) Summary of the sequencing analysis for the three independent Pol II ChIA-PET experiments performed in this project. QC stands for quality check. **(B)** Number (black) and percentage (blue) of Paired-End Tags (PET) based on the distance between the two reads for the three independent Pol II ChIA-PET experiments. Reads mapping to two different chromosomes are labeled as extra-chrom. reads. **(C)** Percentage of PET with non-chimeric half-linker barcodes (specific products, grey) and chimeric half-linker barcodes (non-specific products, black) for each of the three independent Pol II ChIA-PET experiments. **(D)** Distribution of the PET length for the non-chimeric PET (specific products, grey) and the chimeric PET (non-specific products, black), for the mouse liver Pol II ChIA-PET experiments performed with single crosslinked nuclei (left) or dual crosslinked nuclei (right). The ratio between non-chimeric PET and chimeric PET is overlaid in red. Both y-axis are represented in $\log_{10}$ scale. **(E)** Genome browser view of mouse liver BMAL1 ChIP-seq (this study), DNase-seq (ENCODE), and Pol II ChIP-seq (from Sobel et al., 2017b). PETs with both reads mapped to DHSs are in red, while PETs with one read mapped to a DHS are in orange and those not mapped to a DHS are in grey.

A

	Single X-link	Dual X-link (1)	Dual X-link (2)
Nb of Pol II ChIA-PET lib	2	4	2
ChIP starting material per library (ng)	24,311 ± 1,779 (29,827; 21,796)	338 ± 91 (140; 533; 319;361)	304 ± 14 (290; 318)
Nb amplification cyles	14	20	16
Nb reads (total)	17,029,738	341,886,784	340,510,620
Reads passing QC	15,686,931	284,983,965	317,109,401
Nb uniquely mapped reads	2,026,322	44,020,678	45,238,532
Non-chimeric reads	1,498,691	31,339,229	27,954,216
Unique non-chimeric reads (percentage)	1,439,048 (96.02%)	559,254 (1.78%)	851,265 (3.04%)
Chimeric reads	527,631	12,681,449	17,284,316
Unique chimeric reads (%) (percentage)	504,807 (95.67%)	232,707 (1.84%)	562,020 (3.25%)

B

	Single X-link		Dual X-link (1)		Dual X-link (2)	
	Non-chimeric	Chimeric	Non-chimeric	Chimeric	Non-chimeric	Chimeric
Pairs < 3kb (%)	88,790 (6.17%)	1,248 (0.25%)	128,276 (22.9%)	583 (0.25%)	123,326 (14.4%)	3,466 (0.62%)
3kb < pairs < 8kb (%)	871 (0.06%)	21 (0.04%)	1068 (0.20%)	7 (0.003%)	2,462 (0.28%)	141 (0.025%)
8kb < pairs < 200kb (%)	588 (0.04%)	84 (0.016%)	1,140 (0.20%)	34 (0.01%)	2,487 (0.29%)	163 (0.029%)
Pairs > 200kb (%)	72,743 (5.05%)	27,102 (5.39%)	23,229 (4.15%)	12,149 (5.22%)	40,220 (4.72%)	29,872 (5.32%)
Extra-chrom. reads (%)	1,276,056 (88.7%)	467,352 (94.4%)	405,541 (72.5%)	219,776 (94.4%)	683,160 (80.2%)	528,378 (94.0%)

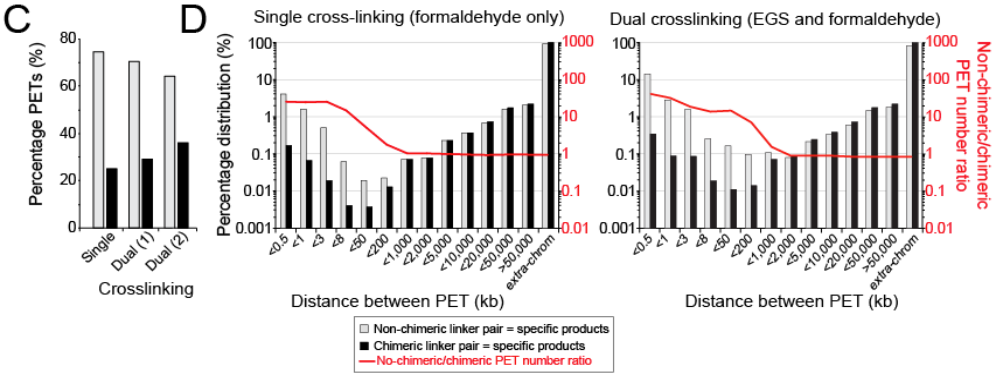

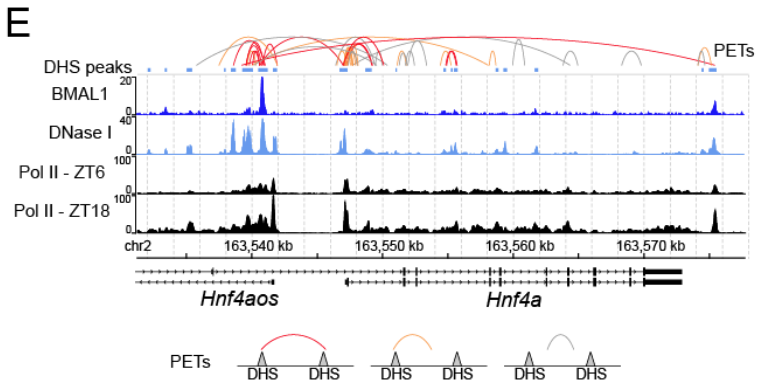

interactions between a BMAL1 peak and a non-DHS site revealed that while the proportion of PETs between ZT6 and ZT18 was similar for rhythmically and arrhythmically expressed targets, more PETs were found at ZT18 for the target genes rhythmically expressed at a similar phase (Fig. 17C, 17D).

To further characterize chromatin interactions between BMAL1-bound DHSs and other DHSs, we analyzed the type of DHSs to which BMAL1-bound DHSs interacts with (*i.e*., liver-specific DHS or DHS common to the kidney and/or heart) as well as their genomic location (*i.e*., promoter, intron, *etc*.). We found that interactions between BMAL1-bound DHSs and DHSs common to several tissues were enriched for rhythmically expressed genes (Fig. 17E), and that interactions with DHSs located in introns were enriched for rhythmically expressed genes with a peak of expression at ZT9-15, *i.e*., a few hours after maximal BMAL1 DNA binding (Fig. 17F). Future experiments will be required to determine if these differences in the type and location of chromatin interactions are relevant for BMAL1-mediated rhythmic gene expression.

Taken together, these results indicate that BMAL1-bound DHSs interacts with other DHSs, and that these interactions are more prevalent when BMAL1 is bound to DNA at ZT6 for rhythmic targets expressed at ZT3-15. Because the number of interactions is not rhythmic for arrhythmically expressed targets, this suggests that rhythmic chromatin interactions between BMAL1-bound DHSs and other DHS may contribute to rhythmic gene expression.

Figure 17: Rhythmic chromatin interactions are more prevalent for rhythmically expressed genes.
(A-D) Percentage of PETs detected at ZT6 (empty/white bar and dashed black line) or ZT18 (solid bar and solid black line) are displayed as the average ± s.e.m. of 3 independent experiments based on the type of PET, the rhythmicity of gene expression, the presence of a BMAL1-bound DHS, and the phase of gene expression. R = rhythmic expression; AR = arrhythmic expression. Triangles represent DHSs, and may be located within a gene or not. * denotes $p < 0.05$ between ZT6 and ZT18. **(E)** Type of DHS (liver-specific DHS or DHS common to the liver, kidney and heart) interacting with a BMAL1 DHS is displayed based on the transcriptional output of BMAL1 target genes (rhythmic or non-rhythmic) and the time at which the ChIA-PET experiment was performed (ZT6 or ZT18). Results are shown as percentage of PETs per ChIA-PET time point (as in panel 17A, top) or as the ratio of common DHS over liver-specific DHS (bottom). **(F)** Genomic location of DHSs interacting with BMAL1-bound DHS is displayed based on the transcriptional output of BMAL1 target genes (phase of expression, and rhythmic or non-rhythmic) and the time at which the ChIA-PET experiment was performed (ZT6 or ZT18). Location of DHSs consists of exon and transcription termination site (TTS) in black, introns in grey, promoter and transcription start site (TSS) in dark orange (-1 kb to +100 bp from TSS), and extended promoter in light orange (-10 kb to -1 kb from TSS). **(G)** Hypothetical model illustrating how CLOCK:BMAL1 generates tissue-specific rhythmic transcriptional programs. This model incorporates mechanisms on how BMAL1 binds to DNA in a tissue-specific manner (chromatin accessibility and co-binding with ts-TFs), and how u-TFs might contribute to BMAL1 DHS rhythmic transcriptional activity. It also illustrates how functional interaction between BMAL1 DHSs and other DHSs (including tissue-specific DHS) may contribute to rhythmic transcription.

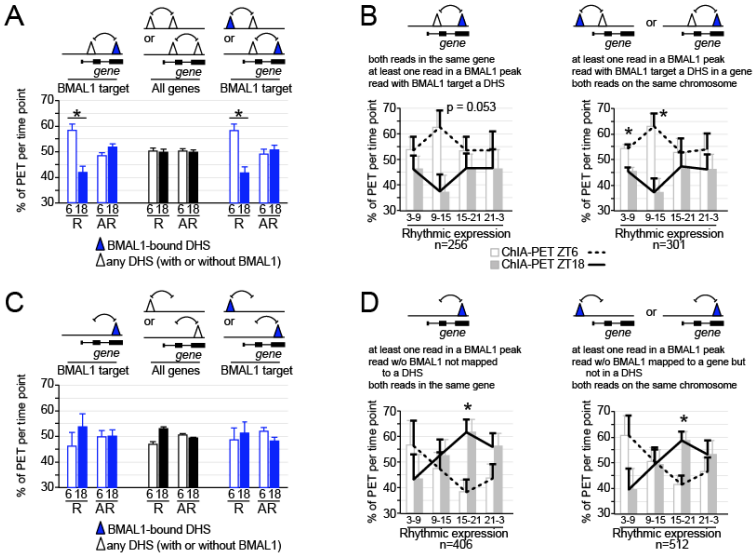

Figure 17 Continued.

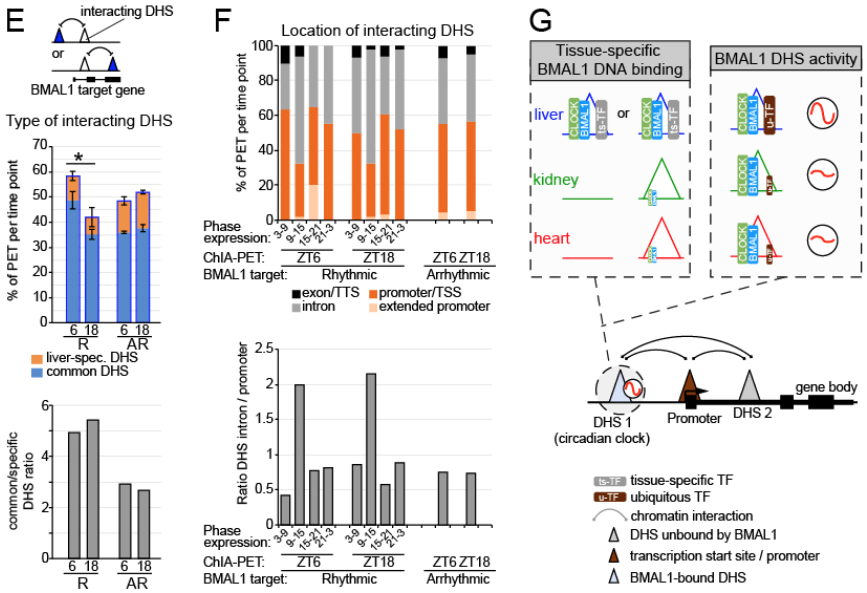

2.4 Discussion

Although the same clockwork mechanism is found in essentially all tissues, clock-controlled gene rhythmic expression is mainly tissue-specific, reflecting the large number of biological functions that are clock controlled (Mure et al., 2018a; Panda et al., 2002; Storch et al., 2002; Zhang et al., 2014). By characterizing BMAL1 cistromes in three

mammalian tissues, we show that tissue-specific circadian transcriptional programs can be directly initiated by the core circadian clock. We provide evidence that BMAL1 DNA binding profiles are largely tissue-specific, which coincides with tissue-specific chromatin accessibility and co-binding with ts-TFs. Our analysis of BMAL1 target gene expression also indicates that rhythmic CLOCK:BMAL1 transcriptional output relies, at least in part, on the rhythmic interaction between BMAL1-bound DHSs and other DHSs.

Given that some of these other DHSs are either tissue-specific or more accessible in specific tissues (e.g., Fig. 13D, 14B), our data suggest that enhancer-enhancer interactions can drive rhythmic BMAL1 target gene expression in a tissue-specific fashion (Fig. 17E). Taken together, chromatin accessibility and enhancer-enhancer interactions may explain how the circadian clock generates tissue-specific circadian transcriptional programs, thereby regulating biological functions in a tissue-specific manner. We anticipate that these mechanisms apply to other TFs that regulate gene expression in a tissue-specific manner.

Recent characterization of the chromatin accessible landscape revealed that most TFs bind to regions that are hypersensitive to nuclease digestion (Thurman et al., 2012b; Yue et al., 2014b). Because many of these DHSs are tissue-specific (Fig. 8A), it is not surprising that differences in the openness of the chromatin between tissues can promote tissue-specific BMAL1 binding. However, the majority of tissue-specific BMAL1 peaks are located in chromatin regions accessible in other tissues (Fig. 7C, 8C, 8D). DHSs are clusters of TF binding motifs, and TF recruitment to DHSs often results from cooperative binding between TFs. In particular, ts-TFs can cooperate with u-TFs to facilitate DNA binding: CEBPB cooperates with glucocorticoid receptor in the mouse liver (Grontved et al., 2013), FOXA1 and GATA3 with the estrogen receptor in primary breasts tumors (Hurtado et al., 2011; Theodorou et al., 2013), and OPA and SERPENT with *Drosophila* CLK:CYC (Meireles-Filho et al., 2014). Our finding that binding motifs, genomic footprints and ChIP-Seq signal for liver-specific TFs are enriched at liver-specific BMAL1 peaks, but not at common peaks, strongly suggests that this ts-TF/u-TF

cooperation applies to BMAL1 and that ts-TFs facilitate tissue-specific CLOCK:BMAL1 binding (Fig. 17C).

By analyzing the genome-wide nucleosome positioning in the mouse liver over the course of the day, it has recently been shown that CLOCK:BMAL1 promotes rhythmic nucleosome removal at its binding sites and proposed that CLOCK:BMAL1 is a pioneer-like TF (Menet et al., 2014). Our findings that BMAL1 binds in a tissue-specific manner even at DHSs common to several tissues seems contradictory to BMAL1 pioneering-like function. Instead of generating new DHSs (an expected feature from pioneer TF; Zaret and Carroll, 2011), our data rather suggest that BMAL1 DNA binding prevents the folding of DNA around histones and thus nucleosome formation. As a result, BMAL1 DNA binding would increase the exposure of naked DNA for other TFs and DNase I and facilitate their binding on DNA. This scenario, which is consistent with the analysis of nucleosome signal at tissue-specific BMAL1 peaks in *Bmal1*$^{-/-}$ mice (Fig. 12H), would explain why DNase I signal is decreased in *Bmal1*$^{-/-}$ mice not only around E-boxes but also around ts-TFs motifs (Fig. 9H, 9I). Conversely, ts-TFs may play a similar role at tissue-specific DHSs, *i.e*., their binding to DNA may facilitate the access of CLOCK:BMAL1 to exposed E-boxes by preventing nucleosome formation. This mechanism, which has been previously proposed to illustrate cooperative TF binding to DHSs (Mirny, 2010), may explain at least in part tissue-specific BMAL1 binding at DHSs common to several tissues. Future experiments will be required to experimentally validate this hypothesis, and eventually clarify BMAL1 pioneering like function.

Genes targeted by BMAL1 in all three tissues do not exhibit a higher rate of rhythmic expression and display a remarkable heterogeneity in the rhythmic output (Fig.

13A, 13B), indicating that even robust BMAL1 binding is not sufficient to drive rhythmic transcription. As recently suggested (Trott and Menet, 2018b), this may be explained by the contribution of u-TFs in regulating the transcriptional activity of BMAL1 DHSs and promoting gene expression. However, our analysis suggests an additional level of regulation that includes DHSs unbound by BMAL1, and through which interactions between BMAL1-bound DHSs and other DHSs would contribute to the regulation of rhythmic gene expression (Fig. 13D). To characterize if DHSs not bound by BMAL1 might contribute to rhythmic BMAL1 transcriptional output, we conducted mouse liver Pol II ChIA-PET to identify physical interactions between DHSs within genes engaged in active transcription (Fig. 6). In agreement with the literature, we found that the number of DHS-DHS interactions correlates with transcriptional levels. Relevant to how the circadian clock might regulate rhythmic gene expression, we identified a large number of interactions between BMAL1-bound DHSs and other DHSs, suggesting that BMAL1 target gene transcription relies more on the functional interaction between DHSs rather than just BMAL1-bound DHSs. In addition, and consistent with previous reports that used the 4C technique (Aguilar-Arnal et al., 2013; Mermet et al., 2018; Yeung et al., 2017), we found that the number of interactions between BMAL1 DHSs and other DHSs is higher at ZT6, *i.e.*, at time of maximal BMAL1 DNA binding. Importantly, this higher number of chromatin interactions at ZT6 was observed for rhythmically expressed target genes that peak during the day and not at arrhythmically expressed targets, suggesting that BMAL1-mediated rhythmic transcription relies on the capacity of BMAL1 to regulate rhythmic enhancer-enhancer interactions. These results are concordant with recent reports showing that rhythmic transcription in mammals is associated with rhythmic

long-range interactions between cis-regulatory elements and rhythmic gene looping (Aguilar-Arnal et al., 2013; Kim et al., 2018b; Mermet et al., 2018; Yeung et al., 2017). While the mechanisms underlying rhythmic enhancer-enhancer interactions remain vastly unknown, they likely involve the Mediator complex and transcriptional regulators recognizing histone modifications associated with transcriptional activation (Kim et al., 2018b). In addition, our and others findings raise the hypothesis that the expression of BMAL1 target genes relies on the relative contribution of BMAL1-bound DHSs *vs.* other DHSs, and that changes in the activity of other DHSs can impair the rhythmic expression of BMAL1 targets without affecting the molecular clockwork mechanism. Such a mechanism may well explain why circadian transcriptional programs can be reprogrammed by environmental challenges without affecting much of the clockwork mechanism (Eckel-Mahan et al., 2013; Murakami et al., 2016; Sato et al., 2017).

In summary, our results provide novel insights into how BMAL1 regulates rhythmic gene expression in a tissue-specific manner, and shed light on the role of enhancer-enhancer interactions in generating circadian transcriptional programs. We anticipate that these findings will be relevant for our understanding of how the circadian clock regulates a wide array of biological functions under normal and diseased states, and will apply more generally to how other TFs regulate tissue-specific gene expression.

2.5 Methods

2.5.1 Animals

Male C57BL/6J and *Bmal1-/-* mice were housed under 12-h light:12-h dark (LD12:12) with food and water available *ad libitum*. *Bmal1-/-* were kindly provided by Christopher Bradfield (Bunger et al., 2000). The age of animals collected was between three and six months old. All experiments were approved by the TAMU Institutional Animal Care and Use Committee (AUP# 2016-0199 and AUP 2013-0158).

2.5.2 BMAL1 chromatin immunoprecipitation

Mice were euthanized by isoflurane anesthesia followed by decapitation, and livers, kidneys, and hearts were collected, rinsed in ice-cold 1X PBS, minced, and immediately homogenized in 1X PBS containing 1% formaldehyde for 10 minutes at room temperature (4ml for livers, 2ml for kidneys, and 1ml for heart). Formaldehyde cross-linking was quenched by adding 2M glycine to a final concentration of 140 mM. Samples were then kept on ice for ten minutes, washed twice with hypotonic buffer (10mM Hepes pH 7.6, 15mM KCl, 0.15% NP-40, 1mM DTT, and 1mM PMSF), and centrifuged at 1500g for 2 minutes at 4ºC. Nuclei were purified by centrifuging on a sucrose cushion (10mM Hepes pH7.6, 15mM KCl, 0.15% NP-40, 24% sucrose, 1mM DTT, 1mM PMSF) at 20,000g for 10 minutes at 4°C, and then washed with hypotonic buffer four times. Sonication for the liver and kidneys were done by resuspending the samples in 12ml per liver and 4.5 ml per kidney of sonication buffer (10mM Tris pH 7.5, 150mM NaCl, 2mM EDTA, 0.25% SDS, 0.2% Triton). Sonication of the heart was done by resuspending the heart in 500 µl of sonication solution (10mM Tris pH 7.5, 150mM

NaCl, 2mM EDTA, 0.5% Sarkosyl, 1X protease inhibitor cocktail). Samples were sonicated in 500 µl aliquots to obtain chromatin fragments of about 100-600 bp in length. After sonication, samples were centrifuged at 15,000g for 10 minutes at 4°C, supernatants were moved to a new tube, and inputs (25 µl) and ChIP (200 µl) samples were made. The 200 µl ChIP aliquots were diluted (final concentration: 10mM Tris-Cl pH 7.5, 150mM NaCl, 1% Triton X-100, 0.1% sodium deoxycholate, 0.1% SDS or sarkosyl, 2mM EDTA), 1 µl of BMAL1 antibody (chicken anti-BMAL1) was added and left to rotate overnight at 4ºC. Dynabeads antibody coupling kit (#14311D, Invitrogen) was used with rabbit anti-chicken IgY antibody (# 31104, Invitrogen) to immunoprecipitate BMAL1 chromatin complexes. Dynabeads were washed with IP buffer twice (10mM Tris-Cl pH 7.5, 150mM NaCl, 1% Triton X-100, 0.1% sodium deoxycholate, 0.1% SDS or sarkosyl, 2mM EDTA), resuspended in blocking solution (IP buffer with 1 mg/ml bovine serum albumin and 0.1 mg/ml yeast tRNA) and left rotating overnight at 4°C. After overnight incubation, dynabeads were washed once with final IP buffer, the chromatin was added, and left rotating at 4°C for two hours. BMAL1 immunoprecipitated chromatin was then washed twice with TSEI buffer (10mM Tris pH 7.5, 0.1%SDS, 1% Triton X-100, 2mM EDTA, 150mM NaCl, 1mM DTT, 1X Protease Inhibitor Cocktail), twice with TSEII buffer (10mM Tris pH 7.5, 0.1%SDS, 1% Triton X-100, 2mM EDTA, 500mM NaCl, 1mM DTT, 1mM PMSF), twice with LiCl Buffer III (10mM Tris pH 7.5, 0.25M LiCl, 1% NP-40, 1% Na Deoxycholate, 1mM EDTA, 1mM DTT, 1mM PMSF), twice with TENT buffer (10mM Tris pH 7.5, 1mM EDTA, 150NaCl, 0.1% Triton X-100), and once with TET buffer (10mM Tris pH 7.5, 1mM EDTA, 0.1% Triton). ChIP samples were then resuspended in 200uL of ChIP Elution Buffer (50mM Tris-HCl pH8, 10mM EDTA, 1% SDS, 1mMDTT)

while input samples were supplemented with 175 µl of ChIP Elution buffer, and incubated for 6-18 hours at 65ºC. After the incubation, samples were purified using Qiagen PCR purification columns (# 28106), and efficiency of BMAL1 ChIP was verified by qPCR as described below.

2.5.3 Generation of BMAL1 ChIP-seq libraries and sequencing

BMAL1 and input ChIP-Seq libraries were generated from liver, kidney, and heart samples (n = 3 mice per tissue) using NEBNext® ChIP-Seq Library Prep Master Mix Set (# E6240, NEB) as per the manufacturer's instructions. DNA from ChIP and input were quantified using a Quantus Fluorometer (# E6150, Promega), and 10 ng was used to generate the libraries. DNA end repair was performed with NEBNext End Repair Reaction Buffer and Enzyme Mix for 30 minutes at 20°C. dA-Tailing of end-repaired DNA was performed with NEBNext dA-Tailing Reaction Buffer and Klenow Fragment (3'→5' exo) for 30 minutes at 37°C. Adapter ligation of dA-tailed DNA was performed with Quick Ligation Reaction Buffer, NEBNext Adaptor (1.5 µM), and Quick T4 DNA Ligase. Libraries were generated by PCR amplification of adaptor ligated DNA using NEBNext Multiplex oligonucleotides and Phusion Taq (M0530S). Libraries were amplified for 16 cycles. Libraries were quantified with qPCR with TRUseq library standards, and with a Quantus Fluorometer. DNA cleanup between each reaction was performed using Solid Phase Reversible Immobilization (SPRI) beads generated in the lab from Sera-mag SpeedBeads (# catalog number 09-981-123, Thermo-Fisher). BMAL1 ChIP-seq and input libraries were sequenced using an Illumina NextSeq with a sequence length of 76 bp.

2.5.4 BMAL1 ChIP-qPCR

Chromatin Immunoprecipitation was performed as described above with the following exceptions. After tissue collection, tissues were flash frozen in liquid nitrogen and kept at -80ºC. Nuclei extraction was conducted using seven samples at a time (6 time points in wild-type mice -ZT2, ZT6, ZT10, ZT14, ZT18, and ZT22-, and the ZT6 sample from *Bmal1-/-* mouse) to minimize inter-individual variations, and nuclei were flash-frozen in glycerol storage buffer (10mM Tris-Cl pH 7.5, 50mM NaCl, 2mM EDTA, 50% glycerol, 1mMDTT, 0.15mM spermine, 0.5mM spermidine, 1X PIC). BMAL1 ChIPs were also performed using seven samples at a time as described above, except for the BMAL1 antibody (# ab3350, abcam) and the Dynabeads protein G (# 10004D, Invitrogen).

qPCR was performed using the BIO-RAD iTaq Universal SYBR Green Supermix (# 1725124, and BIO-RAD CFX Connect). ChIP fold enrichment was calculated as the ratio between *Dbp* 1st intron ChIP signal normalized to input and intergenic region ChIP signal normalized to input. The primer sequences used are:

Dbp 1st intron (forward): ATGCTCACACGGTGCAGACA

Dbp 1st intron (reverse): CTGCTCAGGCACATTCCTCAT

Intergenic region (forward): CTTTTAATGAGGCTGTGTGGA

Intergenic region (reverse): ACTCCCTTGCGAATGTCCTA

2.5.5 Sequencing datasets and alignment to the mouse genome

All public datasets were downloaded from NCBI or https://encodeproject.org (unless noted below) as fastq or Short Read Archive (SRA) file formats. To avoid issues due to

the utilization of different protocols/procedures for each tissue, each of the liver, kidney and heart ChIP-Seq, DNase-Seq and mRNA expression datasets used in cross-comparisons were generated for the from the same research laboratory. Accession number are as follow:

(i) H3K27ac ChIP-seq (comparison between tissues): downloaded from https://encodeproject.org, accession numbers GSM1000093 (heart), GSM1000140 (liver), and GSM1000092(kidney).

(ii) H3K4me1 ChIP-seq: downloaded from https://encodeproject.org, accession numbers GSM769025 (heart), GSM769023 (kidney), and GSM769015 (liver).

(iii) DNase-seq: downloaded from https://encodeproject.org, accession numbers GSM1014166 (heart), GSM1014193 (kidney) and (liver).

(iv) RNA-seq and microarray datasets: downloaded from the NCBI website, accession numbers GSE54652 (Zhang et al., 2014).

Some other datasets were also use to further characterize tissue-specific BMAL1 DNA binding:

(v) Mouse liver H3K27ac and RNA Polymerase II ChIP-seq (time-course in wild-type and *Bmal1*$^{-/-}$ mice): downloaded from the NCBI website, accession number GSE60430 (Sobel et al., 2017b).

(vi) Mouse liver DNase-Seq datasets from wild-type and *Bmal1*$^{-/-}$ mice: downloaded from the NCBI website, accession number GSE60430 (Sobel et al., 2017b).

(vii) Mouse liver PER1, PER2, CRY1, and CRY2 ChIP-Seq datasets: downloaded from the NCBI website, accession number GSE39977 (Koike et al., 2012).

(viii) Mouse liver CREB ChIP-Seq datasets: downloaded from the NCBI website, accession number GSE45674 (Everett et al., 2013).

(ix) Mouse liver MYC and TEAD4 ChIP-Seq datasets: downloaded from the NCBI website, accession number GSE83869 (Croci et al., 2017).

(x) Mouse liver CTCF, GABPA, CBP, p300, HNF4A, CEBPA, HNF1A, and HNF6 ChIP-Seq datasets: downloaded at https://www.ebi.ac.uk/arrayexpress/experiments/E-MTAB-941/ (Faure et al., 2012).

(xi) Mouse liver BCL6 and STAT5 ChIP-Seq datasets: downloaded from the NCBI website, accession number GSE31578 (Zhang et al., 2012b).

(xii) Mouse liver ERα ChIP-Seq datasets: downloaded from the NCBI website, accession number GSE52351 (Gordon et al., 2014).

(xiii) Mouse liver REV-ERBα ChIP-Seq datasets: downloaded from the NCBI website, accession number GSE34020 (Cho et al., 2012).

(xiv) Mouse liver GR ChIP-Seq datasets: downloaded from the NCBI website, accession number GSE59752 (Lim et al., 2015).

(xv) Mouse liver PPARα, LXR, and RXRα ChIP-Seq datasets: downloaded from the NCBI website, accession number GSE35262 (Boergesen et al., 2012).

(xvi) Mouse liver FOXA1 and FOXA2 ChIP-Seq datasets: downloaded from the NCBI website, accession number GSE17067 (MacIsaac et al., 2010).

SRA files were converted to fastq files using SRA toolkit (Leinonen et al., 2011). ChIP-seq and DNase-seq datasets were aligned to the mouse genome (version mm10) using bowtie2 (Langmead and Salzberg, 2012) using the parameters: -x and --end-to-end. Uniquely mapped reads were only considered for analysis, and up to 3 duplicated sequences were kept for each BMAL1 ChIP-Seq dataset. The heart BMAL1 ChIP-Seq replicate 1 dataset contains two technical replicates that were merged into a single bam file, which was then randomly downsampled using samtools from 47,936,219 read to 17,253,305 reads to avoid overrepresentation of one replicate in the final merged file comprising the three biological replicates. All bam files from the heart were then merged for a total read count of 36,975,623 reads (replicate 1: 17,253,305 reads; replicate 2: 11,994,180 reads; replicate 3: 7,728,138 reads). The kidney biological replicate 1 was also downsampled using samtools from 26,840,611 reads to 8,856,833 reads. All bam files from the kidney were then merged for a total of 26, 930,789 reads (replicate 1: 8,856,833 reads; replicate 2: 7,381,236 reads; replicate 3: 10,692,720 reads). None of the liver samples were downsampled, and the bam files were merged using samtools for a total of 34,846,537 reads (replicate 1: 10,966,215 reads; replicate 2: 11,265,139 reads; replicate 3: 12,615,183 reads). Visualization files were generated using bedtools (Quinlan and Hall, 2010) and normalized to 10,000,000 reads. Input files were processed individually and then merged as bam files using samtools.

For DNase-seq datasets, bam files from all technical and biological replicates were merged and no downsampling was performed. Reads from the RNA-Seq dataset were trimmed using fastx_trimmer (http://hannonlab.cshl.edu/fastx_toolkit/) with the following parameters -f 1 -l 100 -Q 33, and aligned to the genome using STAR (Dobin et

al., 2013) with the default parameters and the option: --outFilterIntronMotifs RemoveNoncanonica. Gene expression data were retrieved using cufflinks (Trapnell et al., 2012) and the genome version GRCm38.p5_M14 and default parameters.

2.5.6 BMAL1 ChIP-seq and DNase-seq peak calling

Peak calling for both BMAL1 ChIP-seq and DNase-seq data was performed with findPeaks from the HOMER suite (Heinz et al., 2010). A minimum local enrichment of 4-fold was set up as necessary, and the following parameters were used: -style factor and -i (for BMAL1 ChIP-Seq) or -style dnase and -region (for DNase-Seq). No input was used to identify DNase-seq peaks. Overlap between ChIP-Seq or DNase-Seq peaks was determined using the function intersectBed from Bedtools suite (Quinlan and Hall, 2010) using default parameters. Heatmaps were using the Rscript pheatmap.R.

2.5.7 Assignment of BMAL1 peaks to their target genes

BMAL1 peaks were assigned to their target genes using the perl script annotatePeaks.pl from the HOMER suite with the mm10 mouse genome as a reference (Heinz et al., 2010). The HOMER gene annotation script outputs each peak into the following categories: (i) Promoter-TSS, corresponding to TSS - 10kb to TSS + 1kb, (ii) Transcription termination site (TTS), corresponding to TTS - 100 bp to TTS + 1kb, (iii) exons, (iv) introns, and (v) intergenic, which corresponds to peaks located upstream of the TSS by more than 10 kb and downstream the TTS by more than 1 kb. Intron and

exon assignments were not adjusted from the output of HOMER annotatepeaks.pl. BMAL1 peaks labeled as intergenic were not assigned to a target gene.

2.5.8 Quantification of ChIP-Seq and DNase-Seq signal at BMAL1 ChIP-Seq peaks

ChIP-seq and DNase-seq signal was calculated using scripts from Bedtools (Quinlan and Hall, 2010), the uniquely mapped reads (mm10 version) and the genomic coordinates of BMAL1 ChIP-seq peaks or mouse liver DHS peaks. Signal was calculated in a ± 250 bp region from the peak center for DNase-seq as well as for BMAL1 and other TF ChIP-seq signal, and in a ± 1 kb region from the peak center for H3K27ac ChIP-Seq signal.

2.5.9 Footprint detection

Detection of footprints was performed using the python script wellington_footprints.py from the pyDNase suite (Piper et al., 2015; Piper et al., 2013). All parameters were set to default, and a p-value of -20 was used along with an FDR of 0.01. Wig files generated by wellington_footprints.py were converted to BigWig files with the wigToBigWig algorithm downloaded at https://genome.ucsc.edu/.

2.5.10 Motif analysis at BMAL1 peaks and footprints

Motif analysis was performed at BMAL1 DNA binding sites (genomic location of BMAL1 ChIP-Seq peaks) using the perl script findMotifsGenome.pl from the HOMER suite (Heinz et al., 2010), using the parameter -size 200. Motifs were considered as significantly enriched if the q-value was less than 0.05. Motif enrichment was calculated

based on the background from the output of findMotifsGenome.pl. Motif analysis at footprints located with BMAL1 peaks and BMAL1 DNase I hypersensitive sites (peak center ± 15bp) has been performed similarly.

2.5.11 Quantification of DNase I cuts at E-boxes and other TF binding motifs

The genomic location of DNase I cuts was retrieved from DNase-Seq datasets by reporting the position and strandness of the first nucleotide of each read in a bam file. Average DNase I cut signal was calculated at E-boxes and other TF binding motifs using scripts from Bedtools (Quinlan and Hall, 2010). Quantification of the average DNase I cut signal at control peaks (*i.e*., TF ChIP-Seq peaks that do not exhibit BMAL1 ChIP-Seq signal; Fig. 9I) was performed by randomly selecting an equivalent number of TF ChIP-Seq peaks without BMAL1 to the number of peaks with BMAL1. Because most TF ChIP-Seq peaks with BMAL1 signal exhibit strong DNase-Seq signal (*i.e*., most of them are within the strongest DHSs), the random selection was performed by matching the number of peaks within each DNase-Seq signal decile. This process was repeated 1,000 times, and the average of 1,000 iterations calculated.

2.5.12 Detection of E-box and dual E-box motifs

Generation of motifs for E-boxes and dual E-boxes was performed with the perl script seq2profile.pl from the HOMER suite (Heinz et al., 2010). The E-boxes considered for analysis were as follows CACGTG, CACGNG and CACGTT. These E-boxes contained only one mismatch from the canonical motif and were found to be functional CLOCK-binding motifs *in vitro* (Yoshitane et al., 2014). The dual E-box motif tolerates up to two

mismatches between the two E-boxes and contains a spacer of either six or seven base pair.

2.5.13 Gene ontology analysis

Gene ontology was performed using the perl script annotatePeaks.pl from the HOMER suite (Heinz et al., 2010), with the parameter -go and mm10 genome. HOMER assigns target genes based on the closest gene to the BMAL1 binding region, and then searches for enriched functional categories.

2.5.14 Rhythmic expression analysis

Rhythmic expression of BMAL1 target genes was determined using public microarray datasets performed in the same research lab (Zhang et al., 2014). Files containing expression values for each microarray probe were downloaded from the NCBI website (GSE54652), and no analysis of the original files were performed. Rhythmic gene expression was determined using JTK cycle (Hughes et al., 2010) with the following parameters: timepoints 18-64, and all other parameters were left to default, and was considered significant if q-value < 0.05. The output regarding phase of expression, which is reported for every gene, was used in the ChIA-PET analysis. For results presented in Fig. 13A and 13B, genes targeted by two or more BMAL1 ChIP-Seq peaks assigned to different categories (*e.g.*, a gene targeted by two BMAL1 peaks: one common to all three tissues, and one specific to the liver) were not considered.

2.5.15 Data from GTEX portal

Graphs in Fig. 10C displaying the RPKM values of different TFs in human liver, kidney, and heart (atrial appendage and left ventricle) were retrieved from GTEX portal (Consortium, 2013) in April 2016.

2.5.16 Mouse liver Pol II ChIA-PET

Pol II ChIA-PET experiments were performed using mouse livers collected at either ZT6 or ZT18, with three biological replicates per time point and following previously published protocols (Fullwood and Ruan, 2009; Li et al., 2010; Zhang et al., 2012a). Pol II ChIP, which is the starting point of the ChIA-PET experiment (Fig. 15A), was performed similarly to BMAL1 ChIP with the following modifications:

(i) Livers were collected, rinsed in ice-cold 1X PBS, flash frozen in liquid nitrogen, and stored at -80°C. Frozen livers were crushed to a fine powder in liquid nitrogen using a mortar, and resuspended in 1X PBS containing the crosslinking reagents. One ChIA-PET experiment (JM11) was performed on livers crosslinked with 1% formaldehyde for 10 minutes at room temperature (single crosslinking), and two experiments (JM08 and JM12) were performed on livers first crosslinked with 1.5 mM EGS for 20 minutes at room temperature, and then for 10 additional minutes with 1% formaldehyde (dual crosslinking).

(ii) Nuclei were sonicated in 10 mM Tris pH 7.5, 150 mM NaCl, 2 mM EDTA, 0.5% SDS, 0.2% Triton, 1X protease inhibitor cocktail. Because large amounts of starting material were required, sonicated liver chromatin from 3-7 mice were pulled together, resulting in chromatin amounts ranging from 1.3 mg to 4.1 mg in a volume of ~10 ml. Chromatin samples were diluted 5-fold to obtain a final concentration of ChIP buffer of

10mM Tris-Cl pH 7.5, 150mM NaCl, 1% Triton X-100, 0.1% sodium deoxycholate, 0.1% SDS, 1X protease inhibitor cocktail. Pol II ChIP were performed in 50 ml canonical tube with 65 µg of anti-RNA Polymerase II 8WG16 monoclonal antibody (# MMS-126R, Covance). Immunoprecipitated chromatin was washed once with TSEI buffer, once with TSEII buffer, once with LiCl Buffer III, and once with TET buffer (see above for buffer composition). Beads were finally resuspended in 2 ml of 1X TE buffer supplemented with 1X protease inhibitor cocktail.

(iii) A sample corresponding to 1/40th of each ChIP was set apart and processed for DNA purification and assessment of ChIP enrichment by qPCR. Enrichment was calculated as the ratio between *Aldob* TSS ChIP signal normalized to input and intergenic region ChIP signal normalized to input. The *Aldob* primer sequences used are (forward) TGTTATCATTAACCCAGCTTGC and (reverse) CTGCCACCTCACACAGCTT. The intergenic region primer sequences are described above.

Libraries were generated following published protocols (Fullwood and Ruan, 2009; Li et al., 2010; Zhang et al., 2012a). Immunoprecipitated chromatin was end-repaired, processed for ligation with biotinylated half-linkers, and 5' phosphorylated while still complexed with Pol II antibodies on magnetic beads. Chromatin was then eluted, diluted to a final volume of 10 ml, and used for the proximity ligation step (performed for a minimum of 16 hours at 4ºC under extremely diluted conditions, i.e., < 0.2 ng DNA/µL, to favor ligation events within individual crosslinked chromatin complexes). Following the proximity ligation step, chromatin was treated with proteinase K, reverse crosslinked, and the DNA purified. ChIA-PET DNA was then digested with

MmeI, immobilized on streptavidin beads, and ligated to the ChIA-PET adapters. The DNA samples were finally proceeded through nick translation and a PCR amplification step to generate the library (number of cycles indicated in Fig. S16A). Libraries were ran on an agarose gel, and fragment of ~229 bp were gel-extracted, purified, and quantified using a quantus fluorometer.

2.5.17 Sequencing and computational analysis of Pol II ChIA-PET libraries

ChIA-PET libraries were sequenced on a HiSeq 2000 (JM08 and JM12) or a MiSeq (JM11) to a length of 90 bp (JM08), 100 bp (JM11), and 125 bp (JM12). Reads from the fastq files were processed to extract the tag 1 and 2 (i.e., read 1 and 2) along with their accompanying half-linker code using a custom-made Python script and generate two fastq files (R1 and R2 file) containing the sequence identifier, the raw sequence, and the sequence quality values for each tag. These two files were then aligned to the mouse genome (mm10 version) as paired-end reads using bowtie2 and the options -X 5 and --fast.

2.5.18 Paired-End Tags (PETs) filtering

Only paired tags with both reads mapping uniquely to the mouse genome were considered in our analysis. First, PETs were parsed based on the half-linker barcodes into non-chimeric PETs (specific products) or chimeric PETs (non-specific products) (Fig. 15A). Then, duplicated PETs (i.e., PCR duplicates) were removed for both chimeric and non-chimeric products. PETs with a tag location shifted by 1 bp compared to an existing PET were also considered as PCR duplicates and removed. Identical PET

found at both ZT6 and ZT18 for the same experiment (JM08, JM11 or JM12), and which likely originate from PCR errors due to priming from half-linkers, were also filtered out. Quality of the ChIA-PET experiments was assessed by determining the percentage of non-chimeric/specific *vs.* chimeric/non-specific PETs (Fig. 16C), the proportion of PETs with both tags being on the same chromosome (Fig. 16D), and the distance between each tag (Fig. 16B, D).

2.5.19 Functional analysis of the mouse liver Paired-End Tags (PETs)

PETs with both reads on the same chromosome and with a distance between reads ≥ 500 bp were only considered in our analysis (n = 218,639 PETs). For all PETs, each of the two tags was extended to 200 bp (tag location ± 100 bp) and this tag genomic location (chr:start-end) was used to map tags to (i) a gene, and (ii) a DNase I hypersensitive site, using intersectBed from bedtools (Quinlan and Hall, 2010). Gene coordinates were defined at TSS - 10kb to TTS + 1kb. Mapping to DHS was performed using a more stringent analysis of the mouse liver DNase-Seq datasets from ENCODE, and which mostly reports stronger DHSs (see Fig. 15D). This is because relaxation of the parameters for DNase-Seq analysis often consolidate several distinct DHS peaks into one DHS of several kilobases, thereby resulting into reporting PETs into the same DHS when both reads were distinctively located into two different DHS peaks. DHSs harboring a mouse liver BMAL1 peak were identified with intersectBed between the DHS peak list described above and the list of mouse liver ChIP-Seq peaks generated in this manuscript. To validate that mouse liver PETs contribute to gene transcription (Fig. 15B, 15C), we used public mouse liver Nascent-Seq datasets (Menet et al., 2012), and

averaged values for each of the 12 independent samples. Finally, we considered genes to be rhythmically expressed based on the analysis of the microarray datasets from Zhang and collaborators (Zhang et al., 2014), as described above.

2.5.20 Statistical analysis

Statistical analysis was carried out in JMP®, Version 12.0.1 SAS Institute., Cary, NC, 1989-2007. ChIP-Seq and DNase-Seq signals were analyzed using a Kruskal-Wallis test, and post-hoc analysis with a Wilcoxon each pair test. Analysis of TF mRNA expression between the three tissues was performed using a one-way ANOVA. Analysis of the differences in BMAL1 peaks genomic locations was performed using a chi-square test, and differences in the number of BMAL1 peaks per genomic locations we analyzed by a Fisher's exact test. Spearman correlation was used to determine the degree of correlation between signals (e.g., ChIP-Seq with DNA-Seq) or signal between tissues. Results were considered significant if p-value < 0.05 for the Kruskal-Wallis, student t-test and ANOVA tests, and p-value < 0.01 for Fisher's exact test.

2.5.21 Data availability

The sequencing datasets generated in this paper (BMAL1 ChIP-seq and Pol II ChIA-PET) have been deposited to GEO under the accession code GSE110604.

2.6 References

Aguilar-Arnal L, Hakim O, Patel VR, Baldi P, Hager GL, Sassone-Corsi P. 2013. Cycles in spatial and temporal chromosomal organization driven by the circadian clock. *Nature structural & molecular biology* **20**: 1206-1213.

Boergesen M, Pedersen TA, Gross B, van Heeringen SJ, Hagenbeek D, Bindesboll C, Caron S, Lalloyer F, Steffensen KR, Nebb HI et al. 2012. Genome-wide profiling of liver X receptor, retinoid X receptor, and peroxisome proliferator-activated receptor alpha in mouse liver reveals extensive sharing of binding sites. *Molecular and cellular biology* **32**: 852-867.

Bunger MK, Wilsbacher LD, Moran SM, Clendenin C, Radcliffe LA, Hogenesch JB, Simon MC, Takahashi JS, Bradfield CA. 2000. Mop3 is an essential component of the master circadian pacemaker in mammals. *Cell* **103**: 1009-1017.
Cho H, Zhao X, Hatori M, Yu RT, Barish GD, Lam MT, Chong LW, DiTacchio L, Atkins AR, Glass CK et al. 2012. Regulation of circadian behaviour and metabolism by REV-ERB-alpha and REV-ERB-beta. *Nature* **485**: 123-127.

Consortium GT. 2013. The Genotype-Tissue Expression (GTEx) project. *Nature genetics* **45**: 580-585.

Croci O, De Fazio S, Biagioni F, Donato E, Caganova M, Curti L, Doni M, Sberna S, Aldeghi D, Biancotto C et al. 2017. Transcriptional integration of mitogenic and mechanical signals by Myc and YAP. *Genes & development* **31**: 2017-2022.

Cusanovich DA, Hill AJ, Aghamirzaie D, Daza RM, Pliner HA, Berletch JB, Filippova GN, Huang X, Christiansen L, DeWitt WS et al. 2018. A Single-Cell Atlas of *In Vivo* Mammalian Chromatin Accessibility. *Cell*.
Dobin A, Davis CA, Schlesinger F, Drenkow J, Zaleski C, Jha S, Batut P, Chaisson M, Gingeras TR. 2013. STAR: ultrafast universal RNA-seq aligner. *Bioinformatics* **29**: 15-21.

Doi R, Oishi K, Ishida N. 2010. CLOCK regulates circadian rhythms of hepatic glycogen synthesis through transcriptional activation of Gys2. *The Journal of biological chemistry* **285**: 22114-22121.

Eckel-Mahan KL, Patel VR, de Mateo S, Orozco-Solis R, Ceglia NJ, Sahar S, Dilag-Penilla SA, Dyar KA, Baldi P, Sassone-Corsi P. 2013. Reprogramming of the circadian clock by nutritional challenge. *Cell* **155**: 1464-1478.

Endo M, Shimizu H, Nohales MA, Araki T, Kay SA. 2014. Tissue-specific clocks in Arabidopsis show asymmetric coupling. *Nature* **515**: 419-422.
Everett LJ, Le Lay J, Lukovac S, Bernstein D, Steger DJ, Lazar MA, Kaestner KH. 2013. Integrative genomic analysis of CREB defines a critical role for transcription factor networks in mediating the fed/fasted switch in liver. *BMC genomics* **14**: 337.
Faure AJ, Schmidt D, Watt S, Schwalie PC, Wilson MD, Xu H, Ramsay RG, Odom DT, Flicek P. 2012. Cohesin regulates tissue-specific expression by stabilizing highly occupied cis-regulatory modules. *Genome research* **22**: 2163-2175.
Fullwood MJ, Ruan Y. 2009. ChIP-based methods for the identification of long-range chromatin interactions. *Journal of cellular biochemistry* **107**: 30-39.

Gertz J, Savic D, Varley KE, Partridge EC, Safi A, Jain P, Cooper GM, Reddy TE, Crawford GE, Myers RM. 2013. Distinct properties of cell-type-specific and shared transcription factor binding sites. *Molecular cell* **52**: 25-36.

Gordon FK, Vallaster CS, Westerling T, Iyer LK, Brown M, Schnitzler GR. 2014. Research resource: Aorta- and liver-specific ERalpha-binding patterns and gene regulation by estrogen. *Mol Endocrinol* **28**: 1337-1351.

Gnocchi D, Pedrelli M, Hurt-Camejo E, Parini P. 2015. Lipids around the Clock: Focus on Circadian Rhythms and Lipid Metabolism. *Biology (Basel)* **4**: 104-132.

Grontved L, John S, Baek S, Liu Y, Buckley JR, Vinson C, Aguilera G, Hager GL. 2013. C/EBP maintains chromatin accessibility in liver and facilitates glucocorticoid receptor recruitment to steroid response elements. *The EMBO journal* **32**: 1568-1583.

He HH, Meyer CA, Hu SS, Chen MW, Zang C, Liu Y, Rao PK, Fei T, Xu H, Long H et al. 2014. Refined DNase-seq protocol and data analysis reveals intrinsic bias in transcription factor footprint identification. *Nature methods* **11**: 73-78.

Heinz S, Benner C, Spann N, Bertolino E, Lin YC, Laslo P, Cheng JX, Murre C, Singh H, Glass CK. 2010. Simple combinations of lineage-determining transcription factors prime cis-regulatory elements required for macrophage and B cell identities. *Molecular cell* **38**: 576-589.

Hesselberth JR, Chen X, Zhang Z, Sabo PJ, Sandstrom R, Reynolds AP, Thurman RE, Neph S, Kuehn MS, Noble WS et al. 2009. Global mapping of protein-DNA interactions *in vivo* by digital genomic footprinting. *Nature methods* **6**: 283-289.
Hughes ME, Hogenesch JB, Kornacker K. 2010. JTK_CYCLE: an efficient nonparametric algorithm for detecting rhythmic components in genome-scale data sets. *Journal of biological rhythms* **25**: 372-380.

Hu Z, Gallo SM. 2010. Identification of interacting transcription factors regulating tissue gene expression in human. *BMC genomics* **11**: 49.

Hurtado A, Holmes KA, Ross-Innes CS, Schmidt D, Carroll JS. 2011. FOXA1 is a key determinant of estrogen receptor function and endocrine response. *Nature genetics* **43**: 27-33.

Kieffer-Kwon KR, Tang Z, Mathe E, Qian J, Sung MH, Li G, Resch W, Baek S, Pruett N, Grontved L et al. 2013. Interactome maps of mouse gene regulatory domains reveal basic principles of transcriptional regulation. *Cell* **155**: 1507-1520.

Kim YH, Marhon SA, Zhang Y, Steger DJ, Won KJ, Lazar MA. 2018. Rev-erbalpha dynamically modulates chromatin looping to control circadian gene transcription. *Science* **359**: 1274-1277.

Koike N, Yoo SH, Huang HC, Kumar V, Lee C, Kim TK, Takahashi JS. 2012. Transcriptional architecture and chromatin landscape of the core circadian clock in mammals. *Science* **338**: 349-354.

Langmead B, Salzberg SL. 2012. Fast gapped-read alignment with Bowtie 2. *Nature methods* **9**: 357-359.

Leinonen R, Sugawara H, Shumway M, International Nucleotide Sequence Database C. 2011. The sequence read archive. *Nucleic acids research* **39**: D19-21.

Li G, Fullwood MJ, Xu H, Mulawadi FH, Velkov S, Vega V, Ariyaratne PN, Mohamed YB, Ooi HS, Tennakoon C et al. 2010. ChIA-PET tool for comprehensive chromatin interaction analysis with paired-end tag sequencing. *Genome biology* **11**: R22.

Li G, Ruan X, Auerbach RK, Sandhu KS, Zheng M, Wang P, Poh HM, Goh Y, Lim J, Zhang J et al. 2012. Extensive promoter-centered chromatin interactions provide a topological basis for transcription regulation. *Cell* **148**: 84-98.

Lim HW, Uhlenhaut NH, Rauch A, Weiner J, Hubner S, Hubner N, Won KJ, Lazar MA, Tuckermann J, Steger DJ. 2015. Genomic redistribution of GR monomers and dimers mediates transcriptional response to exogenous glucocorticoid *in vivo*. *Genome research* **25**: 836-844.

Ma D, Liu T, Chang L, Rui C, Xiao Y, Li S, Hogenesch JB, Chen YE, Lin JD. 2015. The Liver Clock Controls Cholesterol Homeostasis through Trib1 Protein-mediated Regulation of PCSK9/Low Density Lipoprotein Receptor (LDLR) Axis. *The Journal of biological chemistry* **290**: 31003-31012.

MacIsaac KD, Lo KA, Gordon W, Motola S, Mazor T, Fraenkel E. 2010. A quantitative model of transcriptional regulation reveals the influence of binding location on expression. *PLoS computational biology* **6**: e1000773.

Meireles-Filho AC, Bardet AF, Yanez-Cuna JO, Stampfel G, Stark A. 2014. cis-regulatory requirements for tissue-specific programs of the circadian clock. *Current biology : CB* **24**: 1-10.

Menet JS, Pescatore S, Rosbash M. 2014. CLOCK:BMAL1 is a pioneer-like transcription factor. *Genes & development* **28**: 8-13.

Menet JS, Rodriguez J, Abruzzi KC, Rosbash M. 2012. Nascent-Seq reveals novel features of mouse circadian transcriptional regulation. *eLife* **1**: e00011.

Mermet J, Yeung J, Hurni C, Mauvoisin D, Gustafson K, Jouffe C, Nicolas D, Emmenegger Y, Gobet C, Franken P et al. 2018. Clock-dependent chromatin topology modulates circadian transcription and behavior. *Genes & development* **32**: 347-358.

Mirny LA. 2010. Nucleosome-mediated cooperativity between transcription factors. *Proceedings of the National Academy of Sciences of the United States of America* **107**: 22534-22539.

Murakami M, Tognini P, Liu Y, Eckel-Mahan KL, Baldi P, Sassone-Corsi P. 2016. Gut microbiota directs PPARgamma-driven reprogramming of the liver circadian clock by nutritional challenge. *EMBO reports* **17**: 1292-1303.

Mure LS, Le HD, Benegiamo G, Chang MW, Rios L, Jillani N, Ngotho M, Kariuki T, Dkhissi-Benyahya O, Cooper HM et al. 2018. Diurnal transcriptome atlas of a primate across major neural and peripheral tissues. *Science*.

Neph S, Vierstra J, Stergachis AB, Reynolds AP, Haugen E, Vernot B, Thurman RE, John S, Sandstrom R, Johnson AK et al. 2012. An expansive human regulatory lexicon encoded in transcription factor footprints. *Nature* **489**: 83-90.

Panda S. 2016. Circadian physiology of metabolism. *Science* **354**: 1008-1015.
Panda S, Antoch MP, Miller BH, Su AI, Schook AB, Straume M, Schultz PG, Kay SA, Takahashi JS, Hogenesch JB. 2002. Coordinated transcription of key pathways in the mouse by the circadian clock. *Cell* **109**: 307-320.

Paquet ER, Rey G, Naef F. 2008. Modeling an evolutionary conserved circadian cis-element. *PLoS computational biology* **4**: e38.

Partch CL, Green CB, Takahashi JS. 2014. Molecular architecture of the mammalian circadian clock. *Trends in cell biology* **24**: 90-99.

Piper J, Assi SA, Cauchy P, Ladroue C, Cockerill PN, Bonifer C, Ott S. 2015. Wellington-bootstrap: differential DNase-seq footprinting identifies cell-type determining transcription factors. *BMC genomics* **16**: 1000.
Piper J, Elze MC, Cauchy P, Cockerill PN, Bonifer C, Ott S. 2013. Wellington: a novel method for the accurate identification of digital genomic footprints from DNase-seq data. *Nucleic acids research* **41**: e201.
Quinlan AR, Hall IM. 2010. BEDTools: a flexible suite of utilities for comparing genomic features. *Bioinformatics* **26**: 841-842.

Rey G, Cesbron F, Rougemont J, Reinke H, Brunner M, Naef F. 2011. Genome-wide and phase-specific DNA-binding rhythms of BMAL1 control circadian output functions in mouse liver. *PLoS biology* **9**: e1000595.
Sato S, Solanas G, Peixoto FO, Bee L, Symeonidi A, Schmidt MS, Brenner C, Masri S, Benitah SA, Sassone-Corsi P. 2017. Circadian Reprogramming in the Liver Identifies Metabolic Pathways of Aging. *Cell* **170**: 664-677 e611.

Sherwood RI, Hashimoto T, O'Donnell CW, Lewis S, Barkal AA, van Hoff JP, Karun V, Jaakkola T, Gifford DK. 2014. Discovery of directional and nondirectional pioneer

transcription factors by modeling DNase profile magnitude and shape. *Nature biotechnology* **32**: 171-178.

Sobel JA, Krier I, Andersin T, Raghav S, Canella D, Gilardi F, Kalantzi AS, Rey G, Weger B, Gachon F et al. 2017. Transcriptional regulatory logic of the diurnal cycle in the mouse liver. *PLoS biology* **15**: e2001069.

Stergachis AB, Neph S, Sandstrom R, Haugen E, Reynolds AP, Zhang M, Byron R, Canfield T, Stelhing-Sun S, Lee K et al. 2014. Conservation of trans-acting circuitry during mammalian regulatory evolution. *Nature* **515**: 365-370.

Storch KF, Lipan O, Leykin I, Viswanathan N, Davis FC, Wong WH, Weitz CJ. 2002. Extensive and divergent circadian gene expression in liver and heart. *Nature* **417**: 78-83.

Sung MH, Guertin MJ, Baek S, Hager GL. 2014. DNase footprint signatures are dictated by factor dynamics and DNA sequence. *Molecular cell* **56**: 275-285.

Takahashi JS. 2016. Transcriptional architecture of the mammalian circadian clock. *Nature reviews Genetics*.

Theodorou V, Stark R, Menon S, Carroll JS. 2013. GATA3 acts upstream of FOXA1 in mediating ESR1 binding by shaping enhancer accessibility. *Genome research* **23**: 12-22.

Thurman RE, Rynes E, Humbert R, Vierstra J, Maurano MT, Haugen E, Sheffield NC, Stergachis AB, Wang H, Vernot B et al. 2012. The accessible chromatin landscape of the human genome. *Nature* **489**: 75-82.

Trapnell C, Roberts A, Goff L, Pertea G, Kim D, Kelley DR, Pimentel H, Salzberg SL, Rinn JL, Pachter L. 2012. Differential gene and transcript expression analysis of RNA-seq experiments with TopHat and Cufflinks. *Nature protocols* **7**: 562-578.

Trott AJ, Menet JS. 2018. Regulation of circadian clock transcriptional output by CLOCK:BMAL1. *PLoS genetics* **14**: e1007156.

Vierstra J, Rynes E, Sandstrom R, Zhang M, Canfield T, Hansen RS, Stehling-Sun S, Sabo PJ, Byron R, Humbert R et al. 2014. Mouse regulatory DNA landscapes reveal global principles of cis-regulatory evolution. *Science* **346**: 1007-1012.

Wang N, Yang G, Jia Z, Zhang H, Aoyagi T, Soodvilai S, Symons JD, Schnermann JB, Gonzalez FJ, Litwin SE et al. 2008. Vascular PPARgamma controls circadian variation in blood pressure and heart rate through Bmal1. *Cell metabolism* **8**: 482-491.

Xie Z, Su W, Liu S, Zhao G, Esser K, Schroder EA, Lefta M, Stauss HM, Guo Z, Gong MC. 2015. Smooth-muscle BMAL1 participates in blood pressure circadian rhythm regulation. *The Journal of clinical investigation* **125**: 324-336.

Yeung J, Mermet J, Jouffe C, Marquis J, Charpagne A, Gachon F, Naef F. 2017. Transcription factor activity rhythms and tissue-specific chromatin interactions explain circadian gene expression across organs. *Genome research*.

Yoshitane H, Ozaki H, Terajima H, Du NH, Suzuki Y, Fujimori T, Kosaka N, Shimba S, Sugano S, Takagi T et al. 2014. CLOCK-controlled polyphonic regulation of circadian rhythms through canonical and noncanonical E-boxes. *Molecular and cellular biology* **34**: 1776-1787.

Yue F Cheng Y Breschi A Vierstra J Wu W Ryba T Sandstrom R Ma Z Davis C Pope BD et al. 2014. A comparative encyclopedia of DNA elements in the mouse genome. *Nature* **515**: 355-364.

Zaret KS, Carroll JS. 2011. Pioneer transcription factors: establishing competence for gene expression. *Genes & development* **25**: 2227-2241.

Zhang J, Poh HM, Peh SQ, Sia YY, Li G, Mulawadi FH, Goh Y, Fullwood MJ, Sung WK, Ruan X et al. 2012a. ChIA-PET analysis of transcriptional chromatin interactions. *Methods* **58**: 289-299.

Zhang R, Lahens NF, Ballance HI, Hughes ME, Hogenesch JB. 2014. A circadian gene expression atlas in mammals: implications for biology and medicine. *Proceedings of the National Academy of Sciences of the United States of America* **111**: 16219-16224.

Zhang Y, Fang B, Emmett MJ, Damle M, Sun Z, Feng D, Armour SM, Remsberg JR, Jager J, Soccio RE et al. 2015. GENE REGULATION. Discrete functions of nuclear receptor Rev-erbalpha couple metabolism to the clock. *Science* **348**: 1488-1492.

Zhang Y, Laz EV, Waxman DJ. 2012b. Dynamic, sex-differential STAT5 and BCL6 binding to sex-biased, growth hormone-regulated genes in adult mouse liver. *Molecular and cellular biology* **32**: 880-896.

CHAPTER III

DESIGNING AN ASSAY TO TEASE APART THE ROLE OF ENHANCER-ENHANCER INTERACTIONS AND THE INTRINSIC ACTIVITY OF AN ENHANCER

3.1 Overview

Nearly every mammalian cell harbors a molecular circadian clock that relies on the heterodimeric transcription factor (TF) CLOCK:BMAL1 to drive rhythmic gene expression in a tissue-specific manner. Previous findings from our lab and others indicate that the rhythmic transcription of CLOCK:BMAL1 target genes coincides with rhythmic interactions between CLOCK:BMAL1-bound enhancers and other enhancers (Aguilar-Arnal and Sassone-Corsi, 2013; Beytebiere et al., 2019; Kim et al., 2018a; Mermet et al., 2018; Yeung et al., 2018). Based on these findings, we hypothesized that CLOCK:BMAL1-bound enhancers rhythmically interact with other enhancers to regulate their activity and initiate rhythmic target gene transcription. In this chapter, I describe the development of a technique that aims at assessing *in vivo* in mouse liver the activity of individual enhancers when they are free from interactions with other enhancers. This technique relies on cloning an enhancer-of-interest upstream of a reporter gene in a plasmid and transfecting this plasmid in the mouse liver cells by hydrodynamic tail vein injection. Our data, which are still preliminary, strongly suggest that this technique may be valuable to not only determine the intrinsic activity of enhancers, but also assess whether enhancer-enhancer interactions impact enhancer activity to initiate rhythmic gene expression.

3.2 Introduction

The circadian clock drives the rhythmic expression of about twenty percent of the mouse liver transcriptome, and over half the mouse genome is rhythmically expressed in at least one tissue (Menet et al., 2012; Zhang et al., 2014). In mammals, the molecular clock relies on the heterodimeric transcription factor (TF) CLOCK:BMAL1 to initiate directly and indirectly genome-wide rhythmic transcription. Recent characterization of BMAL1 cistromes in different tissues revealed that BMAL1 DNA binding is largely tissue-specific, mostly because BMAL1 binds tissue-specific *cis*-regulatory regions (i.e., enhancers and promoters) and cooperates with tissue-specific TFs (ts-TFs) to bind DNA at *cis*-regulatory regions common to several tissues (Beytebiere et al., 2019; Perelis et al., 2015). Surprisingly however, CLOCK:BMAL1 tissue-specific binding is not sufficient to account for tissue-specific rhythmic gene expression. Recent characterization of the 3-D genome by us and others suggests that enhancer-enhancer interactions play a crucial role in driving rhythmic gene expression (Aguilar-Arnal et al., 2013; Beytebiere et al., 2019; Kim et al., 2018a; Mermet et al., 2018; Yeung et al., 2018). Based on these data, we hypothesize that CLOCK:BMAL1-bound enhancers rhythmically interact with other enhancers to regulate their activity and drive rhythmic gene expression. A corollary of this hypothesis is that when other non-rhythmic enhancers regulate the activity of CLOCK:BMAL1-bound enhancers by constitutive interactions that in turn drives constitutive expression. The consequences of this hypothesis are that CLOCK:BMAL1-bound enhancers intrinsic activity when

removed from the chromatin context (without enhancer-enhancer interactions) will be rhythmically active. Non-rhythmic enhancers intrinsic activity when removed from the chromatin context (without enhancer-enhancer interactions) will be unable to drive rhythmic gene expression, regardless of the expression in the genomic context.

To test our hypothesis, we sought to design an assay to determine the intrinsic activity of an enhancer *in vivo*, *i.e*., when this enhancer is removed from functional enhancer-enhancer interactions, and to compare enhancer intrinsic activity to enhancer activity when in chromatin, *i.e.*, when subjected to enhancer-enhancer regulation. Additionally, we aimed at using our previously published ChIA-PET dataset to assess the contribution of CLOCK:BMAL1 enhancers and of enhancer-enhancer interactions to rhythmic gene expression. Our results, which are based on the utilization of vectors designed for long-term reporter expression when transfected in the liver by hydrodynamic tail vein injection, suggest that our strategy will be successful at measuring the intrinsic activity of an enhancer *in vivo*. For example, transfection of a vector carrying a reporter gene under the transcriptional control of a circadian enhancer located in the *Nr1d1* gene loci was sufficient to drive rhythmic expression of the reporter gene. We predict that this technique will be useful to address the role of enhancer-enhancer interactions in coordinating enhancer activity and driving rhythmic gene expression.

Figure 18. The contribution of enhancer-enhancer interactions and intrinsic enhancer activity to rhythmic gene expression.
A graphical depiction of the hypothesis for enhancer activity in a native chromatin state versus the intrinsic activity of an enhancer in the episomal state.

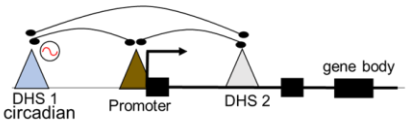

	Rhythmic BMAL1 targets				Arrhythmic BMAL1 targets		
	DHS 1	Prom	DHS 2		DHS 1	Prom	DHS 2
chromosomal	∿	∿	∿		—	—	—
episomal	∿	—	—		∿	—	—

3.3 Results

3.3.1 Cloning strategy for the long-term measurement of enhancer activity *in vivo* in mouse liver

To measure the intrinsic activity of enhancers *in vivo* in mouse liver, we decided to use the pLIVE® plasmid system along with hydrodynamic tail vein injection. Previous findings have shown that utilization of liver-specific gene promoter (*e.g.*, minimal albumin promoter) is more efficient than exogenous/generic promoter (*e.g.*, cytomegalovirus -CMV- promoter) to maintain sustained episomal reporter expression over weeks and even months (Herweijer et al., 2001; Stenler et al., 2014). Indeed, exogenous promoters like CMV can generate high transcription levels, yet, this high expression is only maintained for about a day because exogenous promoters are quickly targeted for DNA methylation on CpG and their activity is subsequently downregulated (Herweijer et al., 2001). pLIVE® vectors carry a reporter gene (either *β-galactosidase* or *Secreted embryonic alkaline phosphatase -Seap-*) under the control of mouse cis-regulatory elements: an *Albumin* minimal promoter and an *Alpha-fetoprotein* (*Afp*) enhancer. Previous studies have shown that the minimal albumin promoter is

necessary but not sufficient to drive transcription (Descombes et al., 1990; Izban and Papaconstantinou, 1989; Maire et al., 1989; Milos and Zaret, 1992), and that the *Afp* enhancer region can promote transcription when linked to the the *Albumin* promoter (Jin et al., 2009). Based on this data, we reasoned that replacing the *Afp* enhancer with our enhancers of interest would enable us to assay for intrinsic enhancer activity.

To determine if our strategy would be sufficient to measure rhythmic enhancer activity, we chose an enhancer located in the *Nr1d1* gene locus because *Nr1d1* is a core clock gene that is targeted by CLOCK:BMAL1 and it is strongly rhythmically expressed with a phase coincidental to CLOCK:BMAL1 DNA binding (Fig 19A, 19C). We also chose to insert three repeats of a small portion of the *Nr1d1* enhancer rather than inserting a single copy of the full enhancer for several reasons. First, we sought to include CLOCK:BMAL1 DNA binding sites and eliminate other potential binding sites for other TFs. Previous studies have also shown that CLOCK:BMAL1 binds E-boxes (CACGTG sequence), and preferentially when separated by a six or seven base pair spacer (Yoshitane et al., 2014). Analysis of the candidate *Nr1d1* enhancer revealed the presence of two perfect E-boxes, as well as a degenerate E-Box seven base pair away of each perfect E-box (Fig 19A, 19C). We thus selected this 65 base pair region that contain two perfect E-boxes for our cloning strategy. Second, we chose to multimerize this CLOCK:BMAL1 DNA binding region three times, because many reports in the literature indicate that multimerization of DNA binding sites enhances transcription activation (Blain et al., 2010; Hollevoet et al., 2018; Rushton, 2016; Su et al., 2002).

Finally, we chose to use *Seap* as the reporter gene. First, SEAP is secreted into the bloodstream and thus reporter gene expression can be measured in the blood without

having to euthanize the animal. SEAP phosphatase activity can be measured from blood samples using commercially available kits such as the Applied Biosystems Phospha-Light™ SEAP Reporter Gene Assay System. (Fig 19A, 19B).

Cloning the *Nr1d1* enhancer into the pLIVE® *Seap* plasmid has been performed using standard cloning protocols. We first removed the *Afp* enhancer using restriction enzymes and added the three *Nr1d1* enhancers to the same plasmid in triplicate.

Figure 19. Cloning the *Nr1d1* upstream enhancer in the pLIVE® *Seap* vector

(A) A gene browser view of the BMAL1 ChIP-seq signal in the mouse liver at ZT6 the peak phase of BMAL1 binding. (B) A graph depicting the gene expression from microarray data for *Nr1d1* from Zhang et al., 2014. (C) A schematic design of the altered pLIVE® *Seap* vector with three copies of the *Nr1d1* enhancer and without the AFP enhancer. The red box contains the sequence of the triplicate *Nr1d1* enhancer. The yellow highlight signifies a perfect E-box, and the blue highlight signifies a degenerate E-box. The plasmid also contains a minimal albumin promoter.

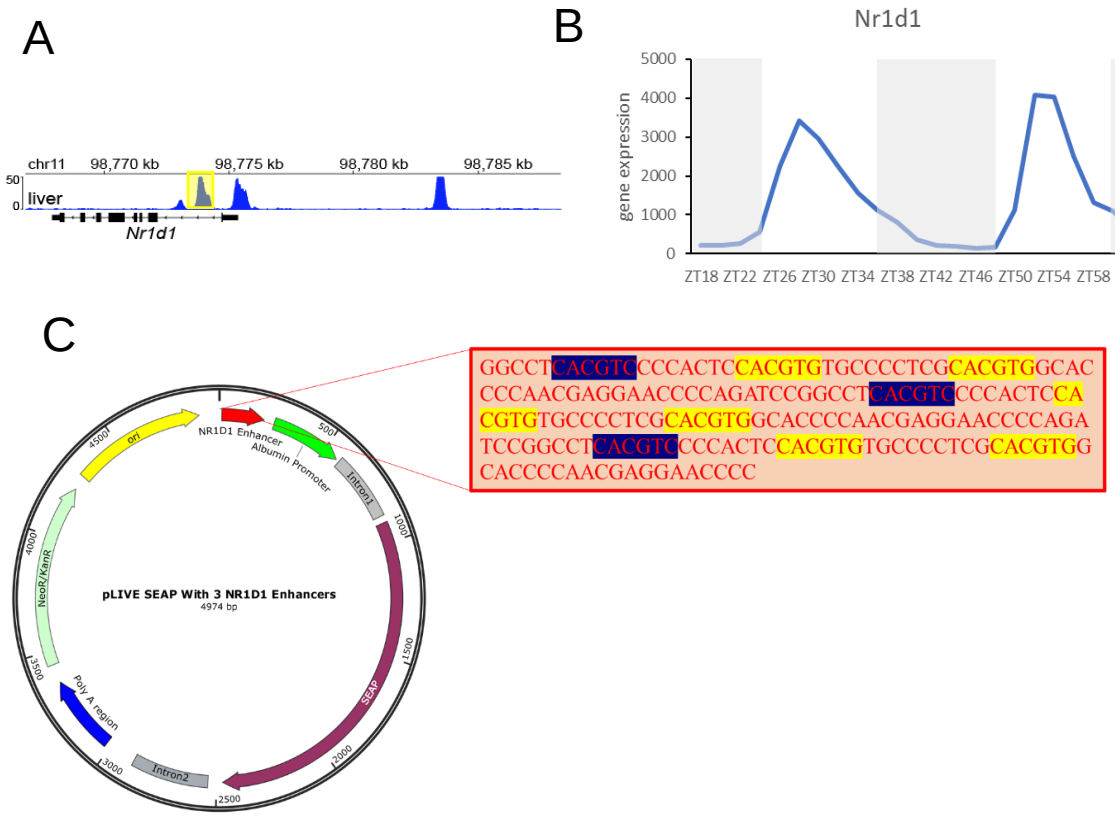

3.3.2 Hydrodynamic tail vein injection as an effective means for delivery of plasmids to the mouse liver for *in vivo* expression studies

We used the technique of hydrodynamic tail vein injection to deliver plasmids to the mouse liver. Previous studies have shown that this technique is efficient at targeting plasmids to the liver, with very little expression in other tissues (Kovacsics and Raper, 2014; Meyer-Kovac et al., 2017; Nguyen et al., 2008). Hydrodynamic tail vein injections rely on an injection of a large volume of fluid containing plasmids into the mouse tail vein (roughly ten percent of the body weight of the mouse) which exceeds the cardiac output. This injection of fluid then causes a development of a high pressure which leads to a backflow of solution towards the organs where the vast majority will be absorbed by the liver (Fig 20) (Meyer-Kovac et al., 2017; Nguyen et al., 2008).

Figure 20. Hydrodynamic tail vein injection of plasmids as a means to assay enhancer activity.

A diagram for the hydrodynamic tail vein injection technique. The technique relies on a large volume of fluid (ten percent of the mouse's body weight) to be injected into the tail vein with 50 micrograms of plasmid such that the cardiac output is exceeded. This leads to the development of a high pressure, a backflow of solution towards the organs through the inferior vena cava, and the liver will absorb most of the injected solution and the plasmids.

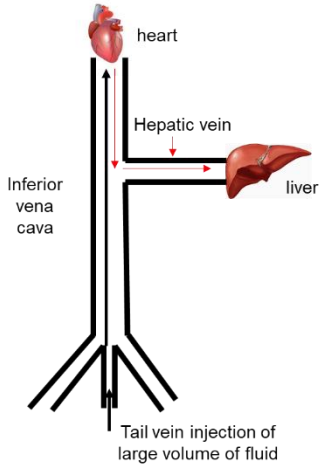

To determine the rate of transfection using the hydrodynamic tail vein injection, we injected fifty micrograms of the pLIVE® lacZ vector under the control of the minimal albumin promoter and the AFP enhancer (Fig 21A). Two weeks post-injection, mice were euthanized, and the liver collected and processed for *β-galactosidase* activity assay using standard X-Gal staining on 20 µm liver sections. X-gal staining could be observed in roughly ten percent of the cells, indicating that we were able to successfully transfect plasmids in the liver (Fig 21B). The injections of both the pLIVE® lacZ and triplicate *Nr1d1* pLIVE® resulted in a modest degree of transfection, however the transfection efficiency was better for the *Nr1d1*-driven *Seap* plasmid and this may be due to this plasmid being smaller in size or the injection of 50µg of plasmid instead of 25 µg of plasmid (Fig 21C).

Figure 21. The pLIVE® lacZ vector confirms successful hydrodynamic tail vein injection.

(A) Depicts a X-gal staining of a liver from a male wild-type mouse that underwent a hydrodynamic tail vein injection. The mouse was injected with fifty micrograms of plasmid in a 2.5mL total volume of TRANSIT-EE® solution. The liver was sectioned in 12 micrometer slices and then stained with X-gal and counterstained with picrosirius red. (B) Schematic of the pLIVE® lacZ vector that was used for the hydrodynamic tail vein injection. The expression of lacZ is driven by a minimal albumin promoter and the AFP enhancer. (C) The number of plasmids found on average in a mouse liver cell based on qPCR analysis with a 50µg injection for *Seap* and a 25µg injection for lacZ. The error bars represent the standard error.

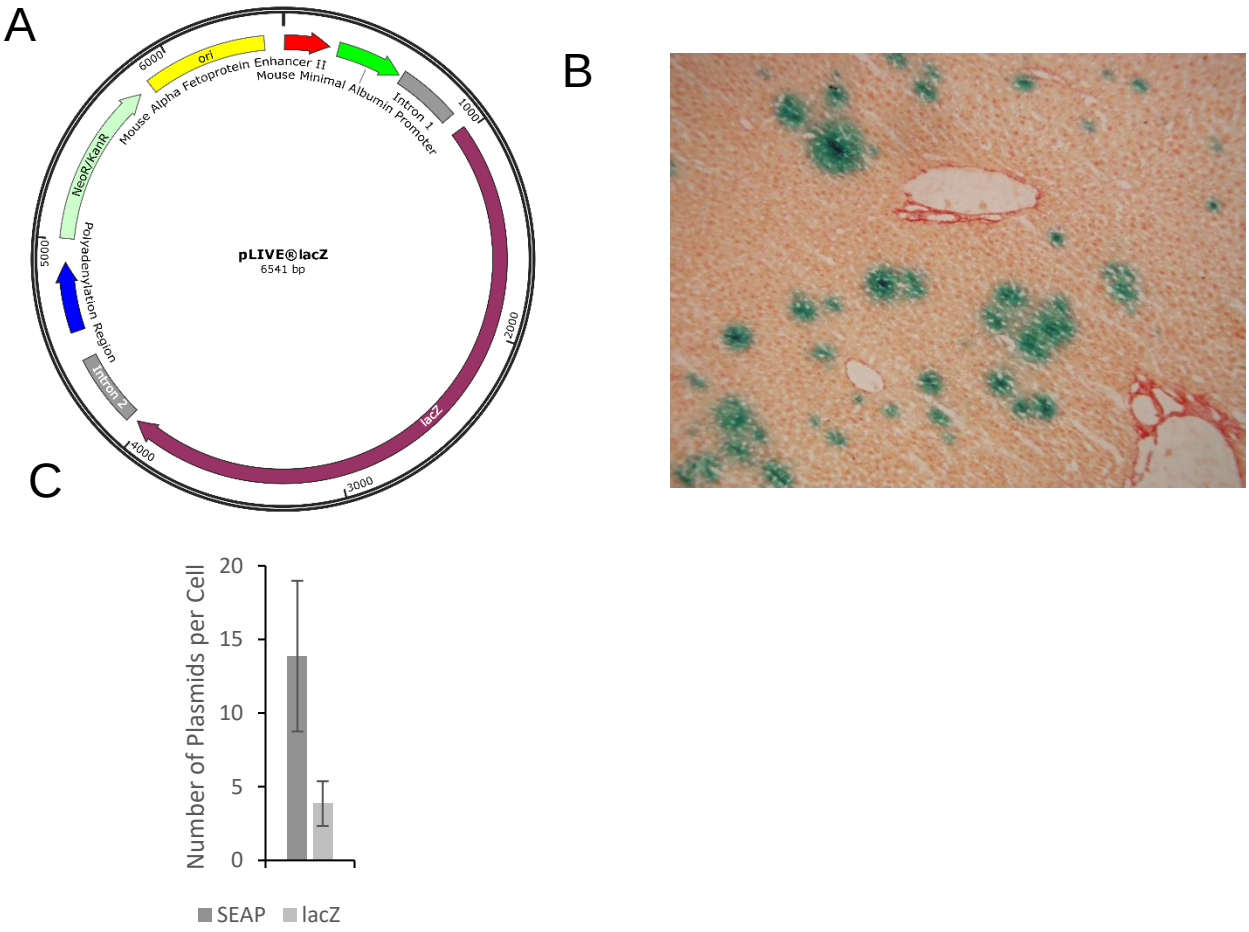

3.3.3 SEAP Protein Levels Can be Measured in the Blood but do Not Show Rhythms

To determine the intrinsic activity of the *Nr1d1* enhancer, six male mice were injected with EE-solution (Mirus) (a patented solution that has shown to deliver higher

transfection efficiency using hydrodynamic tail vein injection) with fifty micrograms of the pLIVE® vector containing three copies of the *Nr1d1* enhancer and twenty-five micrograms of the lacZ vector such that the level of SEAP protein could be measured from the blood without euthanizing the animal over the course of the day. We performed blood draws of 5μL every four hours for twenty-four hours for the six injected mice. We found the overall SEAP activity levels to be highly variable and there were no discernable rhythms in the levels of SEAP phosphatase activity between the six animals (Fig 22A). The results were thus inconclusive as to whether the transcription driven by *Nr1d1* is rhythmic. There were three major reasons that could account for *Seap* failing to be expressed rhythmically: (i) the D-box element in the minimal *Albumin* promoter, which has a significant effect on the transcription of *Albumin* (Maire et al., 1989), is causing a negative interaction since it is a target of another circadian component DBP, (ii) the *Nr1d1* enhancer is unable to drive expression, and/or (iii) the transcription driven by the three *Nr1d1* enhancers is rhythmic but the secretion of SEAP into the blood is not rhythmic and/or in phase between animals. We decided to test this last possibility by measuring *Seap* mRNA in mouse liver.

To further test these hypotheses, we euthanized three mice at ZT6 and three mice at ZT18 such that mRNA levels could be determined for the middle of the day and the middle of the night.

Figure 22. *Nr1d1* drives strong and rhythmic expression of *Seap* from the pLIVE® vector
(A) Measurement of the luminescence of the Seap vector using a kit from applied biosystems from 2.5 µL of blood from male mice. The enrichment was calculated by taking the wavelength the substrate luminesces at over a wavelength without luminescence. Measurements were recorded every four hours over a twenty-four hour time period. (B) The level of protein enrichment in the blood for the pLIVE® *Seap* vector driven by the AFP enhancer, a single *Nr1d1* enhancer, and triplicate *Nr1d1* enhancer. (C) The level of mRNA expression from the pLIVE® *Seap* and pLIVE® lacZ vector normalized to the plasmid copy number. (D) The level of mRNA expression from the pLIVE® *Seap* vector over the mRNA expression from pLIVE® lacZ vector. The *Nr1d1* and *Bmal1* expression from the same mice. (E) The mRNA expression level of *Nr1d1* and *Bmal1* at ZT6 and ZT18 from the mice that were injected with the pLIVE® *Seap* and lacZ vectors.

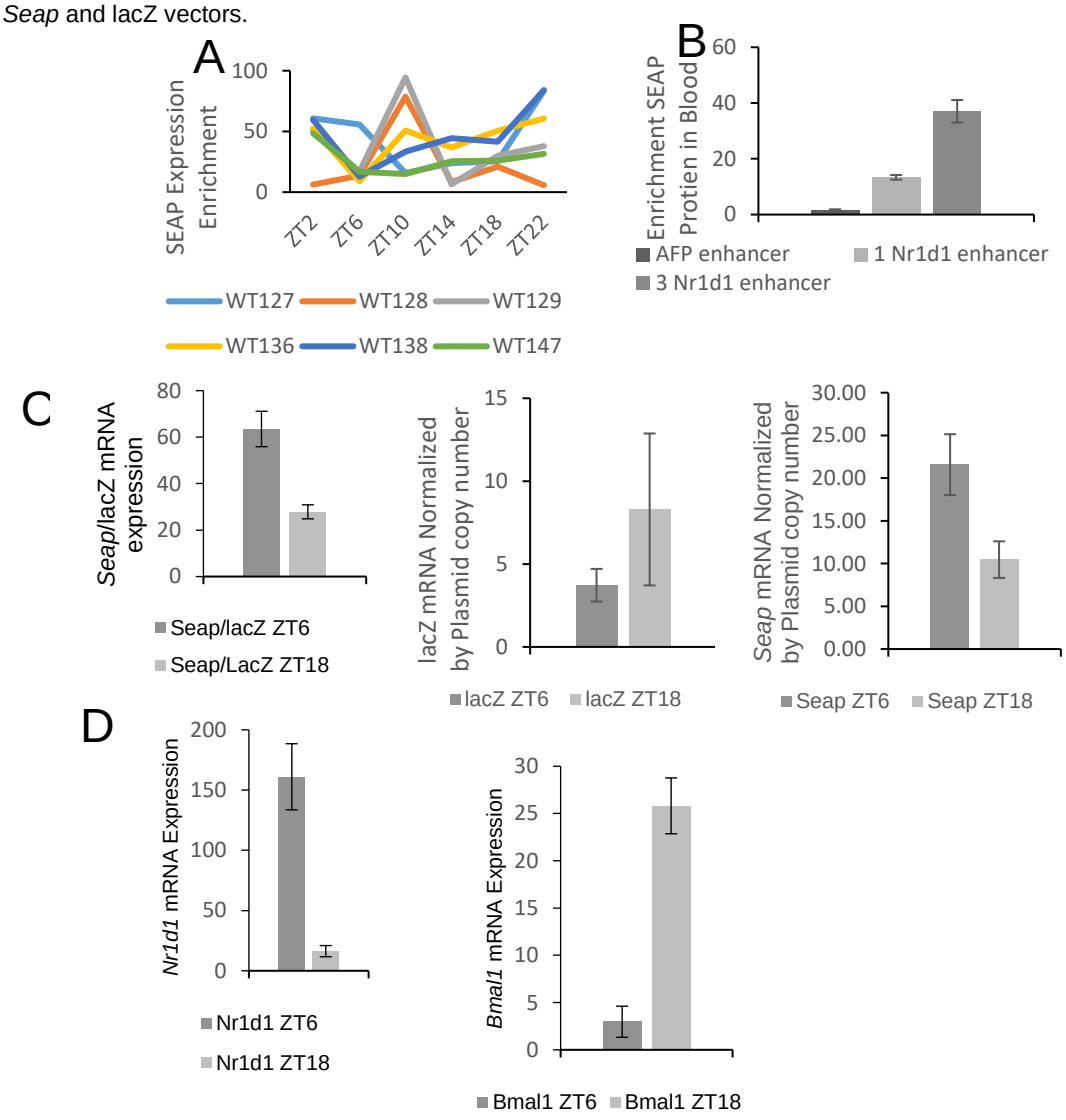

3.3.4 The pLIVE *Seap* vector is highly expressed and in-phase with *Nr1d1* enhancer driven expression

To determine if the triplicate *Nr1d1* enhancer construct is able to drive rhythmic gene expression, we euthanized three mice during the middle of the light phase (ZT6)

and three mice during middle of the dark phase (ZT18), and collected the liver. Total RNA was then extracted and processed to determine if there were day/night differences in gene expression. To first confirm that hydrodynamic tail vein injection did not impair endogenous circadian rhythms in mouse liver, we performed qPCR for *Nr1d1* and *Bmal1* pre-mRNA transcripts (Fig. 22D). We found that the data was in line with the peak phase of both *Nr1d1* and *Bmal1*, with *Nr1d1* being expressed ten-fold higher during the day and *Bmal1* being expressed five-fold more during the night. We then examined *Seap* mRNA expression and found that the *Seap* transcripts levels were two-fold higher at ZT6 than ZT18 (Fig 22C). We standardized the expression of *Seap* with the expression of lacZ as lacZ expression should remain relatively constant throughout the course of the day as it does not contain the three *Nr1d1* enhancers. *Seap* mRNA enrichment at ZT6 showed the same day night enrichment when standardized to the number of plasmids in the mouse liver (Fig 22B). The rhythm of *Seap* mRNA does not reflect the level of rhythm with *Nr1d1* expression. Together, our data showed that the *Nr1d1* enhancers can drive rhythmic gene expression, and thus indicate that this technique can be used to measure the intrinsic activity of enhancers.

3.3.5 The *Nr1d1* Enhancer is a Stronger Driver of Transcription Than AFP in the pLIVE® Vector

To determine the strength of the *Nr1d1* enhancer, we injected the *Seap* pLIVE® plasmid that either contained the *Afp* enhancer, one *Nr1d1* enhancer (*i.e.*, the 65 base pair region, see above), or the triplicate *Nr1d1* enhancer. We found that the *Afp* enhancer had the lowest levels of SEAP activity in the blood, while the triplicate *Nr1d1*

enhancer was able to produce the highest levels of SEAP activity (Fig 22B). Moreover, the triplicate *Nr1d1* enhancer resulted in about three times more SEAP activity than the single *Nr1d1* enhancer, indicating that additional E-boxes were able to promote increased transcription activation. Our data also showed a strong correlation between the protein levels measured in the blood and the mRNA measured via qPCR.

Together, these results suggest that assaying SEAP activity in the blood can be used to test for transfection efficiency of the pLIVE® plasmids, but that it is not appropriate for measuring 24-hour rhythms in enhancer activity (Fig 22A).

3.4 Discussion

The circadian clock plays a vital role in driving rhythmic gene expression allowing organisms to anticipate rhythmic daily oscillations. Previous reports have shown that even though CLOCK:BMAL1 target many genes in the mouse liver, only a fraction of these genes are rhythmically expressed in phase with the rhythmic binding of CLOCK:BMAL1 to DNA (Beytebiere et al., 2019). The fact that many CLOCK:BMAL1 targets are arrhythmic is counterintuitive to the idea that CLOCK:BMAL1 is the sole driver of rhythmic gene expression and highlights the importance of the enhancer-enhancer interactions in driving rhythmic gene expression. Circadian enhancers have been shown to have an important role in driving rhythmic gene expression (Beytebiere et al., 2019; Kim et al., 2018a; Yeung et al., 2018). For these reasons, we sought to develop a technique that would allow us to tease apart the contribution to rhythmic gene expression from both the enhancer-enhancer interactions as well as the role of the intrinsic activity of the enhancer.

The delivery of multiple plasmids per liver cell and the visible transfection of about ten percent of the liver indicate that plasmid delivery via hydrodynamic tail vein injection will provide sufficient resolution to address the role of the intrinsic enhancer activity to rhythmic gene expression. The data shows that the quantity of SEAP protein in the blood provides insight into the amount of expression of the protein. However, the time resolution does not match the expression data which is possibly due to complications with the secretion of the protein. The expression data suggest that the *Nr1d1* enhancer is capable of driving rhythmic gene expression in both its native chromatin context as well as in an episomal context. Further experiments will be needed to determine if the *Nr1d1* enhancer drives rhythmic expression across a six time-point rhythm as currently only day-night differences have been observed.

Future directions for this project would be to perform hydrodynamic tail vein injections with multiple plasmids. Anywhere from ten to one hundred plasmids at a time could be used with a barcode in the 3' UTR to differentiate them. It remains unclear how many plasmid constructs could be used in one animal, and the optimal number of plasmids will need to be experimentally determined. Different nucleotide barcodes could be added to the 3'UTR of each plasmid, such that each plasmid could use a unique primer for amplification in qPCR to determine the amount of gene expression for each enhancer. To dissect the role of the individual enhancer and enhancer-enhancer interactions, it would be relevant to add enhancers to the plasmids that target the exact same gene in their native chromatin context. This would allow us to tease apart the role of intrinsic enhancer activity and enhancer-enhancer interactions. Future studies should address this role in genes that are BMAL1 targets, and which are either rhythmic in-

phase with BMAL1 binding, rhythmic out-of-phase with BMAL1 binding, arrhythmic, or not expressed.

Further studies will also likely need to address the role of enhancer-enhancer interactions to a greater depth. The ChIA-PET performed previously in the Menet laboratory would provide a deeper insight if it was sequenced at a much greater depth (Beytebiere et al., 2019). Indeed, the current resolution of the ChIA-PET datasets is not sufficient enough to draw conclusions about individual interactions between enhancers. After these techniques are established in the mouse liver, they could be carried over to other tissues such as the kidneys and the heart to determine if enhancer-enhancer interactions have a similar role across multiple tissues to drive rhythmic gene expression (Woodard et al., 2018). This would allow stronger conclusions on the role of the circadian clock in driving tissue-specific rhythmic gene expression.

3.5 Methods

3.5.1 Animals

Male C57BL/6J and were housed under 12 h light:12 h dark (LD12:12) with food and water available *ad libitum*. All experiments were approved by the Texas A&M University Institutional Animal Care and Use Committee.

3.5.2 Hydrodynamic tail vein injection

Hydrodynamic tail vein injections were performed as described by Kovacsics and colleagues. The mice were first weighed and a volume equivalent to ten percent the

body weight was injected. The syringes were prepared for injection with TRANSIT-EE® solution (Mirus) biosciences. The plasmid was mixed in the solution according to the weight of the mouse such that each mouse would receive 50 µg of plasmid. A sterile twenty-gauge one-half inch needle was used for the injections. Mice cages were placed on heating pads, and the mice were sufficiently warmed prior to the injection. The mice were placed on heating pads between 38-39°C for twenty to thirty minutes prior to injection such that the blood vessels would dilate. Once the mice were prepared for injection, they were inserted into a fifty-milliliter falcon tube were the tail was wiped with an ethanol wipe to make the vein easier to see. The falcon tube was restrained by taping it to a flat surface with laboratory tape. The solution is then completely injected in one slow steady motion over the course of a few seconds. After the injection the mice are then returned to the 38-39°C cage for several minutes until they have recovered from the injection at which point, they are then returned to their original cage. The mice were monitored for several days to ensure no complications would arise.

3.5.3 SEAP detection from blood

To detect SEAP from the blood we first snipped a ~1mm portion of the mouse tail. Then collected the blood via capillary tube, and then add the blood to a heparinized tube. After collection the blood was kept on ice for the remainder of the collection. The blood is then centrifuged at 10,000g for 5 minutes. The plasma was then removed in 5µL increments and frozen in a -80°C freezer. The 5µL of plasma is diluted to 50µL with water and the applied biosystems kit (Phospha-Light™ SEAP Reporter Gene

Assay System catalog number T1015) is then used to determine the amount of SEAP in the blood.

3.5.4 mRNA expression detection

Mouse livers were flash frozen and crushed with a mortar and pestle and divided into twelve tubes. One tube was taken and resuspended in Trizol and then phenol chloroform extracted. Reverse transcription was performed with MMLV reverse transcriptase made in house. qPCR was performed with a Bio-Rad CFX connect and Bio-Rad qPCR master mix.

3.6 References

Aguilar-Arnal, L., and Sassone-Corsi, P. (2013). The circadian epigenome: how metabolism talks to chromatin remodeling. Curr Opin Cell Biol.

Beytebiere, J.R., Trott, A.J., Greenwell, B.J., Osborne, C.A., Vitet, H., Spence, J., Yoo, S.-H., Chen, Z., Takahashi, J.S., Ghaffari, N.*, et al.* (2019). Tissue-specific BMAL1 cistromes reveal that rhythmic transcription is associated with rhythmic enhancer–enhancer interactions. Genes & Development *33*, 294-309.

Blain, M., Zeng, Y., Bendjelloul, M., Hallauer, P.L., Kumar, A., Hastings, K.E.M., Karpati, G., Massie, B., and Gilbert, R. (2010). Strong Muscle-Specific Regulatory Cassettes Based on Multiple Copies of the Human Slow Troponin I Gene Upstream Enhancer. *21*, 127-134.

Descombes, P., Chojkier, M., Lichtsteiner, S., Falvey, E., and Schibler, U. (1990). LAP, a novel member of the C/EBP gene family, encodes a liver-enriched transcriptional activator protein. Genes Dev *4*, 1541-1551.

Herweijer, H., Zhang, G., Subbotin, V.M., Budker, V., Williams, P., and Wolff, J.A. (2001). Time course of gene expression after plasmid DNA gene transfer to the liver. *3*, 280-291.

Hollevoet, K., De Smidt, E., Geukens, N., and Declerck, P. (2018). Prolonged in vivo expression and anti-tumor response of DNA-based anti-HER2 antibodies. Oncotarget *9*.

Izban, M.G., and Papaconstantinou, J. (1989). Cell-specific expression of mouse albumin promoter. Evidence for cell-specific DNA elements within the proximal promoter region and cis-acting DNA elements upstream of -160. J Biol Chem *264*, 9171-9179.

Jin, L., Long, L., Green, M.A., and Spear, B.T. (2009). The alpha-fetoprotein enhancer region activates the albumin and alpha-fetoprotein promoters during liver development. Dev Biol *336*, 294-300.

Kim, Y.H., Marhon, S.A., Zhang, Y., Steger, D.J., Won, K.-J., and Lazar, M.A. (2018). Rev-erbα dynamically modulates chromatin looping to control circadian gene transcription. Science *359*, 1274-1277.

Kind, J., Pagie, L., Sandra, Nahidiazar, L., Siddharth, Bienko, M., Zhan, Y., Lajoie, B., Carolyn, Amendola, M*., et al.* (2015). Genome-wide Maps of Nuclear Lamina Interactions in Single Human Cells. Cell *163*, 134-147.

Kovacsics, D., and Raper, J. (2014). Transient expression of proteins by hydrodynamic gene delivery in mice. J Vis Exp.

Maire, P., Wuarin, J., and Schibler, U. (1989). The role of cis-acting promoter elements in tissue-specific albumin gene expression. *244*, 343-346.

Meireles-Filho, A.C., Bardet, A.F., Yanez-Cuna, J.O., Stampfel, G., and Stark, A. (2014). cis-regulatory requirements for tissue-specific programs of the circadian clock. Curr Biol *24*, 1-10.

Menet, J.S., Rodriguez, J., Abruzzi, K.C., and Rosbash, M. (2012). Nascent-Seq reveals novel features of mouse circadian transcriptional regulation. eLife *1*, e00011

Mermet, J., Yeung, J., Hurni, C., Mauvoisin, D., Gustafson, K., Jouffe, C., Nicolas, D., Emmenegger, Y., Gobet, C., Franken, P*., et al.* (2018). Clock-dependent chromatin topology modulates circadian transcription and behavior. Genes Dev *32*, 347-358.

Meyer-Kovac, J., Kolbe, I., Ehrhardt, L., Leliavski, A., Husse, J., Salinas, G., Lingner, T., Tsang, A.H., Barclay, J.L., and Oster, H. (2017). Hepatic gene therapy rescues high-fat diet responses in circadian Clock mutant mice. Mol Metab *6*, 512-523.

Milos, P.M., and Zaret, K.S. (1992). A ubiquitous factor is required for C/EBP-related proteins to form stable transcription complexes on an albumin promoter segment in vitro. Genes Dev *6*, 991-1004.
Rushton, P.J. (2016). What Have We Learned About Synthetic Promoter Construction? Methods Mol Biol *1482*, 1-13.

N., K.M.A. (2013). The hydrodynamic tail vein assay as a tool for the study of liver promoters and enhnacers. Methods Mol Biology, 279-289.

Nguyen, A.T., Dow, A.C., Kupiec-Weglinski, J., Busuttil, R.W., and Lipshutz, G.S. (2008). Evaluation of Gene Promoters for Liver Expression by Hydrodynamic Gene Transfer. *148*, 60-66.

Nora, E.P., Goloborodko, A., Valton, A.-L., Gibcus, J.H., Uebersohn, A., Abdennur, N., Dekker, J., Mirny, L.A., and Bruneau, B.G. (2017). Targeted Degradation of CTCF Decouples Local Insulation of Chromosome Domains from Genomic Compartmentalization. Cell *169*, 930-944.e922.

Stenler, S., Wiklander, O.P., Badal-Tejedor, M., Turunen, J., Nordin, J.Z., Hallengärd, D., Wahren, B., Andaloussi, S.E., Rutland, M.W., Smith, C.E.*, et al.* (2014). Micro-minicircle Gene Therapy: Implications of Size on Fermentation, Complexation, Shearing Resistance, and Expression. *2*, e140.

Su, H., Arakawa-Hoyt, J., and Kan, Y.W. (2002). Adeno-associated viral vector-mediated hypoxia response element-regulated gene expression in mouse ischemic heart model. *99*, 9480-9485.

Szabo, Q., Bantignies, F., and Cavalli, G. (2019). Principles of genome folding into topologically associating domains. Science Advances *5*, eaaw1668.

Yeung, J., Mermet, J., Jouffe, C., Marquis, J., Charpagne, A., Gachon, F., and Naef, F. (2018). Transcription factor activity rhythms and tissue-specific chromatin interactions explain circadian gene expression across organs. Genome Res *28*, 182-191.

Yoshitane, H., Ozaki, H., Terajima, H., Du, N.H., Suzuki, Y., Fujimori, T., Kosaka, N., Shimba, S., Sugano, S., Takagi, T.*, et al.* (2014). CLOCK-controlled polyphonic regulation of circadian rhythms through canonical and noncanonical E-boxes. Mol Cell Biol *34*, 1776-1787.

Zhang, R., Lahens, N.F., Ballance, H.I., Hughes, M.E., and Hogenesch, J.B. (2014). A circadian gene expression atlas in mammals: implications for biology and medicine. Proc Natl Acad Sci U S A *111*, 16219-16224.

CHAPTER IV

Bmal1$^{-/-}$ MICE CAN BE ENTRAINED TO NIGHT-RESTRICTED FEEDING

4.1 Overview

The circadian clock plays an extremely vital role for organisms' anticipation of daily oscillations of the environment. When the circadian clock is disrupted or desynchronized, this leads to physiological and psychological disorders in animal models and humans (Hatori and Panda, 2015). Chronic disruption of circadian rhythms has been linked to obesity, metabolic diseases, cancer, coronary heart disease, mood disruption, and dementia (Barclay et al., 2012; Bass, 2012; Davis et al., 2001; Fonken et al., 2010; Karlsson, 2001). Deletion of *Bmal1*, which constitutes the major component of the positive arm of the circadian clock, leads to many similar detrimental health effects in mice as are observed from chronic disruption of circadian rhythms (Kondratov et al., 2006). Reports from the literature suggest that some of the effects observed in organisms bearing a disrupted or desynchronized clock arise from the loss of rhythmic food intake. Importantly, restoration of rhythmic food intake in clock-deficient mice has been proposed as a means to alleviate symptoms associated with disruption or desynchronization of the clock. In this study, we aimed to design a system to test whether rhythmic food intake can mitigate the negative health effects experienced by *Bmal1*$^{-/-}$ mice. Our results show that the majority of *Bmal1*$^{-/-}$ mice eat in an arrhythmic manner when fed *ad libitum* regardless of gender, and those that are rhythmic have a dampened rhythm as compared to wild type. In addition, we found that male *Bmal1*$^{-/-}$ mice are able to entrain to the night-restricted pattern without decreasing their daily

intake of calories, and eat in a rhythmic manner. Together, our data suggest that the lack of *Bmal1*$^{-/-}$ mice feeding rhythms can be restored when forced to eat in a night restricted manner, which could in turn lead to a decrease in the amount of metabolic issues, for example decreased glucose homeostasis experienced by these mice.

4.2 Introduction

The circadian clock is found ubiquitously throughout nature from cyanobacteria to flies, plants, and mammals. The circadian clock is an important mechanism that allows for the anticipation of rhythmic daily oscillations. The mammalian circadian clock is composed of a transcriptional feedback loop that relies on the positive arm CLOCK:BMAL1 to activate the transcription of the negative arm PER:CRY, which in turn feedback to inhibit CLOCK:BMAL1 activated transcription. CLOCK:BMAL1 does not only activate the transcription of *Per* and *Cry*, but also of many other clock controlled genes. Many processes are controlled by the circadian clock such as rhythms in metabolism, sleep-wake cycles, rhythmic blood pressure, and many other processes (Cheng et al., 2002; Gnocchi et al., 2015a; Jeyaraj et al., 2012; Kaasik et al., 2013; Kramer, 2001; Wang et al., 2008). Upon knock out of *Bmal1*, *i.e.*, part of the positive arm of the circadian clock, many of the daily biological processes that were once rhythmic now become arrhythmic. There are also many negative health defects experienced by *Bmal1*$^{-/-}$ mice such as sarcopenia, cataracts, decrease in subcutaneous fat, organ shrinkage, infertility, defective glucose homeostasis, and ossification of ligaments and tendons, and premature aging (Kondratov et al., 2006). Mice are nocturnal animals, and they consume the majority of their food during the active phase

(seventy-five percent of their food intake occurs at night) (Yang et al., 2009). It has been shown previously that *Bmal1*$^{-/-}$ mice consume more food during the night than during the day, however less so that the contrast seen for wild-type mice (Marcheva et al., 2010). While wild-type mice eat about 75% of their daily food intake during their active phase, *Bmal1*$^{-/-}$ mice eat ~60% at night (Marcheva et al., 2010). This could result from two possibilities: either *Bmal1*$^{-/-}$ mice eat in a rhythmic fashion with a dampened amplitude, or *Bmal1*$^{-/-}$ mice eat more food at night but are not eating rhythmically. It has been shown previously that much of the rhythmic gene expression in wild-type mice is arrhythmic in *Bmal1*$^{-/-}$ mice (Atger et al., 2015; Greenwell et al., 2019). However, mice including *Bmal1*$^{-/-}$ present a masking effect to light (Bunger et al., 2000). This masking effect creates an activity pattern in response to lights on and lights off that is independent of the circadian clock due to the photophobicity of mice (Bunger et al., 2000; Crawley and Goodwin, 1980). It allows for the mouse behavior to occur in a rhythmic manner due to environmental factors like the light dark cycle and is not driven by the circadian clock. Therefore, we asked first, do *Bmal1*$^{-/-}$ mice eat rhythmically or arrhythmically, and second, if they do not eat in a rhythmic fashion, whether they can be entrained to eat in a rhythmic fashion. Additionally, if *Bmal1*$^{-/-}$ mice eat in an arrhythmic manner, will forcing them to eat rhythmically have an effect on circadian gene expression and physiology? We hypothesized that if *Bmal1*$^{-/-}$ mice do not eat in a rhythmic fashion, then night restricted feeding should allow for increased molecular rhythms in *Bmal1*$^{-/-}$ mice which, consequently, may lead to less issues with glucose homeostasis and metabolism in the *Bmal1*$^{-/-}$ mice. To address this question, we used a

feeding system previously designed in the laboratory (Fig. 23A; see below) (Greenwell et al., 2019).

4.3 Results

4.3.1 *Bmal1*$^{-/-}$ mice eat in an arrhythmic manner regardless of sex

To determine if there were sex-based differences in the feeding patterns of *Bmal1*$^{-/-}$ mice, we performed the feeding experiments in both male and female mice. First, we analyzed the total amount of food consumed by gender between the *Bmal1*$^{-/-}$ mice, and we did not find a statistically significant difference between the amount of food consumed between male or female *Bmal1*$^{-/-}$ mice (Fig. 23B). To test if the male and female mice were eating the same amount of food during the day as at night, we monitored the amount consumed in each three-hour window. We found results that matched previous findings in the field showing that *Bmal1*$^{-/-}$ mice eat about sixty percent of their food at night, and about forty percent of their food during the day (Fig. 23C) (Marcheva et al., 2010). There was a statistically different amount of food eaten during the day for both males and females (Fig. 23C).

Figure 23. Bmal1$^{-/-}$ mice eat more food during the night than day, and do not show sex-based differences in the amount of food eaten daily.
(A)Illustration of the feeding apparatus used for feeding the *Bmal1*$^{-/-}$ mice under all three conditions ad libitum, transition, and night-restricted (Greenwell et al., 2019). (B) Boxplot representing the amount of food consumed by kilocalories for female and male mice fed *ad libitum* across the entire day, and averaged over the course of one week with the dots representing individual feeding values. Statistical tests were performed with a Welch two sample T-test. (C) Boxplot representing the amount of food consumed by males and females in kilocalories during the day (ZT0 to ZT12) and night (ZT12 to ZT24) averaged over the course of one week. The dots represent individual data points. Statistical tests were carried out with an ANOVA and a post-hoc analysis with Tukey HSD.

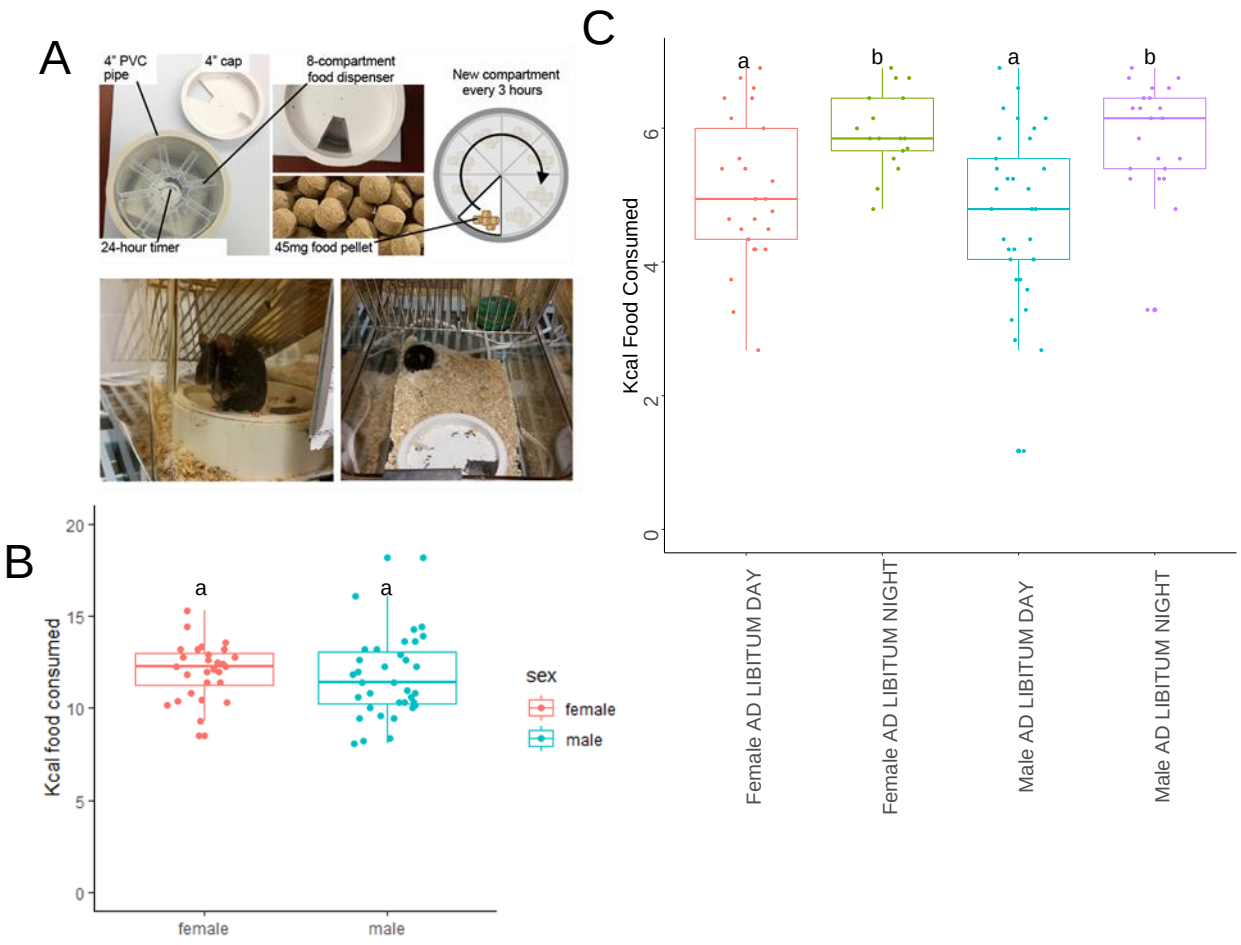

We plotted the amount of food eaten every three hours for a week to visualize the rhythms, and did not see a discernible rhythm in the data (Fig. 24A). Individual plots of the data reveal that there is a lot of noise for each individual animal even those that have were called rhythmic (i.e., BM1858 and BM1859 Fig. 24B). We found that the majority of *Bmal1*$^{-/-}$ mice were arrhythmic with all of the female mice being arrhythmic

and three out of the five male mice being arrhythmic (Fig. 24C). For the mice that were rhythmic they still have a dampened rhythm compared to wild-type which consume 75% of their food at night (Yang et al., 2009).

Figure 24. Eating patterns and rhythmicity of female and male *Bmal1*$^{-/-}$ mice fed *ad libitum.*
(A)Line graph illustration of the amount of food consumed in kilocalories by male and female knockout mice fed ad libitum over the course of a week with each individuals plotted with their own line with measurements being recorded every three hours for twenty-four hours for the course of a week. (B) table of p-values for rhythmic analysis for metacycle and harmonic regression.

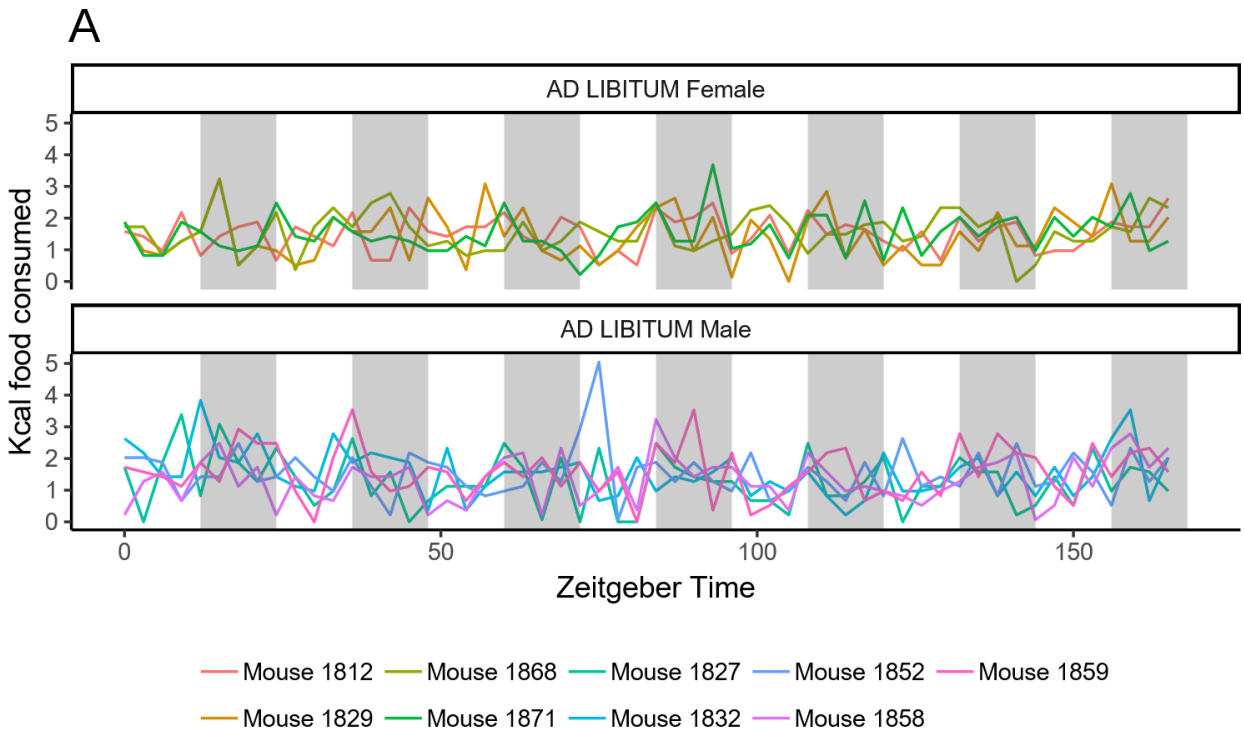

Figure 24 Continued.

B

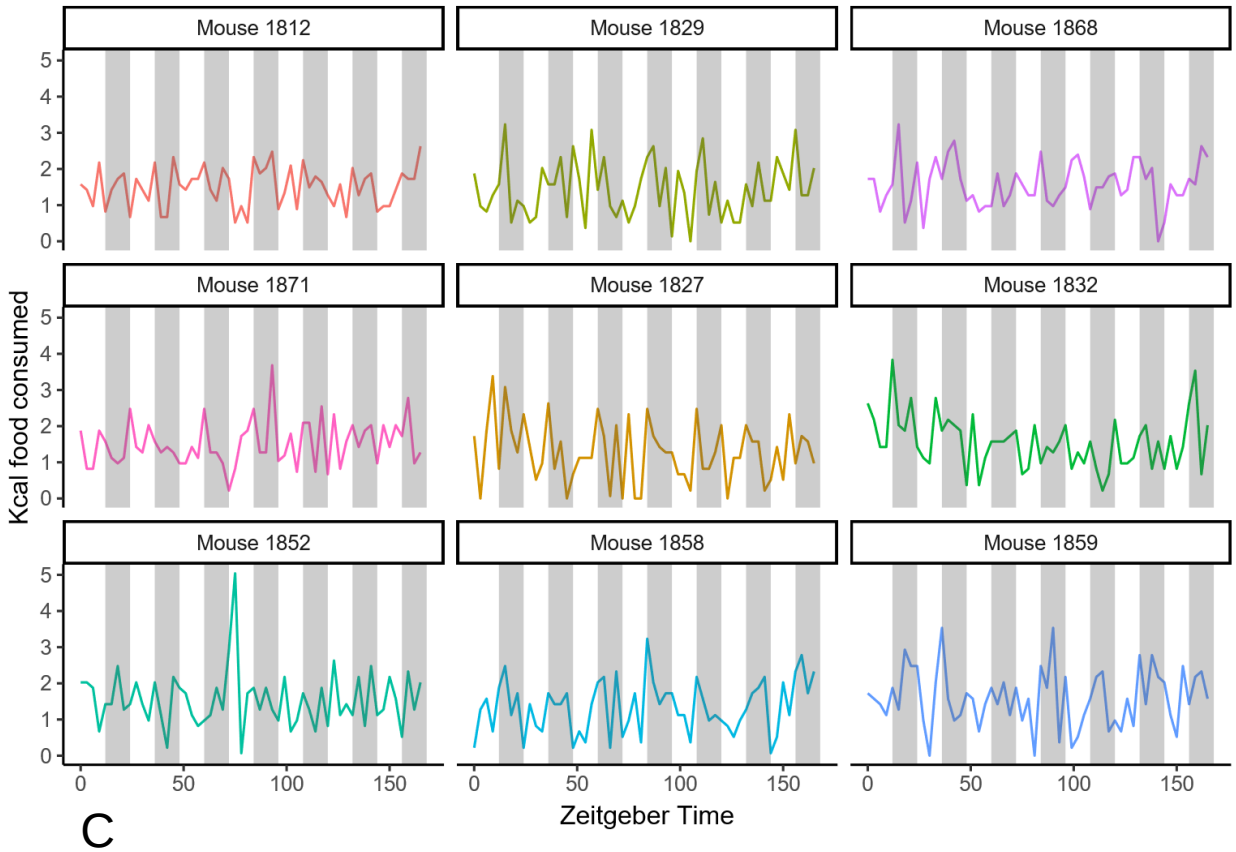

C

male mice	metacycle	harmonic regression
1827	0.49	0.03
1832	1.00	0.20
1852	1.00	0.09
1858	0.00	0.00
1859	0.00	0.00
female mice	metacycle	harmonic regression
1812	0.25	0.11
1829	0.29	0.09
1868	0.29	0.29
1871	0.29	0.28

4.3.2 Male *Bmal1*$^{-/-}$ mice can be entrained to night-restricted feeding

Since *Bmal1*$^{-/-}$ mice eat in an arrhythmic or dampened rhythmic pattern we fed them in a night restricted manner to ascertain if they could eat in a rhythmic manner without consuming a different amount of total kilocalories. These experiments were carried out with the male mice used in the experiments described above (Fig. 24A, 24B). We first transitioned the mice by lowering the amount of food available to the mice during the day (see methods). We found that there was no statistical difference between the amount of food eaten during the *ad libitum* phase and the transition phase, and between the *ad libitum* phase and the night-restricted schedule (Fig. 25A). However, there was a statistically significant difference between the night-restricted and transition paradigms (Fig. 25A). The difference between *ad libitum* and transition could largely be due to the temporal food availability be shifted on the mice as we do not see a significant difference between the night-restricted and the *ad libitum* paradigms once the mice had adjusted. Under the transition and night restricted paradigms, the *Bmal1*$^{-/-}$ mice were able to be forced to eat rhythmically without lowering their total daily food intake (Fig. 25B). Previous publications have shown that rhythmic feeding is a major driver of rhythmic gene expression (Greenwell et al., 2019). These data combined with the current findings suggest that being able to restore *Bmal1*$^{-/-}$ mice to a rhythmic eating pattern will allow our lab to test in future studies whether rhythmic food intake can restore (even partially) the circadian transcriptome in different tissues, and determine if rhythmic food intake can alleviate the physiological issues seen in *Bmal1*$^{-/-}$ mice.

Figure 25. *BMAL1*$^{-/-}$ male mice can be entrained to eat in a rhythmic manner without a reduction in Kcal consumed. (A)Plot for the five male mice over the course of the entire experiment. Each individual line plot is for the different conditions: *ad libitum*, transition, and night restricted. (B) Boxplot illustration of the amount of food consumed by male mice under the three feeding conditions *ad libitum,* transition, and night-restricted. The amount of food consumed is displayed in kilocalories with statistical tests performed with an ANOVA and Tukey's HSD.

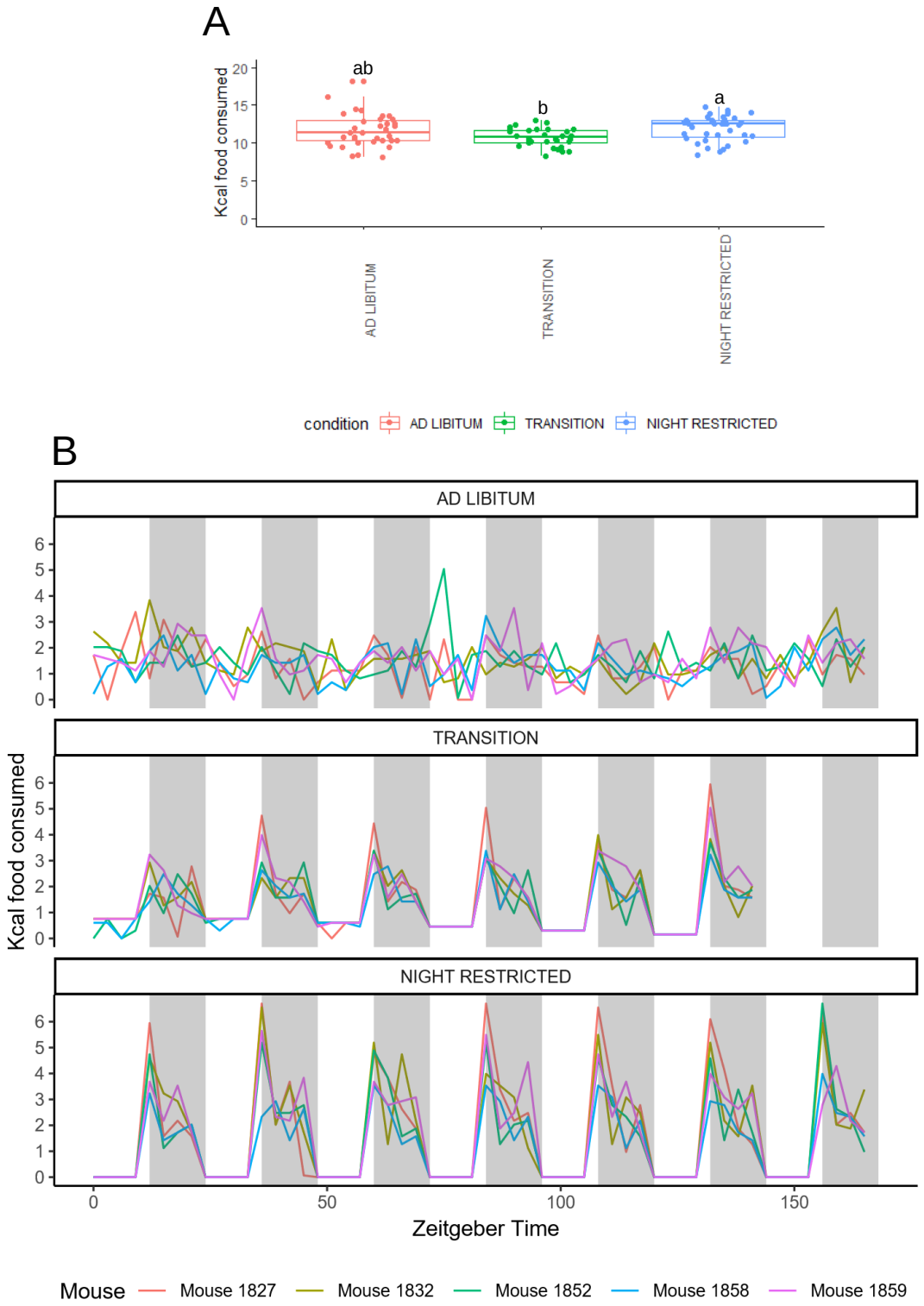

4.4 Discussion

Bmal1$^{-/-}$ mice suffer from a large variety of ailments including ossification of tendons, reduced life-span, infertility, ocular abnormalities, and brain astrogliosis (Kondratov, 2006; Lananna et al., 2018). Previous research has shown that night restricted feeding in *Bmal1*$^{-/-}$ mice increases the amount of rhythmic gene expression, however there are a subset of genes that were not restored (Atger et al., 2015; Greenwell et al., 2019). It was unclear if night-restricted feeding was altering the amount of food eaten daily by *Bmal1*$^{-/-}$ mice, and if this feeding was occurring in a rhythmic manner because of photophobicity/masking. The effect of masking could be tested by housing the mice in constant darkness or constant red light. This is particularly important because it has been shown that calorie restriction can attenuate many age-related diseases and extend the maximal life span (Weindruch et al., 1988). Our results demonstrate that the *Bmal1*$^{-/-}$ mice when fed *ad libitum* will eat in a dampened or arrhythmic manner. Moreover, our results also indicate that the mice can be entrained to a night-restricted eating paradigm without consuming less food during the night-restricted paradigm than during the *ad libitum* paradigm. This suggests that any potential health benefits or increases in rhythmicity are not due to a caloric restriction on the mice. Further studies will be needed to determine how introducing a feeding rhythm in knockout mice effects the physiology and health span of the animals. Potential ways of looking at the health span of the animals would include hair weight, tight wire clinging time, activity in an open field environment, tail collagen, hair growth, wound healing, and hemoglobin concentration tests as described previously (Harrison and Archer, 1988). Further studies would also be needed to determine if the *Bmal1*$^{-/-}$ mice experience an

increased life span with strong rhythms in feeding. This could also translate to potential benefits for humans suffering from circadian related disorders as new potential non-invasive treatment plans such as a strongly rhythmic diet could be employed. Future research will also be needed to determine if strong rhythms in other external cues are able to improve health span and life span in *Bmal1*$^{-/-}$ mice. Some of the other external cues that could likely have an impact are stronger rhythms in light, temperature, and social rhythms that can come from being housed with wild-type mice.

4.5 Methods

4.5.1 Animals

Male C57BL/6J and *Bmal1*$^{-/-}$ mice were housed under 12 h light:12 h dark (LD12:12) with food and water available *ad libitum*. *Bmal1*$^{-/-}$ were kindly provided by Christopher Bradfield (Bunger et al., 2000). All experiments were approved by the Texas A&M University Institutional Animal Care and Use Committee.

4.5.2 Feeding setup

The mice were housed in specially designed cages with a timer that would turn on a continuous basis with a plastic container with the food. It had eight compartments allowing for a three-hour resolution. Two grams of Bio-serv dustless precision rodent pellets (product number F0165) were used per compartment. Each pellet has a weight of 45 milligrams. The food was replaced everyday at ZT8. Mouse cages were changed weekly at the same time as the food change out. For the transition period the feeding during the night remained the same however the day was reduced to five pellets for the

first two days, and was then reduced by one pellet per day until no pellets remained. The night restricted feeding was carried on for one week with no food given during the day and two grams given in each of the four night compartments.

4.5.3 Measuring food consumption

The food in each compartment was weighed out to be 2 grams ± 0.02 grams using pellets that were 45 milligrams each. Then, after each day the container was replaced with a new container. The food from the old container was dumped out one compartment at a time and each pellet was counted and multiplied by 45 milligrams to determine the weigh leftover and the weight consumed.

4.5.4 Statistical analysis

Statistical analysis was performed in R. A welch two sample T-test was used to determine the any differences in the amount of food consumed by sex. An ANOVA and Tukey HSD was used to determine any differences in between the amount of food consumed during the *ad libitum* fed state, transition feeding state, and the night-restricted feeding state. Differences between groups was considered significant if $p < 0.05$.

4.5.5 Rhythmic analysis

Rhythmic analysis was performed with metacycle and harmonic regression (Lück et al., 2014; Wu et al., 2016). Standard conditions were used for each program.

4.6 References

Atger, F., Gobet, C., Marquis, J., Martin, E., Wang, J., Weger, B., Lefebvre, G., Descombes, P., Naef, F., and Gachon, F. (2015). Circadian and feeding rhythms differentially affect rhythmic mRNA transcription and translation in mouse liver. Proceedings of the National Academy of Sciences *112*, E6579-E6588.

Barclay, J.L., Husse, J., Bode, B., Naujokat, N., Meyer-Kovac, J., Schmid, S.M., Lehnert, H., and Oster, H. (2012). Circadian Desynchrony Promotes Metabolic Disruption in a Mouse Model of Shiftwork. *7*, e37150.

Bass, J. (2012). Circadian topology of metabolism. Nature *491*, 348-356.
Bunger, M.K., Wilsbacher, L.D., Moran, S.M., Clendenin, C., Radcliffe, L.A., Hogenesch, J.B., Simon, M.C., Takahashi, J.S., and Bradfield, C.A. (2000). Mop3 is an essential component of the master circadian pacemaker in mammals. Cell *103*, 1009-1017.

Cheng, M.Y., Bullock, C.M., Li, C., Lee, A.G., Bermak, J.C., Belluzzi, J., Weaver, D.R., Leslie, F.M., and Zhou, Q.-Y. (2002). Prokineticin 2 transmits the behavioural circadian rhythm of the suprachiasmatic nucleus. *417*, 405-410.

Crawley, J., and Goodwin, F.K. (1980). Preliminary report of a simple animal behavior model for the anxiolytic effects of benzodiazepines. *13*, 167-170.

Davis, S., Mirick, D.K., and Stevens, R.G. (2001). Night Shift Work, Light at Night, and Risk of Breast Cancer. JNCI Journal of the National Cancer Institute *93*, 1557-1562.

Fonken, L.K., Workman, J.L., Walton, J.C., Weil, Z.M., Morris, J.S., Haim, A., and Nelson, R.J. (2010). Light at night increases body mass by shifting the time of food intake. Proceedings of the National Academy of Sciences *107*, 18664-18669.

Gnocchi, D., Pedrelli, M., Hurt-Camejo, E., and Parini, P. (2015). Lipids around the Clock: Focus on Circadian Rhythms and Lipid Metabolism. *4*, 104-132.

Greenwell, B.J., Trott, A.J., Beytebiere, J.R., Pao, S., Bosley, A., Beach, E., Finegan, P., Hernandez, C., and Menet, J.S. (2019). Rhythmic Food Intake Drives Rhythmic Gene Expression More Potently than the Hepatic Circadian Clock in Mice. Cell Reports *27*, 649-657.e645.

Harrison, D.E., and Archer, J.R. (1988). Biomarkers of aging: Tissue markers. Future research needs, strategies, directions and priorities. Experimental Gerontology *23*, 309-321.

Hatori, M., and Panda, S. (2015). Response of peripheral rhythms to the timing of food intake. Methods Enzymol *552*, 145-161.

Jeyaraj, D., Scheer, F.A., Ripperger, J.A., Haldar, S.M., Lu, Y., Prosdocimo, D.A., Eapen, S.J., Eapen, B.L., Cui, Y., Mahabeleshwar, G.H.*, et al.* (2012). Klf15 orchestrates circadian nitrogen homeostasis. Cell Metab *15*, 311-323.

Kaasik, K., Kivimae, S., Allen, J.J., Chalkley, R.J., Huang, Y., Baer, K., Kissel, H., Burlingame, A.L., Shokat, K.M., Ptacek, L.J.*, et al.* (2013). Glucose sensor O-GlcNAcylation coordinates with phosphorylation to regulate circadian clock. Cell Metab *17*, 291-302.

Karlsson, B. (2001). Is there an association between shift work and having a metabolic syndrome? Results from a population based study of 27 485 people. *58*, 747-752.
Kondratov, R.V. (2006). Early aging and age-related pathologies in mice deficient in BMAL1, the core componentof the circadian clock. Genes & Development *20*, 1868-1873.

Kondratov, R.V., Kondratova, A.A., Gorbacheva, V.Y., Vykhovanets, O.V., and Antoch, M.P. (2006). Early aging and age-related pathologies in mice deficient in BMAL1, the core componentof the circadian clock. Genes Dev *20*, 1868-1873.

Kramer, A. (2001). Regulation of Daily Locomotor Activity and Sleep by Hypothalamic EGF Receptor Signaling. Science *294*, 2511-2515.

Lananna, B.V., Nadarajah, C.J., Izumo, M., Cedeno, M.R., Xiong, D.D., Dimitry, J., Tso, C.F., McKee, C.A., Griffin, P., Sheehan, P.W.*, et al.* (2018). Cell-Autonomous

Regulation of Astrocyte Activation by the Circadian Clock Protein BMAL1. Cell Rep *25*, 1-9 e5.

Lück, S., Thurley, K., Paul, and Pål (2014). Rhythmic Degradation Explains and Unifies Circadian Transcriptome and Proteome Data. *9*, 741-751.

Marcheva, B., Ramsey, K.M., Buhr, E.D., Kobayashi, Y., Su, H., Ko, C.H., Ivanova, G., Omura, C., Mo, S., Vitaterna, M.H.*, et al.* (2010). Disruption of the clock components CLOCK and BMAL1 leads to hypoinsulinaemia and diabetes. Nature *466*, 627-631.

Wang, N., Yang, G., Jia, Z., Zhang, H., Aoyagi, T., Soodvilai, S., Symons, J.D., Schnermann, J.B., Gonzalez, F.J., Litwin, S.E.*, et al.* (2008). Vascular PPARgamma controls circadian variation in blood pressure and heart rate through Bmal1. Cell Metab *8*, 482-491.

Weindruch, R., Naylor, P.H., Goldstein, A.L., and Walford, R.L. (1988). Influences of aging and dietary restriction on serum thymosin alpha 1 levels in mice. J Gerontol *43*, B40-42.

Wu, G., Anafi, R.C., Hughes, M.E., Kornacker, K., and Hogenesch, J.B. (2016). MetaCycle: an integrated R package to evaluate periodicity in large scale data. Bioinformatics *32*, 3351-3353.

Yang, S., Liu, A., Weidenhammer, A., Cooksey, R.C., McClain, D., Kim, M.K., Aguilera, G., Abel, E.D., and Chung, J.H. (2009). The role of mPer2 clock gene in glucocorticoid and feeding rhythms. Endocrinology *150*, 2153-2160.

CHAPTER V

TEMPORAL FOOD PREFERENCES IN MICE SUGGEST STANDARD CHOW MAY NOT MEET MICE TEMPORAL FOOD NEEDS

5.1 Overview

Laboratory mice are often raised on a standard chow diet with the same composition of macronutrients with no difference in what they are fed over the course of the day. However, it has been shown that many metabolic pathways such as glucose metabolism, lipid metabolism, and protein metabolism are rhythmic, and this may suggest that biomolecular needs of organisms vary throughout the course of the day (Barclay et al., 2012; Bass, 2012; Davis et al., 2001; Fonken et al., 2010; Karlsson, 2001). We hypothesized that mice would prefer carbohydrates and fat early on in the night as glycogen is the first choice of energy storage and use, and then would have a selection for proteins later on in the night (Lu et al., 2014). The rationale for this hypothesis is that glycogen is a preferred nutrient for cells as it can be quickly utilized for energy release and will likely be rhythmic in animals that consume food in a rhythmic manner. To test this hypothesis, we developed a novel feeding system based on a feeding apparatus designed in the Menet lab to manipulate the daily food intake rhythm in the mouse (Greenwell et al., 2019). The system consisted of a large cage (25.4 by 45.7 centimeters) containing three feeding systems, with each of them accommodating an eight-compartment food dispenser that rotated continuously and completing one rotation every twenty-four hours, thereby allowing for a three-hour resolution of food consumption. By providing different nutrient sources in each of the three-feeding

systems (carbohydrates, lipids, and proteins), we found that wild-type male and female C57BL/6 mice eat the fat with the earliest phase in the night followed by carbohydrates and then by protein. These promising results will be useful to determine if animals being allowed to choose their source of energy across the 24-hr day exhibit better physiological markers and are overall healthier than animals eating the same food all the time.

5.2 Introduction

There has been a substantial amount of research into food preference, however it has yet to be addressed if there are temporal food preferences for different macronutrients, and if these temporal food preferences have physiological impacts on organisms. Mice are nocturnal animals that are mostly active during the night (ZT12-ZT24) and are less active during the day (ZT0-ZT12), and have been shown to have photophobia and masking (Bunger et al., 2000; Crawley and Goodwin, 1980). ZT or zeitgeber time is a system where ZT0 denotes lights on and ZT12 denotes lights off. Previous studies have shown that mice eat about seventy-five percent of their food during the night (Yang et al., 2009). However, it has been shown that many metabolic pathways such as glucose metabolism, lipid metabolism, and protein metabolism are rhythmic, and this may suggest that biomolecular needs of organisms vary throughout the course of the day (Barclay et al., 2012; Bass, 2012; Davis et al., 2001; Fonken et al., 2010; Karlsson, 2001).

Feeding behavior has been shown to be very important for organisms and can be divided into two major categories, quantity and quality. Quantity simple refers to the

amount of food consumed, while quality refers to what food is eaten and when food is eaten. There are two major systems that have been described to control food preferences: the homeostatic and hedonic systems. The homeostatic system refers to the needs of the organism while the hedonic system refers to the wants of the organism (Berridge and Robinson, 2003; Berridge et al., 2009; Berthoud and Morrison, 2008). Research into the quality of feeding behavior largely addresses two topics: macronutrient-based diet selection and feeding patterns.

Macronutrient based diet selection has shown to be influenced by humoral factors, homeostatic feeding mechanisms, the hedonic system, and genetics (Sasaki, 2017). The humoral factor FGF21 regulates carbohydrate preference, and the humoral factor ghrelin has also been shown to have an impact on food preference (Larson et al., 2019; Stephanie et al., 2016; Talukdar et al., 2016). One way the hedonic system plays a role in food preference is with glucose-containing sugars and fat, that have a potent reward of dopamine (Hajnal, 2003; Steinbusch et al., 2015).

Feeding patterns have shown to play a very important role in controlling weight and health (Asher and Sassone-Corsi, 2015). Ingestion of the same amount of food at different times of day has different health consequences because the systemic metabolic efficiency will fluctuate throughout the course of the day. Current research has shown that a high-fat diet is capable of reprogramming the circadian clock (Eckel-Mahan et al., 2013; Kohsaka et al., 2007). Correcting the feeding schedule of mice on a high-fat diet has shown to relieve them of high-fat diet induced obesity (Fuse et al., 2012; Hatori et al., 2012; Sherman et al., 2012).

Currently a gap in the field exists as it has yet to be fully addressed whether there is a temporal preference for different macronutrients throughout the course of the day. Previous research indicates that mice do have a preference for sugars early in the active phase, however this research did not find a preference for protein later in the night as they had hypothesized (Jensen, 1993). One potential explanation is that they were not using pure forms of the macronutrients and instead used fruits and nuts which would be mixed. We hypothesized that carbohydrates and fats peak consumption would be earlier in the night, and that protein peak consumption would be later in the night. One reason for this is that glycogen is the main energy source used by many areas of the body and is used to provide energy to all cells, and it can be acquired from food or from fatty acids that are beta-oxidized, and gluconeogenesis (Slavin and Carlson, 2014). Glycogen represent the first choice of energy storage and use, and when glycogen needs are met the animals will switch to storing lipids in adipocytes, and protein in muscles (Lu et al., 2014).

Figure 26. Total consumption of food and food preference in wild-type C57/BL6 mice for different macronutrients. (A)Schematic Illustration of the feeding apparatus. Showing the (B) Boxplot for the amount of kilocalories consumed by sex. Data was averaged for males and females based on the total Kcal consumed in a day for six recordings occurring every three days. Kcal consumed for carbohydrate, fat, and protein were added together for each animal and then used to generate the total food consumed for each individual. The dots represent the value for total Kcal consumed for each individual point. (C) Boxplot of Kcal consumed between males and females for the three macronutrients carbohydrate, fat, and protein. The data was recorded for six recordings occurring every three days. The dots represent the individual values.

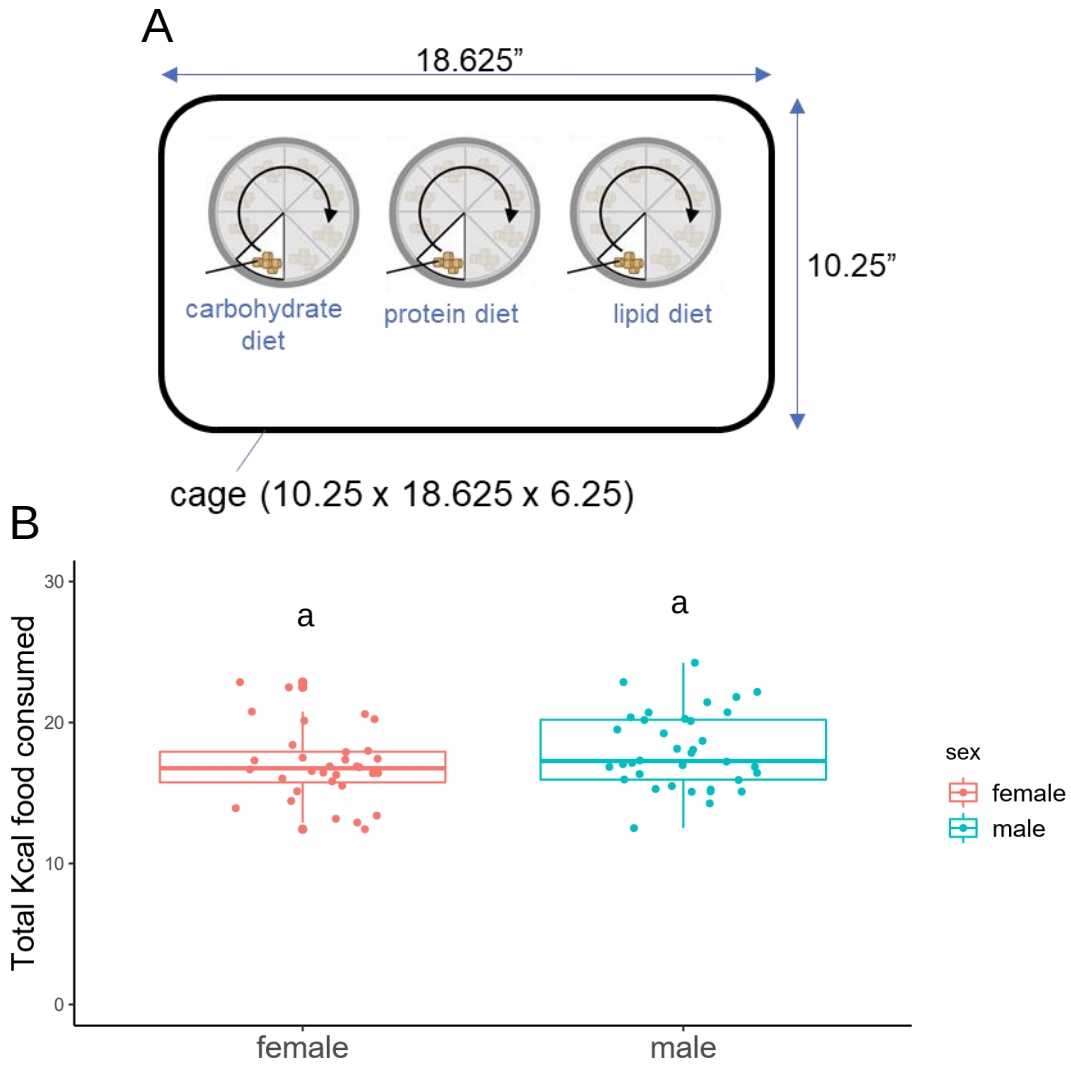

Figure 26 Continued.

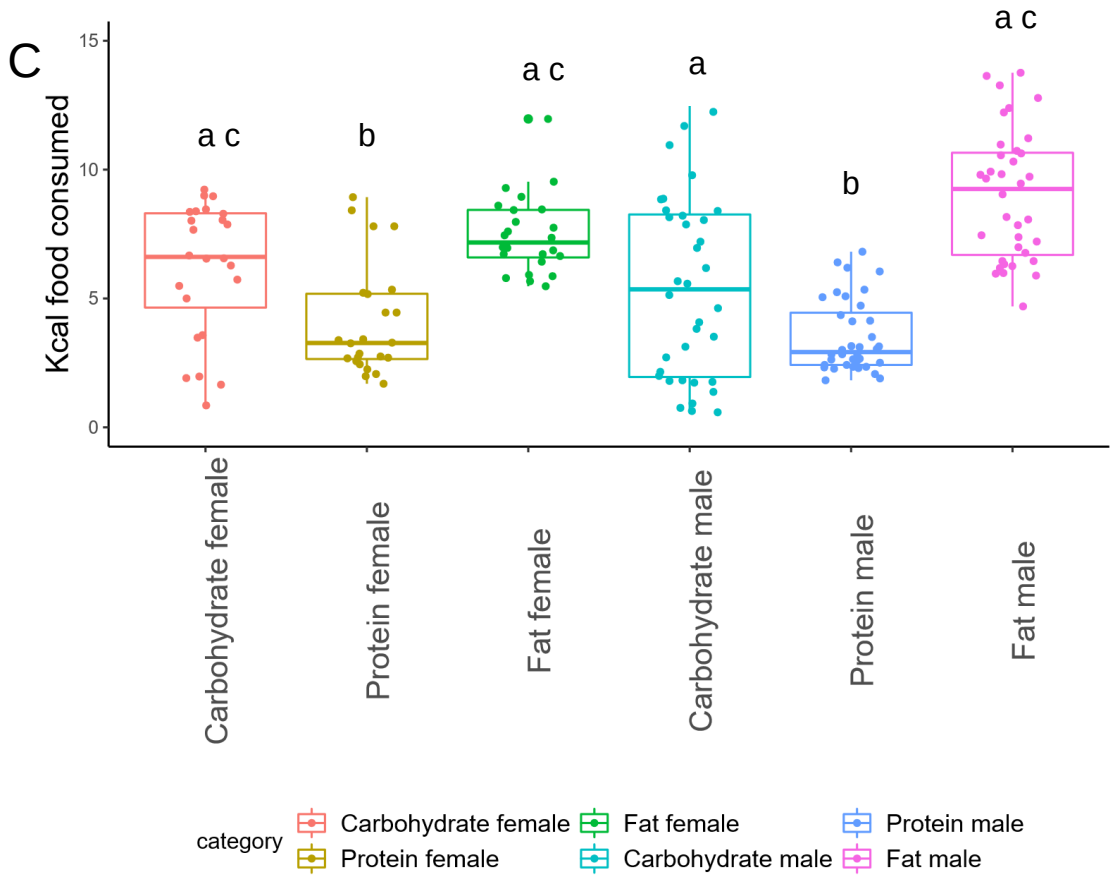

5.3 Results

5.3.1 Male and Female Mice Consume Comparable Amounts of Carbohydrate, Fat, and Protein

To study the temporal food preferences of C57BL/6 male and female mice, we designed a novel feeding system that allows for the detection of the food consumed within a three-hour window (Fig. 26A). We ordered three special diets from Research Diets where 99% of the Kcal originate for only one nutrient source: carbohydrates,

lipids, or proteins (Fig. 27). Each diet contains equal amounts of vitamins, minerals, and fiber (cellulose), such that the only difference between diets comes from the nutrient source. By providing these three diets in our custom-made cages, we were able to measure the exact amount of carbohydrates, fat, and protein consumed with a three-hour resolution across the 24-hour day.

Figure 27. Table consisting of the food makeup of the diets from Research Diets.
Greater than 99% of the Kcal come from one source either carbohydrate, protein, or carbohydrates. All diets have the same mineral and vitamin mix to ensure a consistent delivery of micronutrients.

Product Number	D18111905M(Carbohydrate)		D18111906M (Protein)		D14112201M (Fat)	
	gram%	kcal%	gram%	kcal%	gram%	kcal%
Protein	0	0	90.4	99	0	0
Carbohydrate	91.3	100	0.9	1	1.8	1
Fat	0	0	0	0	80.7	99
Total		100		100		100
kcal/gram	3.65		3.65		7.33	
Ingredients						
Casein, 80 Mesh	0	0	1000	4000	0	0
L-Cystine	0	0	4.25	17	0	0
Corn Starch	710	2840	0	0	0	0
Dextrose	152	608	0	0	0	0
Sucrose	142.25	569	0	0	0	0
Cellulose, BW200	50	0	50	0	50	0
Soybean Oil	0	0	0	0	25	225
Lard	0	0	0	0	421.3	3791.7
Mineral Mix	10	0	10	0	10	0
DiCalcium Phosphate	13	0	13	0	13	0
Calcium Carbonate	5.5	0	5.5	0	5.5	0
Pottasium Citrate	16.5	0	16.5	0	16.5	0
Vitamin Mix	10	40	10	40	10	40
Choline Bitartrate	2	0	2	0	2	0
FD&C Yellow Dye #5	0.05	0	0.025	0	0	0
FD&C Red Dye #40	0	0	0.025	0	0.05	0
FD&C Blue Dye #1	0	0	0	0	0	0

To determine whether there were sex-based differences in food preference in mice, we first examined the total kilocalories (Kcal) of food consumed by male or female mice. We found that there was not a significant difference in the total Kcal consumed by gender (Fig. 26B). Interestingly, we also found that there is a significantly higher amount of Kcal consumed of fat and carbohydrate when compared to the Kcal of protein consumed for both genders (Fig. 26C). There is also a significantly higher Kcal of fat consumed for males than females when compared to male carbohydrate but not when compared to female carbohydrate. We found there to be no significant difference in the amount of carbohydrates, fat, or protein consumed based between males and females.

5.3.2 Wild-type Mice Display a High-degree of Rhythmicity in Eating the Three Major Macronutrients as Well as Phase Preferences

To determine whether there were time-of-day differences in feeding, we fed the mice in a special designed cage system such that we could record the food eaten with a three-hour resolution (Fig 26A). We found that for both male and female mice, for all three macronutrients, there was more food eaten during the night than during the day (Fig. 28A). We found that there were variations between the individual mice for consumption of the macronutrients, but each mouse ate in very similar way across the entire experiment for all three macronutrients (Fig 28B).

We found the majority of the mice eat each macronutrient in a rhythmic manner based on metacycle and harmonic regression (Fig. 29A) (Lück et al., 2014; Wu et al., 2016). All the male mice were rhythmic for each macronutrient according to at least one rhythmic program (Fig. 29A). While all but one of the female mice were rhythmic

Figure 28. Male and female mice have similar food preferences and individual mice eat the same macronutrients at the same time of day.
(A)Line graph of the amount of food consumed on average for male and female mice over the course of the day. The average was calculated with six samples for males and four for females for each macronutrient. The error bars represent the standard error. (B) Is the eating pattern for an individual male mouse number 133 in the experiment that is characteristic of all the mice in the experiment.

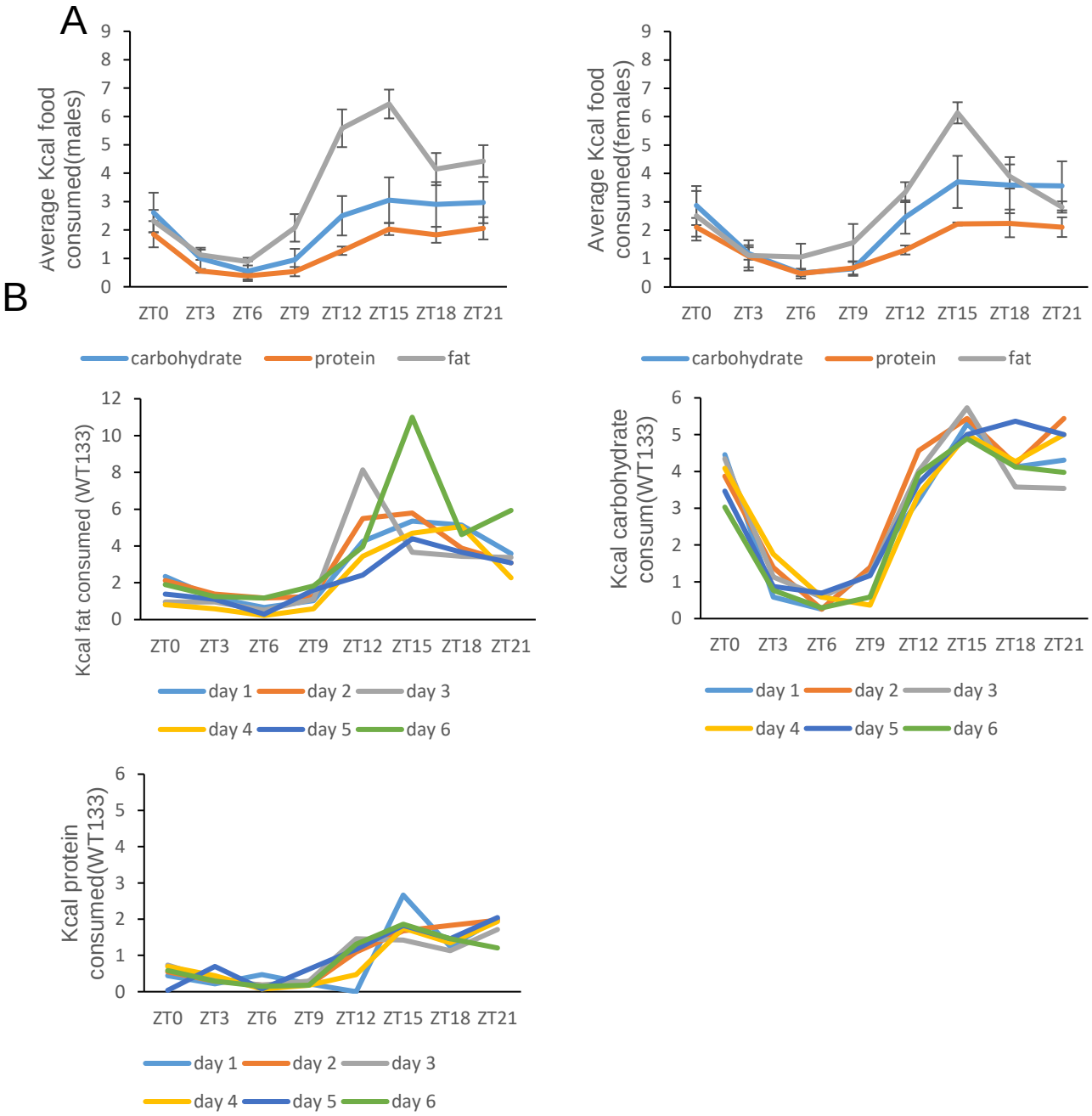

according to at least one program, and the one female that was arrhythmic for carbohydrates and proteins (Fig. 29A). The mice also had different peak phases of consumption between the different macronutrient categories (Fig. 29B). There were slight differences based on gender, but both genders consumed fat the earliest, followed by carbohydrates, and then proteins (Fig. 29 B).

Figure 29. Rhythmicity and phase differences of macronutrient consumption for male and female wild-type mice. (A)Adjusted p-values of metacycle and harmonic regression for male and female mice based on the three macronutrient categories. (B)Phase diagram of the representative peak phase of expression in male and female mice for the three macronutrients carbohydrates, fats, and protein. The bars represent the average phase for the sex and macronutrient type with the standard error on each side. The dots are the individual peak phases for each individual mouse averaged over the course of the six recordings that were taken every three days.

A

males		carbohydrate	fat	protein
rhythmic analysis metacycle	JB162	0.00	0.00	0.00
	JB165	0.00	0.00	0.00
	JB170	0.00	0.00	0.00
	WT133	0.00	0.00	0.00
	WT134	0.01	0.00	0.00
	WT135	0.00	0.00	0.00
rhythmic analysis harmonic regression	JB162	0.00	0.00	0.00
	JB165	0.00	0.00	0.00
	JB170	0.00	0.00	0.00
	WT133	0.00	0.00	0.00
	WT134	0.06	0.00	0.00
	WT135	0.00	0.00	0.00
females		**carbohydrate**	**fat**	**protein**
rhythmic analysis metacycle	BM1817	0.00	0.00	0.00
	BM1822	0.85	0.00	0.65
	BM1830	0.00	0.00	0.44
	BM1861	0.00	0.00	0.13
rhythmic analysis harmonic regression	BM1817	0.00	0.00	0.00
	BM1822	0.81	0.00	0.63
	BM1830	0.00	0.00	0.00
	BM1861	0.00	0.00	0.00

B

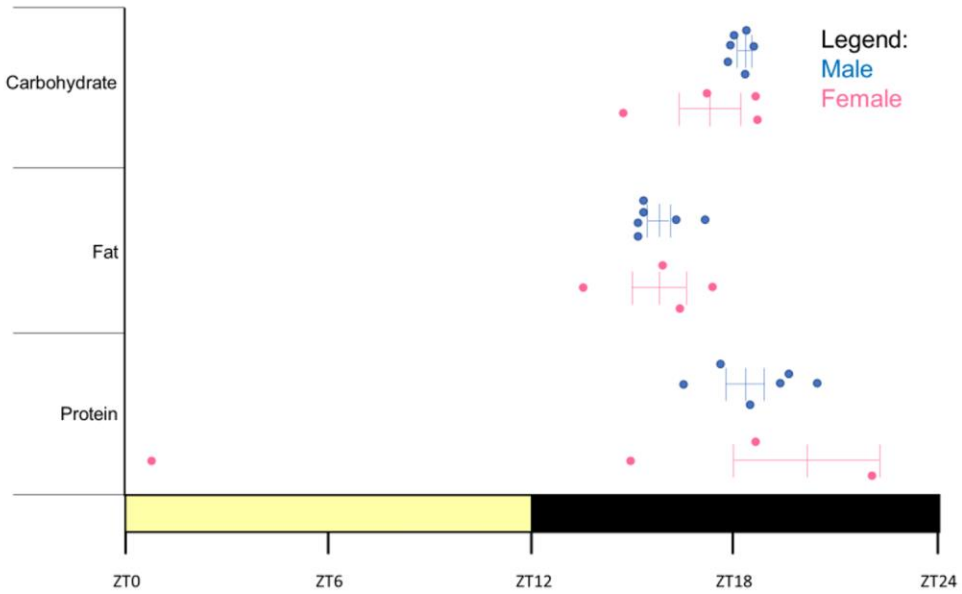

5.4 Discussion

Many aspects of food preferences have been addressed across many species, however temporal changes in food preferences remain largely unaddressed. Previous findings have shown that mice preferred sugars early in their active phase, and that there was no strong temporal preference for proteins (Jensen, 1993). Previous research has also suggested that in natural populations, rodents will go for the highest caloric gain per unit of time spent foraging (Hansson, 1985). This data suggests that the mice may in general prefer the highest caloric foods first, which could also contribute to an earlier consumption of fat in mice.

Our data suggest that there is little difference in the total amount of food consumed in Kcal by male and female mice when fed pure carbohydrate, fat, and protein diets. However, there were differences in the amount of the different macronutrients consumed with fat being the most consumed macronutrient. There were also mouse-to-mouse differences in the amount of each macronutrient consumed, with some of the mice preferring carbohydrates, and others preferring fats. With a larger sample size these individual preferences could likely be minimized such that a stronger conclusion can be reached. The data also suggest that there are differences in the phase of food consumption for the major macronutrients. With only six male mice and four female mice future experiments would benefit from a larger sample size of mice, such as 15 mice or greater of each gender, being used such that the eating pattern of an individual mouse has less overall impact on the results. This is one of the first studies that has directly looked at the temporal food preferences for different macronutrients in mice with a nearly pure form of each macronutrient.

Some future directions that could benefit the scope and impact of the project would be to address elderly mice, effects of pregnancy on temporal macronutrient preference, effects of *Bmal1*$^{-/-}$ on temporal food preferences, effects of injecting glucose, ghrelin, galanin, neuropeptide Y, and oxytocin at different times of day, and treatment with antibiotics. *Bmal1*$^{-/-}$ mice could be used to study the role of the clock in temporal food preferences. Pregnant mice may have different nutrient requirements which this feeding system would be able to address (Butte and King, 2005; Cox and Phelan, 2008; Elango and Ball, 2016). Injections of ghrelin and galanin have shown to increase fat preference and if injecting at different times their temporal effects could be studied (Shimbara et al., 2004; Tempel et al., 1988). Neuropeptide Y injection has been shown to promote carbohydrate preference and could also be used to determine whether it has a different effect at different times of day (Slawecki et al., 2000; Stanley et al., 1985). While oxytocin reduced sensitivity to sweet taste, and knockouts could allow for the role of the hedonic system to be reduced such that the homeostatic systems role can be further determined (Klockars et al., 2015; Olszewski et al., 2010). Antibiotics could also be administered, and the feed paradigm applied to tease apart the role of the microbiome in temporal food preferences. The gut microbiome has been reported to affect multiple aspects of health and a gavage of certain bacteria has been reported to alleviate diet-induced obesity (Liu et al., 2017; Ridaura et al., 2013).

In modern chow for both laboratory and pet animals' temporal food preferences have remained unaddressed. Our data suggest that there are temporal food preferences in mice for different macronutrients. These findings may also translate to other species that are often kept as household pets. The physiological impacts of

temporal changes in food preference remain unclear, and further studies will need to be done to determine the physiological impacts of these temporal changes in food preferences in mice. Further studies will need to be done to look at the metabolic impacts of temporal changes in food preferences versus feeding a single type of chow with the same carbohydrate, fat, and protein composition. Some ways that these physiological and metabolic impacts could be addressed are with O_2 consumption, CO_2 production, temperature, activity measurements, and a metabolic screen to look for the amount of cholesterol, bile acids, blood urea nitrogen, and many other signs of metabolic disorders. These results could also allow for better treatment of humans with circadian related disorders, however further research would need to be done to determine if humans have a biological preference for carbohydrates and fats early in the active phase followed by proteins later on in the active phase.

5.5 Methods

5.5.1 Animals

The mice were housed under 12 h light: 12 h dark (LD12:12) with food and water provided *ad libitum*. All experiments were approved by the Texas A&M University Institutional Animal Care and Use Committee, AUP number 2016-0199.

5.5.2 Cage setup

The mice were housed individually in a rat cage that measured 10.25”X18.625”X6.25”. Three circular holes were drilled into the rat cage with a PVC pipe fitted to the holes (Figure 26A). A timer was then added through the PVC pipe, and the timer was

attached to a grey PVC base for support and so it would not shift during the experiments. A plastic container with eight compartments was then attached to the timer via screws that were embedded into the top of the timer. A plastic lid was then used to cover the eight feeding compartments with a cutout such that one feeding compartment could be accessed at a time.

5.5.3 Data collection

Mice were fed roughly 1.5 grams of each type of food every three days. Every three days the weight of food consumed was recorded, and the mice were checked every day to ensure that they had plenty of food. The weight of food consumed was done by first measuring the weight of food added to the container at least 1.5 grams but potentially slightly higher. The weight after three days was then recorded for each compartment and the difference was used to calculate the amount of food that was consumed. Recordings were taken for each compartment for each of the macronutrients.

5.5.4 Data analysis

The amount of total Kcal consumed was analyzed in R with a Welch two-sample T-test. The comparison of the feeding categories based on gender and biomolecule was done in R with an ANOVA and a post-hoc analysis with TukeyHSD. The graphs showing the average of food consumed by gender have the average plus/minus the standard error. Considered significant with a p-value < 0.05.

5.5.5 Rhythmic analysis

Rhythmic Analysis was performed with metacycle and harmonic regression (Lück et al., 2014; Wu et al., 2016). The peak phase of expression was determined with metacycle. Standard parameters were used.

5.6 References

Asher, G., and Sassone-Corsi, P. (2015). Time for Food: The Intimate Interplay between Nutrition, Metabolism, and the Circadian Clock. Cell *161*, 84-92.

Barclay, J.L., Husse, J., Bode, B., Naujokat, N., Meyer-Kovac, J., Schmid, S.M., Lehnert, H., and Oster, H. (2012). Circadian Desynchrony Promotes Metabolic Disruption in a Mouse Model of Shiftwork. *7*, e37150.

Bass, J. (2012). Circadian topology of metabolism. Nature *491*, 348-356.

Berridge, K.C., and Robinson, T.E. (2003). Parsing reward. Trends in Neurosciences *26*, 507-513.

Berridge, K.C., Robinson, T.E., and Aldridge, J.W. (2009). Dissecting components of reward: 'liking', 'wanting', and learning. Current Opinion in Pharmacology *9*, 65-73.

Berthoud, H.-R., and Morrison, C. (2008). The Brain, Appetite, and Obesity. *59*, 55-92.

Bunger, M.K., Wilsbacher, L.D., Moran, S.M., Clendenin, C., Radcliffe, L.A., Hogenesch, J.B., Simon, M.C., Takahashi, J.S., and Bradfield, C.A. (2000). Mop3 is an essential component of the master circadian pacemaker in mammals. Cell *103*, 1009-1017.

Butte, N.F., and King, J.C. (2005). Energy requirements during pregnancy and lactation. Public Health Nutrition *8*, 1010-1027.

Cox, J.T., and Phelan, S.T. (2008). Nutrition During Pregnancy. *35*, 369-383.
Crawley, J., and Goodwin, F.K. (1980). Preliminary report of a simple animal behavior model for the anxiolytic effects of benzodiazepines. *13*, 167-170.

Davis, S., Mirick, D.K., and Stevens, R.G. (2001). Night Shift Work, Light at Night, and Risk of Breast Cancer. JNCI Journal of the National Cancer Institute *93*, 1557-1562.

Eckel-Mahan, K.L., Patel, V.R., de Mateo, S., Orozco-Solis, R., Ceglia, N.J., Sahar, S., Dilag-Penilla, S.A., Dyar, K.A., Baldi, P., and Sassone-Corsi, P. (2013). Reprogramming of the circadian clock by nutritional challenge. Cell *155*, 1464-1478.

Elango, R., and Ball, R.O. (2016). Protein and Amino Acid Requirements during Pregnancy. *7*, 839S-844S.

Fonken, L.K., Workman, J.L., Walton, J.C., Weil, Z.M., Morris, J.S., Haim, A., and Nelson, R.J. (2010). Light at night increases body mass by shifting the time of food intake. Proceedings of the National Academy of Sciences *107*, 18664-18669.

Fuse, Y., Hirao, A., Kuroda, H., Otsuka, M., Tahara, Y., and Shibata, S. (2012). Differential roles of breakfast only (one meal per day) and a bigger breakfast with a small dinner (two meals per day) in mice fed a high-fat diet with regard to induced obesity and lipid metabolism. J Circadian Rhythms *10*, 4.

Greenwell, B.J., Trott, A.J., Beytebiere, J.R., Pao, S., Bosley, A., Beach, E., Finegan, P., Hernandez, C., and Menet, J.S. (2019). Rhythmic Food Intake Drives Rhythmic Gene Expression More Potently than the Hepatic Circadian Clock in Mice. Cell Reports *27*, 649-657.e645.

Hajnal, A. (2003). Oral sucrose stimulation increases accumbens dopamine in the rat. *286*, 31R-37.

Hansson, L. (1985). The food of bank voles, wood mice and yellow-necked mice, Vol 55.

Hatori, M., Vollmers, C., Zarrinpar, A., Ditacchio, L., Eric, Gill, S., Leblanc, M., Chaix, A., Joens, M., James*, et al.* (2012). Time-Restricted Feeding without Reducing Caloric Intake Prevents Metabolic Diseases in Mice Fed a High-Fat Diet. Cell Metabolism *15*, 848-860.

Jensen, S.P. (1993). Temporal changes in food preferences of wood mice (Apodemus sylvaticus L.). *94*, 76-82.

Karlsson, B. (2001). Is there an association between shift work and having a metabolic syndrome? Results from a population based study of 27 485 people. *58*, 747-752.

Klockars, A., Levine, A.S., and Olszewski, P.K. (2015). Central Oxytocin and Food Intake: Focus on Macronutrient-Driven Reward. *6*.

Kohsaka, A., Laposky, A.D., Ramsey, K.M., Estrada, C., Joshu, C., Kobayashi, Y., Turek, F.W., and Bass, J. (2007). High-fat diet disrupts behavioral and molecular circadian rhythms in mice. Cell Metab *6*, 414-421.

Larson, K.R., Chaffin, A.T.B., Goodson, M.L., Fang, Y., and Ryan, K.K. (2019). Fibroblast growth factor-21 controls dietary protein intake in male mice. Endocrinology.

Liu, R., Hong, J., Xu, X., Feng, Q., Zhang, D., Gu, Y., Shi, J., Zhao, S., Liu, W., Wang, X.*, et al.* (2017). Gut microbiome and serum metabolome alterations in obesity and after weight-loss intervention. Nature Medicine *23*, 859-868.

Lu, B., Bridges, D., Yang, Y., Fisher, K., Cheng, A., Chang, L., Meng, Z.X., Lin, J.D., Downes, M., Yu, R.T.*, et al.* (2014). Metabolic Crosstalk: Molecular Links Between Glycogen and Lipid Metabolism in Obesity. *63*, 2935-2948.

Lück, S., Thurley, K., Paul, and Pål (2014). Rhythmic Degradation Explains and Unifies Circadian Transcriptome and Proteome Data. *9*, 741-751.

Olszewski, P.K., Klockars, A., Olszewska, A.M., Fredriksson, R., Schiöth, H.B., and Levine, A.S. (2010). Molecular, Immunohistochemical, and Pharmacological Evidence of Oxytocin's Role as Inhibitor of Carbohydrate But Not Fat Intake. Endocrinology *151*, 4736-4744.

Ridaura, V.K., Faith, J.J., Rey, F.E., Cheng, J., Duncan, A.E., Kau, A.L., Griffin, N.W., Lombard, V., Henrissat, B., Bain, J.R.*, et al.* (2013). Gut Microbiota from Twins Discordant for Obesity Modulate Metabolism in Mice. Science *341*, 1241214-1241214.
Sasaki, T. (2017). Neural and Molecular Mechanisms Involved in Controlling the Quality of Feeding Behavior: Diet Selection and Feeding Patterns. Nutrients *9*.

Sherman, H., Genzer, Y., Cohen, R., Chapnik, N., Madar, Z., and Froy, O. (2012). Timed high-fat diet resets circadian metabolism and prevents obesity. FASEB J *26*, 3493-3502.

Shimbara, T., Mondal, M.S., Kawagoe, T., Toshinai, K., Koda, S., Yamaguchi, H., Date, Y., and Nakazato, M. (2004). Central administration of ghrelin preferentially enhances fat ingestion. *369*, 75-79.

Slavin, J., and Carlson, J. (2014). Carbohydrates. Advances in Nutrition *5*, 760-761.

Slawecki, C.J., Betancourt, M., Walpole, T., and Ehlers, C.L. (2000). Increases in Sucrose Consumption, But Not Ethanol Consumption, Following ICV NPY Administration. *66*, 591-594.

Stanley, B.G., Daniel, D.R., Chin, A.S., and Leibowitz, S.F. (1985). Paraventricular nucleus injections of peptide YY and neuropeptide Y preferentially enhance carbohydrate ingestion. *6*, 1205-1211.

Steinbusch, L., Labouèbe, G., and Thorens, B. (2015). Brain glucose sensing in homeostatic and hedonic regulation. *26*, 455-466.

Stephanie, Lucas, Peltekian, L., Meghan, Terry, Kristin, Adriana, Andreas, Ratner, C., Holst, B.*, et al.* (2016). FGF21 Mediates Endocrine Control of Simple Sugar Intake and Sweet Taste Preference by the Liver. *23*, 335-343.

Talukdar, S., Bryn, Song, P., Hernandez, G., Zhang, Y., Zhou, Y., William, Paratala, B., Turner, T., Smith, A.*, et al.* (2016). FGF21 Regulates Sweet and Alcohol Preference. Cell Metabolism *23*, 344-349.

Tempel, D.L., Leibowitz, K.J., and Leibowitz, S.F. (1988). Effects of PVN galanin on macronutrient selection. *9*, 309-314.

Wu, G., Anafi, R.C., Hughes, M.E., Kornacker, K., and Hogenesch, J.B. (2016). MetaCycle: an integrated R package to evaluate periodicity in large scale data. Bioinformatics *32*, 3351-3353.

Yang, S., Liu, A., Weidenhammer, A., Cooksey, R.C., McClain, D., Kim, M.K., Aguilera, G., Abel, E.D., and Chung, J.H. (2009). The role of mPer2 clock gene in glucocorticoid and feeding rhythms. Endocrinology *150*, 2153-2160.

CHAPTER VI

DISCUSSION, SUMMARY, AND FUTURE DIRECTIONS

6.1 CLOCK:BMAL1 bind DNA in a tissue-specific manner

To determine how the circadian clock drives tissue-specific rhythmic transcription, we performed BMAL1 ChIP-seq experiments in the mouse liver, kidney, and heart. We identified two major mechanisms that contribute to the tissue-specific binding of CLOCK:BMAL1, the first being the binding of tissue-specific transcription factors (ts-TFs) and the second being a tissue-specific permissive chromatin landscape. Current research suggests that ts-TFs may be at least partially responsible for creating a permissive chromatin landscape which would suggest that these two mechanisms are not mutually exclusive (Cieślik and Bekiranov, 2015; Iwafuchi-Doi et al., 2016; Zaret and Carroll, 2011). The vast majority of CLOCK:BMAL1 binding sites were found to be in open chromatin across the mouse liver, kidney, and heart. This data parallels what has been seen for many other transcription factors, as the ENCODE consortium found that 94.4% of transcription factor binding occurs in an open chromatin environment (Thurman et al., 2012b; Yue et al., 2014a). Previous research has also observed tissue-specific binding of a ubiquitously expressed transcription factor (u-TFs) due to binding with different tissue-specific transcription factors in different tissues (Glass and Natoli, 2016; Grontved et al., 2013; Heinz et al., 2015; Hurtado et al., 2011). This suggests that one major role of ts-TFs is to direct u-TFs such as CLOCK:BMAL1 to the correct locations in the tissue. Previous research suggests that the purpose of the u-TFs is to control the intrinsic activity of the BMAL1 bound enhancers enhancer (Trott and Menet,

2018a). This data suggests that different types of transcription factors will have different roles, and that in many instances ts-TFs will be responsible for controlling the permissiveness of the chromatin landscape, while u-TFs are responsible for the transcriptional output of the enhancers target gene. Much of the BMAL1 binding also occurred in a tissue-specific manner when the chromatin was permissive in all three tissues. This evidence suggests that instead of BMAL1 acting as a pioneer transcription factor and generating a new DHS, that it instead prevents DNA from wrapping around the nucleosomes and creates a permissive chromatin landscape with help from ts-TFs but does not generate new DHS. The idea is that BMAL1 and the ts-TF's are preferred binders as compared to the nucleosomes in these enhancer regions and thus are able to maintain a DHS in these regions. Our current hypothesis is that the nucleosomes found at BMAL1-bound enhancers are often fragile nucleosomes, and thus BMAL1 out competes the nucleosomes at these locations. Further research would be needed to test this hypothesis to determine if there is a difference in the histone modifications at CLOCK:BMAL1 bound enhancers. It has been previously suggested that H3K27ac could be a major component of driving rhythmic transcription (Trott and Menet, 2018a).

We hypothesized that the vast majority of BMAL1 bound enhancers would be responsible for driving rhythmic gene expression. Previous publications from the laboratory have shown that CLOCK:BMAL1 bound enhancers activity are largely determined by the binding of additional u-TFs (Trott and Menet, 2018). While the rhythmicity of BMAL1 bound enhancers was higher than observed for non-BMAL1 bound enhancers, the majority were still expressed in an arrhythmic manner (Fig 13). This evidence suggests that while u-TFs are responsible for controlling the intrinsic

activity of an enhancer, the intrinsic activity may not be sufficient to drive tissue-specific rhythmic transcription. For many genes there are multiple enhancers found within the same gene, and enhancers have shown to interact over very long distances, and in some instances even between different chromosomes (Dekker and Misteli, 2015; Sanyal et al., 2012).

6.2 The Three-dimensional chromatin architecture contributes to rhythmic gene expression

Recent findings have shown that u-TFs are largely responsible for controlling the intrinsic activity of CLOCK:BMAL1 bound enhancers, and our findings expand on this suggesting that transcription is often regulated with another layer of complexity with enhancer-enhancer interactions (Beytebiere et al., 2019; Trott and Menet, 2018a). The three-dimensional chromatin architecture has been shown to be important for gene expression and its mis-regulation has shown to lead to cancer and many disease states (Barutcu et al., 2015; Darío et al., 2015; Flavahan et al., 2016; Franke et al., 2016; Hnisz et al., 2016; Martin et al., 2015; Seaman et al., 2017; Taberlay et al., 2016). Our results show that BMAL1 enhancers and neighboring enhancers have day-night differences in the number of interactions for rhythmic targets, whereas these day-night differences in the number of interactions are not observed for arrhythmic targets. These findings are consistent with previous findings using 4C thus suggesting that BMAL1-mediated rhythmic transcription relies on the ability of BMAL1 to regulate rhythmic enhancer-enhancer interactions (Aguilar-Arnal and Sassone-Corsi, 2013; Mermet et al., 2016; Yeung et al., 2018). Previous research utilizing 4C in the liver showed that

BMAL1 bound enhancers were recruited to promoters during the day to drive liver specific rhythmic gene expression (Yeung et al., 2018). Multiple recent publications have shown that rhythmic transcription in mammals is associated with rhythmic long-range interactions (Aguilar-Arnal and Sassone-Corsi, 2013; Beytebiere et al., 2019; Kim et al., 2018a; Mermet et al., 2016; Yeung et al., 2018). The mechanisms that control rhythmic enhancer-enhancer interactions are still not fully understood, but would likely include the mediator complex, histone modifications, and transcription factors. Recent findings have shown that the mediator acts as a functional bridge rather than an architectural bridge, and the cohesin is required to tether regulatory DNA (El Khattabi et al., 2019). These findings altogether led to the hypothesis that enhancers can either play a dominant or a subordinate role in regulating the transcriptional output of a given gene. It is also hypothesized that a dominant enhancer under one environmental condition could become a subordinate enhancer under another given condition, i.e., it becomes controlled by another enhancer. For example, under *ad libitum* feeding conditions with standard chow, the dominant enhancer for a given gene may no longer be the dominant enhancer under high fat diet conditions suggesting that these enhancer-enhancer interactions offer a very dynamic way to regulate gene expression. It is also very likely that while the dominant enhancers play the major role in regulating transcription, the subordinate enhancers still have an important role in the transcriptional output. Future research could also look to determine whether there is also a circadian link between the enhancer-enhancer interactions and cancer as three-dimensional chromatin interactions have already shown to play a pivotal role in cancer development (Barutcu et al., 2015; Flavahan et al., 2016; Hnisz et al., 2016; Seaman et

al., 2017; Taberlay et al., 2016). Further research will be needed to determine the exact role enhancer-enhancer interactions play in driving rhythmic gene expression. It is currently technically challenging to determine the different effects of enhancer-enhancer interactions and whether these interactions regulate the intrinsic activity of an enhancer. To start addressing this question, we have developed a technique that aims at directly teasing apart the contribution of enhancer-enhancer interactions and of the intrinsic activity of enhancers are to the transcriptional output. As described in Chapter 3, this technique relies on cloning enhancers into a plasmid and delivering it to the mouse liver by hydrodynamic tail vein injection.

Based on the current levels of transfection observed using hydrodynamic tail vein injection, this technique will provide sufficient transfection rate to determine the contribution of the intrinsic activity of an enhancer to rhythmic gene expression. We were able to detect SEAP protein in the blood, but it was not rhythmic over the course of the 24-hr day when driven by the *Nr1d1* enhancer. Because rhythmic *Seap* mRNA expression was observed in the liver, it may be that Seap mRNA is translated rhythmically, but its secretion from hepatocytes into the bloodstream is not clock-controlled and thereby lead to arrhythmic blood levels. Our data also suggest that *Nr1d1* enhancer can drive rhythmic expression in both the native chromatin context and in the episomal context. One interesting point is that the mRNA levels only had a two-fold difference from the episomal context between ZT6 and ZT18 while for the pre-mRNA from *Nr1d1* enhancers native context the amplitude was ten-fold. One plausible explanation is that the four CLOCK:BMAL1 enhancers located in *Nr1d1* locus may have an additive or synergistic effect on the transcriptional output in the native context, and

that this effect is not observed when the enhancer is removed from the chromatin context. Additional experiments will be needed to test this hypothesis. In addition, additional experiments where intrinsic activity of enhancer is measured every four hours for 24-hours (*i.e*., six-time point rhythm) will be required to expand the day-night differences we have uncovered.

Future directions for the project will also include performing the technique with a larger number of enhancers. The technique will need to be scaled up to include between ten to one hundred plasmids per mouse depending on what is found experimentally to be the optimal number. It will also be ideal to add a different barcode to the plasmid for each enhancer such that the transcription rate from each plasmid can be easily determined. The most important part for the future of the project is the determination of which enhancers to use. It would be a good strategy to take multiple enhancers from the same gene. It would also be good to pick genetic targets of BMAL1 that are rhythmic in-phase, rhythmic out-of-phase, arrhythmic, and not-expressed. This would allow for the determination of the role of enhancer-enhancer interactions and the intrinsic activity of enhancers. It would also allow for the determination of whether dominant enhancers and subordinate enhancers work together to drive transcription of the target genes. It may allow for the further elucidation of what makes a dominant and subordinate enhancer take their given role. The enhancer-enhancer interactions can currently be addressed on a genome-wide scale, but further experiments will be needed such that individual interactions can be studied. The ChIA-PET experiments could be performed as previously done in the Menet laboratory but sequenced to a significantly greater depth (Beytebiere et al., 2019). The next step for this project would then be to

address if these interactions similarly dictate rhythmic gene expression across multiple tissues. This would allow for strong claims about how the circadian clock drives rhythmic gene expression throughout the organism and not just in the liver.

6.3 *Bmal1*$^{-/-}$ mice can be entrained to night-restricted feeding

Bmal1$^{-/-}$ mice lack rhythms in much of their behavior and activity, and develop many different physiological disorders as they age (Kondratov et al., 2006). Previous studies have shown that *Bmal1*$^{-/-}$ mice lack rhythmic activity (Park et al., 2015). We fed *Bmal1*$^{-/-}$ mice in a feeding apparatus previously designed in the laboratory to determine their feeding behavior (Greenwell et al., 2019). We found that the knockout mice eat in an arrhythmic manner, but that they could be entrained to eat in a night restricted manner without lowering the amount of food they consumed. Similar food consumption is important so that health benefits of rhythmic food consumption can be teased apart from restricted caloric intake. This suggests that the *Bmal1*$^{-/-}$ mice can respond to external rhythms and that these can set the *Bmal1*$^{-/-}$ mice to have rhythmic feeding behavior. Further research will be needed to determine the effects of night-restricted feeding in knockouts on rhythmic gene expression. Previous publications have shown that mice fed only at night have a set of genes in the liver that are rhythmically transcribed due to the circadian clock (~ 30%) and that ~70% of the rhythmically expressed genes are rhythmic due to rhythmic food intake (Atger et al., 2015; Greenwell et al., 2019). These experiments were only conducted with four days of night-restricted feeding, which is sufficient for differences in gene expression. However, to study the physiological impacts, it is likely that the experiments would need to be run for a much

longer amount of time. Some questions that future studies should address are whether or not the physiological issues observed by *Bmal1*$^{-/-}$ mice can be mitigated by strong environmental rhythms. Some tests that would be worth running are whether rhythmic food intake coupled with strong rhythms in lighting are able to not only restore *Bmal1*$^{-/-}$ behavior rhythms but whether it can diminish the physiological issues.

6.4 Temporal food preferences in mice suggest standard chow may not meet mice temporal food needs

Most laboratory mice are commonly fed standard chow that has the same composition of carbohydrates, fats, and proteins throughout the course of the day. This leads to the mice having the same ratio of macronutrients at every feeding session. However, previous publications suggest that there may be a temporal food preference for sugars early in the active phase (Jensen, 1993). Previous publications did not find a preference for protein later in the active phase as we hypothesized, but one reason could be due to the protein sources they used not being pure protein and having a high source of fat (seeds and nuts). Many factors have shown to regulate food preferences such as humoral factors, homeostatic feeding mechanisms, the hedonic system, and genetics (Sasaki, 2017).

We used a novel feeding system that was adapted from the feeding system previously developed in the laboratory (Greenwell et al., 2019). We found that lipids had the earliest peak phase of consumption, followed by carbohydrates, and then by proteins. This is expected since glycogen is the preferred form of energy. Glycogen can be quickly utilized to meet the energy needs of the cell. The main source of glycogen is

glucose, but fat can also be a source from gluconeogenesis. Adding more replicates for both males and females (fifteen biological replicates for both males and females) will be necessary to expand on this study, and provide more robust results. In any case, our preliminary data suggest that mice have temporal food preferences, and further research will be needed to determine the impacts on physiology and gene expression. Previous publications have shown that rhythmic food intake is capable of driving rhythmic gene expression (Greenwell et al., 2019). This system could be further used to address for preferences in *Bmal1*$^{-/-}$ mice, and in pregnant mice, and could be used to test the effects of different factors controlling food preference such as ghrelin, FGF21, and glucose injections.

6.5 References

Aguilar-Arnal, L., and Sassone-Corsi, P. (2013). The circadian epigenome: how metabolism talks to chromatin remodeling. Curr Opin Cell Biol.

Atger, F., Gobet, C., Marquis, J., Martin, E., Wang, J., Weger, B., Lefebvre, G., Descombes, P., Naef, F., and Gachon, F. (2015). Circadian and feeding rhythms differentially affect rhythmic mRNA transcription and translation in mouse liver. Proceedings of the National Academy of Sciences *112*, E6579-E6588.

Barutcu, A.R., Lajoie, B.R., McCord, R.P., Tye, C.E., Hong, D., Messier, T.L., Browne, G., Van Wijnen, A.J., Lian, J.B., Stein, J.L.*, et al.* (2015). Chromatin interaction analysis reveals changes in small chromosome and telomere clustering between epithelial and breast cancer cells. Genome Biology *16*.

Beytebiere, J.R., Trott, A.J., Greenwell, B.J., Osborne, C.A., Vitet, H., Spence, J., Yoo, S.-H., Chen, Z., Takahashi, J.S., Ghaffari, N.*, et al.* (2019). Tissue-specific BMAL1 cistromes reveal that rhythmic transcription is associated with rhythmic enhancer–enhancer interactions. Genes & Development *33*, 294-309.

Cieślik, M., and Bekiranov, S. (2015). Genome-wide predictors of NF-κB recruitment and transcriptional activity. *8*.

Darío, Kraft, K., Heinrich, V., Krawitz, P., Brancati, F., Klopocki, E., Horn, D., Kayserili, H., John, Laxova, R.*, et al.* (2015). Disruptions of Topological Chromatin Domains Cause Pathogenic Rewiring of Gene-Enhancer Interactions. Cell *161*, 1012-1025.
Dekker, J., and Misteli, T. (2015). Long-Range Chromatin Interactions. *7*, a019356.

El Khattabi, L., Zhao, H., Kalchschmidt, J., Young, N., Jung, S., Van Blerkom, P., Kieffer-Kwon, P., Kieffer-Kwon, K.-R., Park, S., Wang, X.*, et al.* (2019). A Pliable Mediator Acts as a Functional Rather Than an Architectural Bridge between Promoters and Enhancers. Cell.

Flavahan, W.A., Drier, Y., Liau, B.B., Gillespie, S.M., Venteicher, A.S., Stemmer-Rachamimov, A.O., Suvà, M.L., and Bernstein, B.E. (2016). Insulator dysfunction and oncogene activation in IDH mutant gliomas. Nature *529*, 110-114.

Franke, M., Ibrahim, D.M., Andrey, G., Schwarzer, W., Heinrich, V., Schöpflin, R., Kraft, K., Kempfer, R., Jerković, I., Chan, W.-L.*, et al.* (2016). Formation of new chromatin domains determines pathogenicity of genomic duplications. *538*, 265-269.

Glass, C.K., and Natoli, G. (2016). Molecular control of activation and priming in macrophages. Nature Immunology *17*, 26-33.

Greenwell, B.J., Trott, A.J., Beytebiere, J.R., Pao, S., Bosley, A., Beach, E., Finegan, P., Hernandez, C., and Menet, J.S. (2019). Rhythmic Food Intake Drives Rhythmic Gene Expression More Potently than the Hepatic Circadian Clock in Mice. Cell Reports *27*, 649-657.e645.

Grontved, L., John, S., Baek, S., Liu, Y., Buckley, J.R., Vinson, C., Aguilera, G., and Hager, G.L. (2013). C/EBP maintains chromatin accessibility in liver and facilitates glucocorticoid receptor recruitment to steroid response elements. EMBO J *32*, 1568-1583.

Heinz, S., Romanoski, C.E., Benner, C., and Glass, C.K. (2015). The selection and function of cell type-specific enhancers. Nature Reviews Molecular Cell Biology *16*, 144-154.

Hnisz, D., Weintraub, A.S., Day, D.S., Valton, A.L., Bak, R.O., Li, C.H., Goldmann, J., Lajoie, B.R., Fan, Z.P., Sigova, A.A.*, et al.* (2016). Activation of proto-oncogenes by disruption of chromosome neighborhoods. *351*, 1454-1458.

Hurtado, A., Holmes, K.A., Ross-Innes, C.S., Schmidt, D., and Carroll, J.S. (2011). FOXA1 is a key determinant of estrogen receptor function and endocrine response. Nat Genet *43*, 27-33.

Iwafuchi-Doi, M., Donahue, G., Kakumanu, A., Watts, J.A., Mahony, S., Pugh, B.F., Lee, D., Kaestner, K.H., and Zaret, K.S. (2016). The Pioneer Transcription Factor FoxA

Maintains an Accessible Nucleosome Configuration at Enhancers for Tissue-Specific Gene Activation. Mol Cell *62*, 79-91.

Jensen, S.P. (1993). Temporal changes in food preferences of wood mice (Apodemus sylvaticus L.). *94*, 76-82.

Kim, Y.H., Marhon, S.A., Zhang, Y., Steger, D.J., Won, K.-J., and Lazar, M.A. (2018). Rev-erbα dynamically modulates chromatin looping to control circadian gene transcription. Science *359*, 1274-1277.

Kondratov, R.V., Kondratova, A.A., Gorbacheva, V.Y., Vykhovanets, O.V., and Antoch, M.P. (2006). Early aging and age-related pathologies in mice deficient in BMAL1, the core componentof the circadian clock. Genes Dev *20*, 1868-1873.

Martin, P., McGovern, A., Orozco, G., Duffus, K., Yarwood, A., Schoenfelder, S., Cooper, N.J., Barton, A., Wallace, C., Fraser, P.*, et al.* (2015). Capture Hi-C reveals novel candidate genes and complex long-range interactions with related autoimmune risk loci. *6*, 10069.

Mermet, J., Yeung, J., and Naef, F. (2016). Systems Chronobiology: Global Analysis of Gene Regulation in a 24-Hour Periodic World. a028720.

Park, N., Kim, H.D., Cheon, S., Row, H., Lee, J., Han, D.H., Cho, S., and Kim, K. (2015). A Novel Bmal1 Mutant Mouse Reveals Essential Roles of the C-Terminal Domain on Circadian Rhythms. PLoS One *10*, e0138661.

Sanyal, A., Lajoie, B.R., Jain, G., and Dekker, J. (2012). The long-range interaction landscape of gene promoters. Nature *489*, 109-113.

Sasaki, T. (2017). Neural and Molecular Mechanisms Involved in Controlling the Quality of Feeding Behavior: Diet Selection and Feeding Patterns. Nutrients *9*.

Seaman, L., Chen, H., Brown, M., Wangsa, D., Patterson, G., Camps, J., Omenn, G.S., Ried, T., and Rajapakse, I. (2017). Nucleome Analysis Reveals Structure-function Relationships for Colon Cancer. molcanres.0374.0372.

Taberlay, P.C., Achinger-Kawecka, J., Lun, A.T.L., Buske, F.A., Sabir, K., Gould, C.M., Zotenko, E., Bert, S.A., Giles, K.A., Bauer, D.C.*, et al.* (2016). Three-dimensional disorganization of the cancer genome occurs coincident with long-range genetic and epigenetic alterations. Genome Research *26*, 719-731.

Thurman, R.E., Rynes, E., Humbert, R., Vierstra, J., Maurano, M.T., Haugen, E., Sheffield, N.C., Stergachis, A.B., Wang, H., Vernot, B.*, et al.* (2012). The accessible chromatin landscape of the human genome. Nature *489*, 75-82.

Trott, A.J., and Menet, J.S. (2018). Regulation of circadian clock transcriptional output by CLOCK:BMAL1. PLOS Genetics *14*, e1007156.

Yeung, J., Mermet, J., Jouffe, C., Marquis, J., Charpagne, A., Gachon, F., and Naef, F. (2018). Transcription factor activity rhythms and tissue-specific chromatin interactions explain circadian gene expression across organs. Genome Res *28*, 182-191.

Yue, F., Cheng, Y., Breschi, A., Vierstra, J., Wu, W., Ryba, T., Sandstrom, R., Ma, Z., Davis, C., Pope, B.D.*, et al.* (2014). A comparative encyclopedia of DNA elements in the mouse genome. Nature *515*, 355-364.

Zaret, K.S., and Carroll, J.S. (2011). Pioneer transcription factors: establishing competence for gene expression. Genes Dev *25*, 2227-2241.